SUPER-GAIN PARAMETRIC WAVE AMPLIFICATION IN OPTICAL MICRO-RESONATORS USING ULTRASHORT PUMP WAVES

A THESIS SUBMITTED TO
THE GRADUATE SCHOOL OF NATURAL AND APPLIED SCIENCES
OF
MIDDLE EAST TECHNICAL UNIVERSITY

BY

ÖZÜM EMRE AŞIRIM

IN PARTIAL FULFILLMENT OF THE REQUIREMENTS FOR
THE DEGREE OF DOCTOR OF PHILOSOPHY IN ELECTRICAL
AND ELECTRONICS ENGINEERING

JUNE 2020

Approval of the thesis:

SUPER-GAIN PARAMETRIC WAVE AMPLIFICATION IN OPTICAL MICRO-RESONATORS USING ULTRASHORT PUMP WAVES

submitted by **ÖZÜM EMRE AŞIRIM** in partial fulfillment of the requirements for the degree of **Doctor of Philosophy in Electrical and Electronics Engineering Department, Middle East Technical University** by,

Prof. Dr. Halil Kalıpçılar
Dean, Graduate School of **Natural and Applied Sciences** _____

Prof. Dr. İlkay Ulusoy
Head of Department, **Electrical and Electronics Engineering** _____

Prof. Dr. Mustafa Kuzuoğlu
Supervisor, **Electrical and Electronics Engineering, METU** _____

Examining Committee Members:

Prof. Dr. Gönül Turhan Sayan
Electrical and Electronics Engineering, METU _____

Prof. Dr. Mustafa Kuzuoğlu
Electrical and Electronics Engineering, METU _____

Prof. Dr. Özlem Özgün
Electrical and Electronics Engineering, Hacettepe University _____

Prof. Dr. Asım Egemen Yılmaz
Electrical and Electronics Engineering, Ankara University _____

Assoc. Prof. Dr. Serdar Kocaman
Electrical and Electronics Engineering, METU _____

Date: 23.06.2020

I hereby declare that all information in this document has been obtained and presented in accordance with academic rules and ethical conduct. I also declare that, as required by these rules and conduct, I have fully cited and referenced all material and results that are not original to this work.

Name, Surname: Özüm Emre Aşırım

Signature :

ABSTRACT

SUPER-GAIN PARAMETRIC WAVE AMPLIFICATION IN OPTICAL MICRO-RESONATORS USING ULTRASHORT PUMP WAVES

Aşırım, Özüm Emre
Doctor of Philosophy, Department of Electrical and Electronics Engineering
Supervisor: Prof. Dr. Mustafa Kuzuoğlu

June 2020, 135 pages

The aim of this thesis is to show that super-gain electromagnetic wave amplification can be achieved in a small micro-resonator using high-intensity ultrashort pump waves, provided that the frequencies of the ultrashort pulses are tuned to maximize the intracavity magnitude of the wave to be amplified, which is called the *stimulus wave*. In order to accomplish this, a dispersion analysis is performed via numerical modeling of the polarization density in terms of the nonlinear electron cloud motion. The polarization density is then concurrently solved with the wave equation for the electric field. Through a series of nonlinear programming integrated finite difference time domain simulations, we have determined the optimum pump wave frequencies that simultaneously maximize the stored electric energy density and the polarization density inside a micro-resonator by using the Broyden-Fletcher-Goldfarb-Shanno (BFGS) optimization algorithm. Based on the results of our numerical experiments, we propose that micrometer-scale achievement of super-gain electromagnetic wave amplification is possible in a micro-resonator with high-intensity ultrashort "pump wave" pulses, by determining the optimum frequencies that concurrently maximize the stored electric energy density and the polarization density in a dielectric interaction medium.

Keywords: Wave amplification, Nonlinear wave mixing, Micro-resonator, Optimization

ÖZ

OPTİK MİKRO-YANKILAYICILARDA ÇOK KISA SÜRELİ KAYNAK DALGALARI İLE ELEKTROMANYETİK DALGALARIN SÜPER-KAZANÇLI GENLİK YÜKSELTİMİ

Aşırım, Özüm Emre
Doktora, Elektrik Elektronik Mühendisliği Bölümü
Tez Yöneticisi: Prof. Dr. Mustafa Kuzuoğlu

Haziran 2020, 135 Sayfa

Bu tezde mikroyankılayıcıların kısa süreli kaynak dalgaları ile geniş bantlı ve yüksek kazançlı elektromanyetik dalga yükseltgeci olarak kullanılabilmesine yönelik en iyileme ve geliştirme yöntemleri ele alınmaktadır. Denetimsel yöntem olarak bilgisayar hesaplaması kullanılmıştır. Hesaplamalar dalga denkleminin eğrisel elektron hareketi denklemi ile aynı anda çözülmesi yolu ile gerçekleştirilmiştir. Bu hesaplamalar yapılırken zaman boyutunda sonlu fark yönteminden yararlanılmıştır. Öncelikle yankılayıcı içerisinde ki enerji en yüksek seviyeye çıkarılacak şekilde kaynak dalgası titreşim sıklığı ayarlaması yapılmıştır. Bununla birlikte, kaynak dalgasından genliği yükseltilecek dalgaya enerji aktarımının fazla olması için eğrisel bağlantı katsayısının da yüksek olması sağlanmıştır. Bunlara ek olarak, yük kutuplaşması yoğunluğunun fazla olmasını sağlamak ve enerji birikimini arttırmak için sönümlenme katsayısının düşük seçilmesi gerektiğine vurgu yapılmış ve bu vurgu bilgisayar hesaplamaları ile belirtilmiştir. Son olarak, kazanç ortamının yankılayıcı titreşim sıklığının düşük olmasının eğrisel kazancı arttıracağı gösterilmiş ve kazanç ortamının buna göre seçilmesi gerektiği belirtilmiştir. Bugün kü kuramsal önerilere aykırı olarak mikroyankılayıcılarda geniş bantlı ve yüksek kazançlı genlik yükseltmesi yapılabileceği önerilmiş, ve bunun için kaynak dalgasının titreşim sıklığının ayarlanması gerektiği sonucuna varılmştır.

Anahtar Kelimeler: Genlik yükseltimi, doğrusal olmayan dalga karışımı, Mikroyankılayıcı, Optimizasyon

Dedicated to my parents Adil and Gülgün

ACKNOWLEDGMENTS

I would like to express my gratitude to my supervisor Prof. Dr. Mustafa Kuzuoğlu for his guidance, suggestions, criticism, and encouragement during the time of research and writing of this thesis. I would also like to express my deepest gratitude to TÜBİTAK for awarding me the PhD scholarship, investing in me and my research for the hopes of contributing to the research made in our great country, Republic of Turkey.

I am grateful to my parents Gülgün and Adil, for their endless support and patience during my PhD studies.

TABLE OF CONTENTS

LIST OF TABLES

TABLES

LIST OF FIGURES

FIGURES

CHAPTER 1

INTRODUCTION

Parametric wave amplification is a broadband amplification technique that is based on nonlinear wave interaction. It allows for high-gain amplification in a wide spectral band, especially in the optical region. Therefore, it is a commonly used technique of wave amplification, when a sufficiently-long nonlinear gain medium, and an intense pump wave that can supply the input wave with energy, are simultaneously available. In the micrometer scale, even materials with a high second or third order electric susceptibility, are not useful to yield a significant gain factor. Based on many recent studies on optical parametric amplification, a significant gain in the micrometer scale is not achievable. Some previous studies have reported a high-gain optical parametric amplification in the millimeter scale, however, these studies have assumed for a single resonance (emission) frequency and have not considered the case of multiple resonance frequencies for an interaction medium. A more realistic approach is to consider an interaction material with multiple resonance frequencies in a given spectral band. More importantly, the vast majority of studies on optical parametric amplification have treated the nonlinear electric susceptibilities (second and third order) as time independent constants. However, when the pump wave is an ultrashort pulse (with a duration of less than several picoseconds), which is usually the case given that most intense pump waves have practically very short durations, this is not a realistic assumption. Several computational studies have modeled the nonlinear electric susceptibilities as functions of time, though their results were not perfectly reliable as these computational studies have relied on experimental data to create the time dependent nonlinear susceptibility models, which is subject to a variety of errors due to harmonic generation and spectral broadening. Moreover, experimental

data for the nonlinear electric susceptibility of most materials are not available, which limits the applicability of time dependent nonlinear susceptibility models. Recent experimental studies on nonlinear optics, are mostly focusing on improving harmonic conversion efficiencies and generating an ultra-wideband supercontinuum using ultrashort pulses. In the last two decades, optical parametric amplification technique has been investigated to be employed in milimetric "on-chip" optical devices with promising results. However, micro-scale optical amplification seems to be unfeasible and remains uninvestigated.

Optical parametric amplification usually enables the achievement of a high gain factor for interaction mediums with a length of a few centimeters [1]. For interaction mediums with unusually high nonlinear electric susceptibilities, the required length reduces to a few milimeters. In the micrometer scale, the achievement of a high gain factor might be possible with artificially created materials, such as glass doped with gold nanoparticles [2]. However, the fabrication of these materials with necessary interaction lengths is challenging and these materials can be quite expensive. Some experimental studies report novel materials with extraordinarily-high resonant nonlinear susceptibilities for certain frequencies [1-2], which can be used for the applications of nonlinear integrated optics. Though, these materials are not suitable for optical amplification as their dielectric absorption is very strong at these frequencies where nonlinear response displays a resonance behaviour. Hence, experimental studies, for the most part, do not focus on enhancing the gain factor of an optical parametric amplification. In addition, computational studies on nonlinear optics is quite limited as the required interaction length is hundreds of wavelengths long, which requires an enormous computational power. Commercially important optical frequencies are on the nanometer scale and a few centimeters long interaction medium would require a computational domain of thousands of wavelengths, which restricts the duration of simulation and increases the cost of computation [1-3].

Theoretically, high gain optical parametric amplification can be achieved in the micrometer scale by increasing the intensity of the pump wave pulse to a level where the interaction medium starts to couple the pump wave to the input wave to be amplified.

However, this will practically breakdown the interaction medium and will cause ionization of the interaction medium [4-5]. This is due to the optical breakdown of the interaction medium due to very high intensity. Different materials have different optical breakdown intensities, but a pump wave intensity that is high enough to provide amplification (theoretically) in the micrometer scale would breakdown almost any interaction medium. Therefore, increasing the intensity of the pump wave for achieving a considerable gain in the micrometer scale is not feasible and will damage the interaction medium. Furthermore, one may increase the frequencies of the pump wave and the input wave (assuming both are perfectly monochromatic) for a higher gain factor in the micrometer scale, but this would offer a noticably enhanced gain factor only in the near ultraviolet part of the spectrum and beyond[6-8]. For these reasons, a computational study that involves an in-depth dispersion analysis remains necessary for the possibility of achieving wideband high-gain optical parametric amplification in the micrometer scale.

Performing parametric optical amplification in the microscale could offer a wideband high-gain amplification feature for microphotonic devices and might enable wideband optical antennas for future applications in integrated photonics. Currently no experimental study has reported wideband high-gain optical parametric amplification in a microresonator or in any other microscale device based on our investigations of recently available reviews on wave amplification via nonlinear mixing.

A recent computational study [32] has shown the achievement of super-gain optical parametric amplification in a microresonator. In this study, a single resonance interaction medium is considered. Although some media have only a single resonance frequency (such as excitonic materials), in practice most media have multiple resonance frequencies. This thesis aims to investigate the achievement of super-gain optical parametric amplification in an interaction medium with multiple resonance frequencies, using the finite difference time domain method (FDTD), incorporated with a constrained numerical optimization algorithm.

In this study, the dispersion analysis is based on the modeling of polarization density by using the nonlinear equation of electron motion. The treatment is classical instead of a quantum one. The wave equations for the electric field of the pump wave and the input

wave to be amplified, will be solved in parallel with the dispersion equations that involve the polarization density. The total polarization density is considered to be due to the sum of all electron polarizations with respect to the nucleus, based on each different resonance frequency (atomic model "spring constant"). Each resonance frequency will result in the addition of a dispersion equation that involve the corresponding polarization density component. The polarization density components will finally be added to obtain the total polarization density due to all resonance frequencies and all the corresponding damping rates (state lifetimes). It is essential to note that each resonance frequency and each corresponding polarization density component will have a weight factor that is equal to the ratio of the electrons oscillating at that particular resonance frequency. This is a result of the quantum mechanical (probabilistic) interpretation of the atomic model.

This study aims to build on the study given in [32] in order to present a more realistic picture on the feasibility of optical parametric amplification in a microresonator. A simple fabry perot type microresonator will be assumed in the discussion. The basic form of Newton's optimization algorithm that involves penalty functions (constraints) will be incorporated in the FDTD method to optimize the gain factor for an interaction medium with multiple resonance frequencies under certain restrictions.

The propagation of waves in nonlinear dispersive media will be presented firstly as the background subject for the subsequent optimization analysis. Two simulations will be presented and their results will be analyzed in the discussion section. The conclusion of this study aims to provide a recipe for high-gain optical amplification in a microresonator with an ordinary interaction medium with multiple emission frequencies. Importance of careful nonlinear programming for any given experimental setup and the flowchart of the complete algorithm is emphasized in the concluding comments.

1.1 Basics of parametric amplification

Parametric amplification is a nonlinear process in which a low intensity input wave is amplified by a high intensity pump wave. The high intensity of the pump wave is what makes the parametric amplification possible through nonlinear coupling in an interaction

medium. The required intensity for nonlinear coupling depends on the nonlinearity of the interaction medium [9-11]. For strongly nonlinear interaction mediums, the required pump wave intensity can be relatively low. For an interaction medium with minimal nonlinearity, the required intensity can be very high and sometimes high enough to damage the interaction medium, for this reason, interaction mediums exhibiting low nonlinearities are not preferred for the optical parametric amplification process. In most research papers and book chapters about optical parametric amplification, the nonlinearity coefficients of most interaction mediums are assumed to be constant during the interaction of the input wave and the pump wave. This is a valid assumption when the durations of the input wave and the pump wave are much longer than the nonlinear response time of the interaction medium, however, when the nonlinear response time of the interaction medium is long or when the duration of the high-intensity pump wave is very short, such an assumption might be inaccurate [12-13]. Since the period of an electromagnetic wave in the optical frequency range is very small (on the order of femtoseconds), the pump wave is mostly assumed to be monochromatic, even when it is generated by systems that are known to generate ultrashort pump wave pulses, such as mode-locked lasers or Q-switched lasers. The pump wave amplitude is usually assumed to be constant during the interaction time, this is a reasonable assumption when the gain factor of the input wave is not very high. However, for high-gain amplifications of the input wave, the pump wave amplitude decreases significantly over time and the assumption of constant pump wave amplitude is not valid [14-16].

Parametric amplification is more efficient at relatively high frequencies. For example, the amplification efficiency in the ultraviolet range is much higher than the amplification efficiency in the far infra-red frequency range. In the microwave frequency range, the efficiency of parametric amplification is quite low and requires a long interaction medium to compensate for low efficiency. One of the most attractive features of optical parametric amplification is that it can be achieved in a very wide frequency band. The bandwidth of the amplification is not limited to the emission bandwidth of the interaction material as in the case for lasers. The amplification bandwidth is limited only by the pump wave frequency, which has to be higher than the frequency of the input wave. Therefore, in terms of monochromatic description, a visible input wave cannot be amplified by an

infrared pump wave or a visible pump wave cannot be used to amplify an ultraviolet input wave. Hence, it is better to use a high frequency pump wave to increase the amplification bandwidth. An ultraviolet pump wave for example, can be generated via frequency doubling of an intense visible pump wave by using a highly efficient frequency doubler.

One weakness of optical parametric amplification (OPA) technique is that it works very poorly for microscale interaction mediums. OPA relies heavily on the interaction medium length. Even under very intense pump wave excitations, the amplification of an input wave is negligible in the micrometer scale. One practical way of increasing the amplifiation efficiency is to increase the pump wave amplitude to the optical power threshold without causing breakdown, and by increasing the pump wave and the input wave frequencies, however, this will limit the amplification to higher frequencies and most importantly will cause damage to the interaction material over time, since microscale interaction materials are susceptible for optical breakdown, especially at high frequencies. This makes OPA not suitable for the applications of integrated nonlinear photonics.

A possible solution is to use an interaction medium with an extraordinarily high nonlinearity, although such materials are very rare, there are artifical materials that demonstrate superior nonlinear optical response. These artifical materials are usually expensive and exhibit high conduction and scattering losses under excitation, which is not ideal for optical amplification.

The low gain available from a micrometer scale interaction medium is not sufficient to support for a significant optical amplification in a microresonator. This is due to the loss factor exceeding the small signal optical gain. The loss factor of a microresonator is the multiplication of all individual loss factors, such as the reflection losses, the dielectric absorption loss of the interaction medium, the conduction loss of the interaction medium, scattering losses due to material impurities in the interaction medium and any other loss that can occur in a simple cavity [17-19]. The combination of all losses results in a loss factor that is practically much higher than the gain factor achieved from a microscale gain medium. Even if the microresonator walls would be perfect reflectors, the conduction loss would be zero, and the material impurities would be nonexistent, the practical dielectric loss would still exceed the available gain factor. Hence, optical microresonators do not

provide a significant gain factor via the technique of optical parametric amplification, which is why microchip lasers are of high interest for integrated optics.

The gain factor of OPA is highly sensitive to many microresonator parameters. It is most sensitive to the intensity of the pump wave amplitude, even a very small decrease in the pump wave intensity can severely degrade the OPA performance, which is why preserving the pump wave amplitude is of key interest in OPA. Another major parameter that heavily affects the amplification performance is the nonlinearity of the interaction medium. As mentioned before, interaction mediums with low nonlinearities may not yield any amplification via nonlinear wave mixing under intense pump wave excitations, but a highly nonlinear medium can yield a very strong amplification even under moderate pump wave intensities. Silicon is a good example of a highly nonlinear material that is non-centrosymmetric (possesses only third order nonlinearity with second order nonlinearity being zero). Gallium arsenide is another semiconductor that demonstrates a highly nonlinear response under excitation.

The loss factor of the OPA process in a microresonator is highly nonlinear. Any loss that results in the cavity will lead to a decrease in the pump wave amplitude, which will cause more loss at the next round trip due to decreased nonlinearity. Even in a highly nonlinear interaction medium, a small decrease in pump wave amplitude will cause a drastic decrease in input wave amplification (gain factor) [20-22]. For this reason, controlling the pump wave amplitude is crucial. In microresonators, maintaining a stable pump wave amplitude can be achieved by maximizing the constructive interface in the cavity.

The main question is, how to increase the gain factor in a microresonator with a micrometer-scale interaction medium? This depends on the nonlinear dispersion charactheristics of the interaction medium [23-25]. There are many experimental studies that aim to achieve a resonant nonlinear response for certain excitation frequencies (using the "Z-Scan" technique). Currently, there are many materials that are experimentally proven to demonstrate a resonant nonlinear response under certain excitation frequencies. These materials can be used in microresonators for an enhanced gain factor for OPA. However, rather than focusing on certain materials for high-gain microscale OPA, it is better to develop an algorithm that can enable high-gain OPA for any optical microcavity

involving any kind of interaction material. This study involves a computational approach as a recipe for achieving high-gain OPA in an arbitrary microresonator containing an arbitrary interaction medium. The computational method that is used in this study involves the combination of Newton's optimization method and the finite difference time domain method. At each step of the optimization, the wave equation and the dispersion equations that involve the polarization density, are discretized using the finite difference time domain method. A brief summary of the Newton's method will be mentioned for clarification in the following sections.

Assume that we want to amplify the low-intensity input wave E_1 using a high-intensity pump wave E_2. In order to solve for the gain factor of E_1, the following two equations must be solved [26-28]

$$\nabla^2(E_2) - \mu_0\varepsilon_0\left(1+\chi^{(1)}\right)\frac{\partial^2(E_2)}{\partial t^2} = \mu_0\sigma\frac{\partial(E_2)}{\partial t} + \mu_0\varepsilon_0\left(\frac{\partial^2\left\{\chi^{(2)}(E_2)^2 + \chi^{(3)}(E_2)^3\right\}}{\partial t^2}\right) \quad (1)$$

$$\nabla^2 E_1 - \mu_0\varepsilon_0\left(1+\chi^{(1)}\right)\frac{\partial^2 E_1}{\partial t^2} = \mu_0\sigma\frac{\partial(E_1)}{\partial t} + \mu_0\varepsilon_0\frac{\partial^2\left\{\chi^{(2)}({E_1}^2 + 2E_1E_2) + \chi^{(3)}({E_1}^3 + 3{E_1}^2E_2 + 3E_1{E_2}^2)\right\}}{\partial t^2} \quad (2)$$

ε_0: *Permittivity of free space*

μ_0: *Permeability of free space*

$\chi^{(1)}$: *First order electric susceptibility*

$\chi^{(2)}$: *Second order electric susceptibility*

$\chi^{(3)}$: *Third order electric susceptibility*

σ: *Electric conductivity*

Based on equations, the solution for the gain factor of E_1 after the propagation through an interaction medium of length *L*, is given by the following formula

$$\frac{E_1(x=L)}{E_1(x=0)} = G = \cosh\left\{\left(Ld\sqrt{\omega_1(\omega_2-\omega_1)\eta^3}\sqrt{0.5cn\varepsilon_0{E_{pump}}^2}\right)\right\} \quad (3)$$

c: Speed of light, ε_0: Permittivity of free space, L: Medium length

d: Nonlinearity coefficient, n: Refractive index, η: Intrinsic impedance

ω_1: *Angular frequency of the input wave,* ω_2: *Angular frequency of the pump wave*

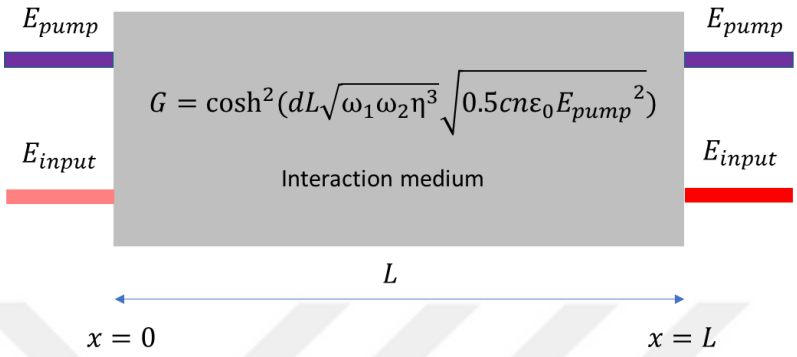

Figure 1.1 Single pass optical parametric amplification

Since the gain factor that can be obtained from a single pass is negligible, we need to investigate the parametric amplification process inside a micro-resonator. Inside a low-loss resonator the gain is expected to be much higher as every round trip yields further amplification, however, since the interaction medium length is very small, the resonator losses prevents the achievement of a significant gain factor. Assuming the gain factor definition in equation, the gain factor that is achieved in a micro-resonator after N round trips is given as

$$Gain(N) = \prod_{i=1}^{N} \zeta^2 \times \cosh^2\left\{Ld\sqrt{h\omega_1(\omega_2 - \omega_1)\eta^3}\sqrt{0.5cn\varepsilon_0 E_{pump}(i)^2}\right\} \quad (4)$$

$$E_{pump}(i) = E_{pump}(0) \times \zeta^i$$

$$i: \ Number\ of\ round\ trips$$

$$Gain(N) = Overall\ gain\ after\ N\ round\ trips$$

Where the round-trip loss ζ is defined as

$$Round\ trip\ loss\ factor = \zeta = R_1\ R_2 \exp(-\alpha_d L)\ \exp(-\alpha_c L)\ \exp(-\alpha_s L) \quad (5)$$

(R_1, R_2): Reflectivity imperfections of the cavity walls (R_1 R_2).

α_d: Dielectric absorption loss, α_c: Conduction loss, α_s: Scattering losses

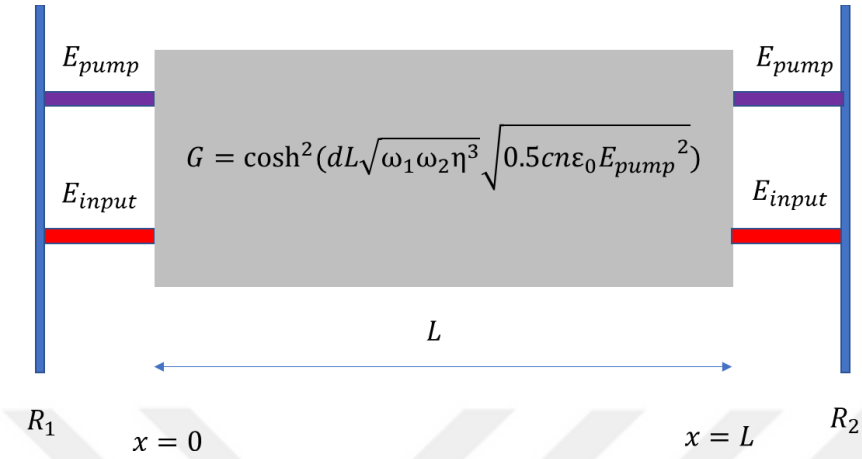

Figure 1.2 Optical parametric amplification in a resonator

In order to show that the overall achievable micro-resonator gain is small, and the optical amplification efficiency is low, as an example, consider the following micro-resonator parameters

$$\omega_1 = 2\pi(120\,THz),\ d = 1 \times 10^{-21}\,C/V^2,\ \sigma \approx 0,\ R_1 = R_2 = 1$$

$$Round\ trip\ loss\ factor = \zeta = \exp(-\alpha_d L)\exp(-\alpha_s L) = 1 - 10^{-3} = 0.999$$

$$\omega_2 = 2\pi(180\,THz),\ L = 10\ \mu m,\ \varepsilon_r = 10,\ I = 0.5cn\varepsilon_0 {E_{pump}}^2\ O\left(\frac{10^{16}\,W}{m^2}\right)$$

$$Input\ wave\ electric\ field\ amplitude\ at\ the\ 1st\ round\ trip = 1\,V/m$$

Note that practically such a round trip loss factor is unattainably low. The resulting input wave amplitude variation with respect to the number of round trips is plotted in Figure. As we can easily notice, the input wave amplitude keeps on increasing while the small signal gain is greater than the loss factor. Since the pump wave amplitude keeps on decreasing due to the resonator losses at each round trip, the small signal gain of the input wave also decreases at each round trip and eventually the loss factor exceeds the gain factor. After this, the input wave amplitude starts to decrease. As the process of parametric amplification strongly depends on the pump wave amplitude, the resonator loss exponentially increases with the number of round trips.

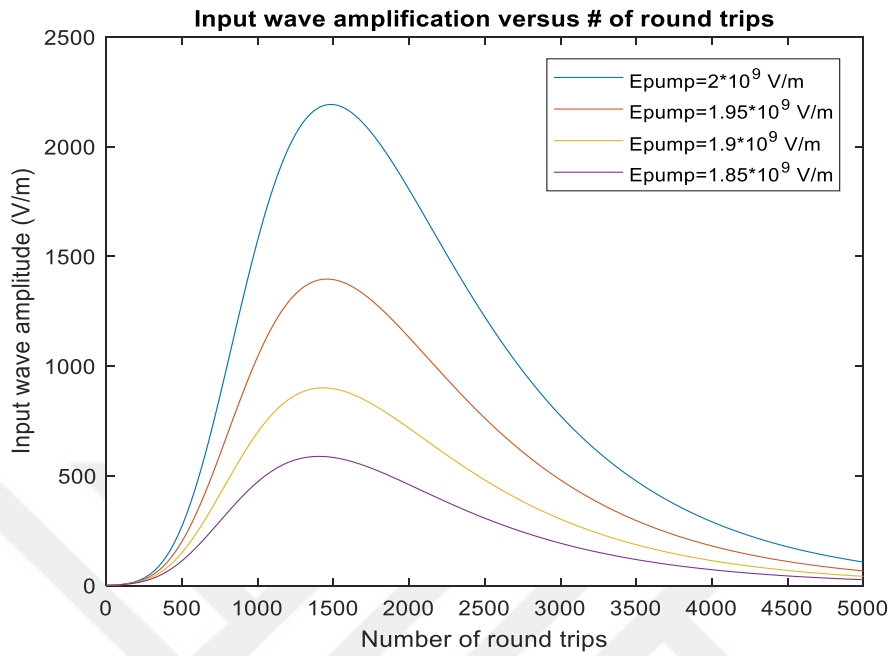

Figure 1.3 Input wave amplitude versus number of round trips in a micro-resonator

Figure1.3 shows the variation of the input wave amplitude with respect to the number of round trips in the micro-resonator when the nonlinearity coefficient is decreased (halved) to $d = 5 \times 10^{-22}\, C/V^2$, notice that the amplification performance has severely decreased, even though the nonlinearity (d) is still considered as quite high.

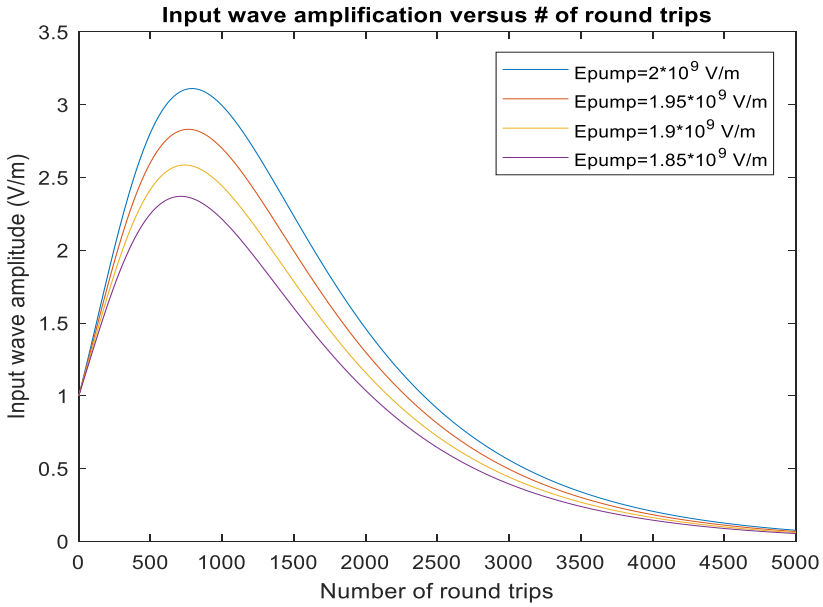

Figure 1.4 Input wave amplitude versus number of round trips in a micro-resonator

Figure1.4 shows the variation of the input wave amplitude with respect to the number of round trips in the micro-resonator when the nonlinearity coefficient is increased to $d = 3 \times 10^{-21}\ C/V^2$, and the round trip loss factor is changed to $\zeta = 1 - 10^{-2} = 0.99$.

Note that, even though this round trip loss is quite small and still practically very hard to ensure, the optical amplification is quite weak and has a low efficiency.

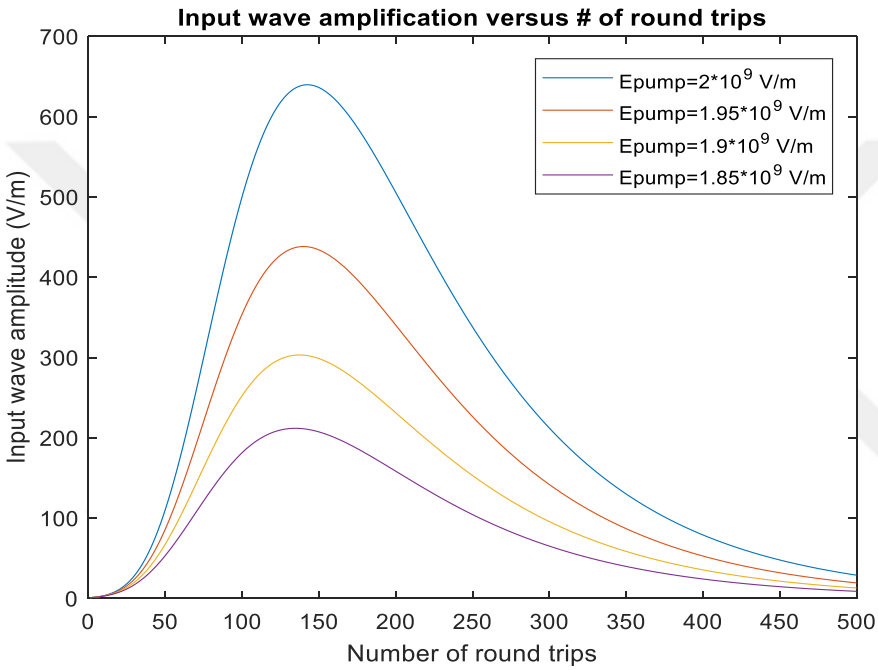

Figure 1.5 Input wave amplitude versus number of round trips in a micro-resonator

These examples clearly indicate that high-gain optical parametric amplification is not feasible in a micro-resonator as the interaction medium length is too small to yield enough small signal gain to compensate for the resonator losses. In this study, a numerical approach will be used to prove that high-gain optical parametric amplification may be achieved by performing an extensive dispersion analysis that measures the nonlinear electrical response of an arbitrary micro-resonator for each quasi-monochromatic pump wave center frequency. This analysis will be carried out by solving the electric field wave equation in parallel with the equation of nonlinear electron cloud motion for an interaction medium with multiple emission (resonance) frequencies. We will often focus our investigation on the dominant resonance frequency for the dispersion analysis.

CHAPTER 2

POLARIZATION DENSITY AND LIGHT MATTER INTERACTION

2.1 Basics of charge polarization and polarization density

The atoms or molecules of a material are stimulated when an electric field is applied. This is because the electrons of an atom are bound to the nucleus by a very strong electrostatic force and the excitation of a material by an electric field will create a distortion in the net force applied on the electrons and they will start to oscillate in space towards the nucleus and back. As a result, the dipole moment of the nucleus-electron pair will keep on changing in time as long as the external electric field is applied. Since the electrical permittivity of a material is related to the vectorial sum of all of the individual electrical dipoles, depending on the frequency and intensity of the applied field, the resulting electrical permittivity of the material can change. It is known that when the intensity of the applied electric field is very strong, the positions of the electrons in the atom are highly distorted and the net force on an electron changes significantly. This significant change of the net force on an electron causes the electrical permittivity of the material to change. As the intensity of the applied electric field increases, the change in the electrical permittivity of the material will also increase. Since the electrostatic binding force applied on the electrons by the nucleus is also very high (usually much higher than the force applied by an external electric field), the resulting change in the electrical permittivity will be very small in percentage. However, even this very small change causes a variety of interesting phenomena, such as the electro-optic effect. The change in the electrical permittivity or the refractive index of a material depends on it's experimentally determined nonlinear susceptibility value. For some materials the nonlinear susceptibility values are extraordinarily high, which makes them suitable for applications that requires refractive index modulation. Gold and silicon are two example materials of this kind.

One important utilization of nonlinear materials in the field of nonlinear optics is the *self focusing* phenomenon. When we apply an intense laser beam to a nonlinear material, the beam automatically focuses itself while propagating inside the material and remains focused after leaving the material [29]. This helps us to overcome the diffraction limit and focus the beam on the nanometer scale. If the beam is precisely focused and controlled, this technique may be used in a variety of applications. In certain conditions, this technique can be used in *nanoscopy* to observe the world in the nanoscale, provided that the focused beam intensity is not damagingly high and will not harm the tissue or the surface that is being investigated[1-4].

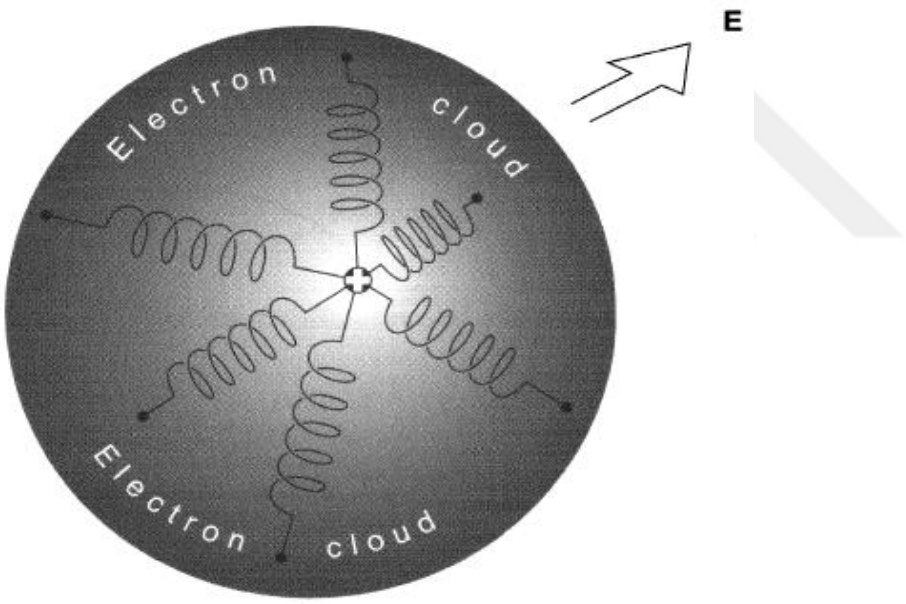

Figure 2.1 Electrons are bounded to the nucleus via the electrostatic force, resembled here as springs. An external electric field will change the relative positions of the electrons [7].

The physical idea behind the nonlinear dielectric polarization is related to the changes in the nucleus of the atom under very high intensity electric field excitation. When the

applied field intensity is extremely high, the relation between the restoring (electrostatic binding) force of the nucleus and the position of the electron becomes nonlinear.

Therefore the polarization density vector becomes nonlinear. Since the position of the electron depends on the applied field strength, the resulting relation between the polarization density vector and the field strength is also nonlinear.

The degree of nonlinearity depends heavily on the crystal structure of a material. Depending on the lattice/crystal structure, some materials only exhibit third order nonlinear polarization density while others can exhibit both second and third order nonlinear polarization density under high electric field excitation. Certain materials have a lattice structure that is symmetric with respect to the lattice center, such materials are called centro-symmetric materials. Centro-symmetric materials only exhibit third order nonlinearity and their associated second order nonlinear susceptibility is zero. One example is silicon, which has an unusually high third order susceptibility value, but since it has a centro-symmetric crystal structure, it's associated second order susceptibility value is zero. There are also materials with a non centrosymmetric crystal structure, for such materials both the second and the third order susceptibilities are nonzero. A well known example of a non centro-symmetric material is Gallium-Arsenide (GaAs). Gallium-Arsenide also has an unusually high third order susceptibility value and it's response to an applied electric field is anisotropic, meaning that in the case of GaAs the associated third order susceptibility is a tensor. As GaAs is non centro-symmetric, it also has a nonzero second order susceptibility tensor and it is known to exhibit a very strong second order electrical nonlinearity. Gold is also known to have a very strong second and third order nonlinear electrical susceptibility and in order to utilize it's nonlinearity, gold nanoparticles are usually doped in glass. Other examples of well known electrically nonlinear materials include some polymers such as polydiacetylenes. Other sorts of materials that are nonlinear in nature include germanium, silver, titanium dioxide, chalcogenide glass, lithium niobate and some nanoparticles [5,6].

Insulators have a certain dielectric strength that can withstand high electric fields up to a certain threshold. After that threshold insulators can break down and may start to act as a

conductor. Some insulators may still remain dielectric, but they can weakly or locally conduct electrical currents. Therefore, even though some materials have a very high nonlinear susceptibility, they might also have a low dielectric strength and before we can observe any nonlinear effects under high electric field excitation, the materials may break down and change their properties.

Recall that the polarization vector for a linear anisotropic material under excitation can be expressed as (assuming either the intensity of the electric field is not very high and $\chi^{(2)}, \chi^{(3)}$ terms can be ignored, or the material exhibits low nonlinearity and has ignorable $\chi^{(2)}, \chi^{(3)}$ values).

$$P_x = \varepsilon_0 {\chi_{xx}}^{(1)} E_x + \varepsilon_0 {\chi_{xy}}^{(2)} E_y + \varepsilon_0 {\chi_{xz}}^{(3)} E_z \quad (6)$$

$$P_y = \varepsilon_0 {\chi_{yx}}^{(1)} E_x + \varepsilon_0 {\chi_{yy}}^{(2)} E_y + \varepsilon_0 {\chi_{yz}}^{(3)} E_z \quad (7)$$

$$P_z = \varepsilon_0 {\chi_{zx}}^{(1)} E_x + \varepsilon_0 {\chi_{zy}}^{(2)} E_y + \varepsilon_0 {\chi_{zz}}^{(3)} E_z \quad (8)$$

In the linear case the susceptibility tensor has only 9 elements. For the nonlinear case the second order susceptibility tensor $\boldsymbol{\chi^{(2)}}$ has 27 elements and the third order suseptibility tensor $\boldsymbol{\chi^{(3)}}$ has 81 elements. Now let us consider the nonlinear case;

The first three orders of the i component of the polarization vector is expressed as;

$$P_i = \varepsilon_0 \sum_{j=1}^{3} {\chi_{ij}}^{(1)} E_j + \varepsilon_0 \sum_{j=1}^{3}\sum_{k=1}^{3} {\chi_{ijk}}^{(2)} E_j E_k + \varepsilon_0 \sum_{j=1}^{3}\sum_{k=1}^{3}\sum_{l=1}^{3} {\chi_{ijkl}}^{(3)} E_j E_k E_l \quad (9)$$

Elements of the higher order susceptibility tensors are negligible in value and can be ignored. For centro-symmetric materials the second order susceptibility tensor is zero, therefore the resulting i component of the polarization vector can be written as;

$$P_i = \varepsilon_0 \sum_{j=1}^{3} {\chi_{ij}}^{(1)} E_j + \varepsilon_0 \sum_{j=1}^{3}\sum_{k=1}^{3}\sum_{l=1}^{3} {\chi_{ijkl}}^{(3)} E_j E_k E_l \quad (10)$$

For an isotropic nonlinear material (though most materials are anisotropic in nature), the {x,y,z} components of the polarization vector can be written as;

$$P_x = \varepsilon_0\chi^{(1)}E_x + \varepsilon_0\chi^{(2)}{E_x}^2 + \varepsilon_0\chi^{(3)}{E_x}^3 \quad (11)$$

$$P_y = \varepsilon_0\chi^{(1)}E_y + \varepsilon_0\chi^{(2)}{E_y}^2 + \varepsilon_0\chi^{(3)}{E_y}^3 \quad (12)$$

$$P_z = \varepsilon_0\chi^{(1)}E_z + \varepsilon_0\chi^{(2)}{E_z}^2 + \varepsilon_0\chi^{(3)}{E_z}^3 \quad (13)$$

The materials that are both nonlinear and anisotropic in nature are way more cumbersome in mathematical description, though for such materials most of the elements of the susceptibility tensor are very small. Furthermore most nonzero elements of the susceptibility tensor are nearly equal to each other, so the mathematical expressions of the wave equation for such materials can be greatly simplified.

Recall that for a linear media under an external electric field excitation $\boldsymbol{E}$, the position $\boldsymbol{x}$ of an electron that is bound to the nucleus by the electrostatic binding force is decribed by the following differential equation [1,7]

$$m\frac{d^2\boldsymbol{x}}{dt^2} + m\nu\frac{d\boldsymbol{x}}{dt} + m{\omega_0}^2\boldsymbol{x} = -e\boldsymbol{E}(t) \quad (14)$$

$$\nu: Damping\ coefficient\ (material\ dependent)$$

$$m: Electron\ mass\ (9.11 \times 10^{-31}\ kg)$$

$$F_{restoring} = m{\omega_0}^2\boldsymbol{x}\ \ (restoring\ force\ of\ the\ nucleus)$$

$$\omega_0 = Resonance\ frequency\ of\ the\ atom$$

$$e: Electron\ charge$$

For a second order nonlinear material, the equation that describes the position of an electron with respect to the nucleus is given by the following equation

$$m\frac{d^2\boldsymbol{x}}{dt^2} + m\nu\frac{d\boldsymbol{x}}{dt} + m{\omega_0}^2\boldsymbol{x} + mn\boldsymbol{x}^2 = -e\boldsymbol{E}(t) \quad (15)$$

Notice the extra term $mn\boldsymbol{x}^2$ in the equation, which is related to the nonlinear restoring force of the nucleus. The term *n* resembles the strength of nonlinearity of the atom and is

therefore material dependent. It has been theoretically established that the nonlinearity coefficient *n* is related to the resonance frequency ω_0 of the atom by the following relation [1]

$$n = \frac{{\omega_0}^2}{d} \qquad (16)$$

$$d: Atomic\ size\ (around\ 3\ Angstroms\ for\ solids)$$

Which suggests that the degree of nonlinearity strongly depends on the resonance frequency of the atom. This makes perfect sense as ω_0 is a measure of strength of the nuclear binding force and the nonlinear susceptibility of an atom depends on nothing but the binding force.

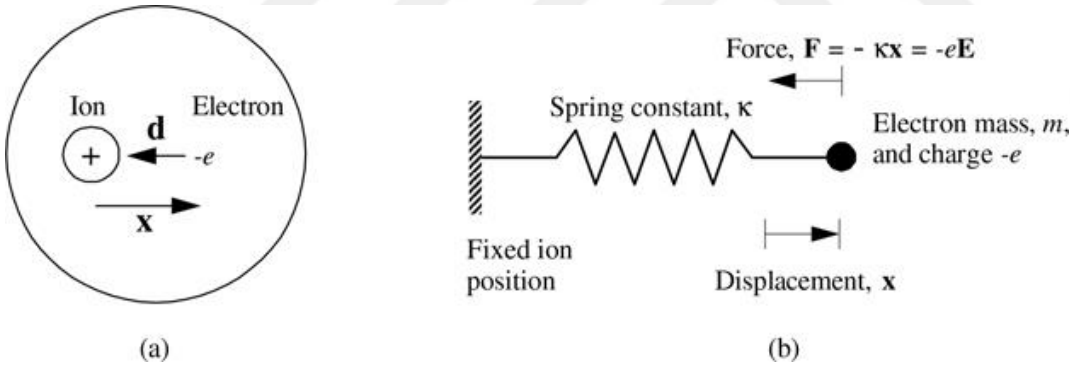

Figure 2.2 Electrostatic restoring force of the nucleus acting on an electron [21].

In order to find a solution for Eq.10, we start with a solution of the form

$$\boldsymbol{x}(t) = \varphi \boldsymbol{x_1}(t) + \varphi^2 \boldsymbol{x}_2(t) + \varphi^3 \boldsymbol{x}_3(t) + \cdots \qquad (17)$$

If the terms in Eq.10 are proportional to the coupling coefficients $\varphi, \varphi^2, \varphi^3$ in Eq.17, then the substitution of this form of solution into the nonlinear differential equation will decouple the nonlinear differential equation into the following linear differential equations

$$m\frac{d^2\boldsymbol{x_1}}{dt^2} + m\nu\frac{d\boldsymbol{x_1}}{dt} + m{\omega_0}^2\boldsymbol{x_1} = -e\boldsymbol{E}(t) \qquad (18)$$

$$m\frac{d^2\boldsymbol{x_2}}{dt^2} + m\nu\frac{d\boldsymbol{x_2}}{dt} + m{\omega_0}^2\boldsymbol{x_2} + n{\boldsymbol{x_1}}^2 = 0 \qquad (19)$$

$$m\frac{d^2\boldsymbol{x_3}}{dt^2} + m\nu\frac{d\boldsymbol{x_3}}{dt} + m{\omega_0}^2\boldsymbol{x_3} + 2n\boldsymbol{x_1}\boldsymbol{x_2} = 0 \qquad (20)$$

And so on so forth for the remaining terms. Notice that the first equation is the differential equation that describes the position of an electron with respect to the nucleus for a linear media. After solving for $\boldsymbol{x_1}$ we can substitute it into the second equation and solve the for $\boldsymbol{x_2}$. Then we can plug $\boldsymbol{x_1}, \boldsymbol{x_2}$ into the third equation and solve for $\boldsymbol{x_3}$ and etc.

For most solids the second order nonlinear susceptibility is found to be approximately around the following value [1]:

$$\chi^{(2)} \approx \frac{{q_e}^3}{\varepsilon_0 m^2 {\omega_0}^4 d^4} = 6.9 \times \frac{10^{-12}\, m}{V} \qquad (21)$$

$$\omega_0 : 1 \times \frac{10^{16}\, rad}{s}, \qquad d = 0.3\, nm, \qquad q_e = 1.6 \times 10^{-19}\, Coulomb$$

However, some solids have much lower resonance frequency values and therefore have a much greater $\chi^{(2)}$ value. The atomic diameter d is assumed to be the same for most solids. Therefore, the only variable in Eq.21 is the angular resonance frequency ω_0 which is material dependent.

Similarly, for most solids the third order nonlinear susceptibility is found to be approximately around the following value [1]

$$\chi^{(3)} \approx \frac{{q_e}^4}{\varepsilon_0 m^3 (0.7\omega_0)^6 d^5} = 344\ \frac{pm^2}{V^2} \qquad (22)$$

Hence, if we determine the $\chi^{(2)}$ value of a material experimentally, we can solve for it's resonance frequency and plug it in the equation for $\chi^{(3)}$ and roughly estimate the value of $\chi^{(3)}$ and vice versa (both for isotropic and anisotropic materials). For anisotropic materials the estimation is usually for the largest tensor element.

Ex: Gallium-Arsenide has a $\chi^{(3)}$ value of $1.4 \times 10^{-18}\ m^2/V^2$ one of the highest $\chi^{(3)}$ values among solids. It's corresponding $\chi^{(2)}$ value can be estimated to be around

$$\omega_0 = \sqrt[1/6]{({q_e}^4)/(\varepsilon_0 m^3 d^5 (0.7)^6)} = 2.5025 \times 10^{15}\ Hz$$

$$\chi^{(2)} \approx \frac{{q_e}^3}{\varepsilon_0 m^2 {\omega_0}^4 d^4} = 1.76 \times 10^{-9}\ m/V$$

Note that the resulting value is not precise. The actual value of the highest tensor element is around $1.48 \times 10^{-9}\ m/V$. However these formulas give a rough estimation of the degree of the second and the third order nonlinearities. One can also estimate the value of the second order susceptibility from *Miller's rule.*

For nanoparticles the corresponding $\chi^{(2)}$ and $\chi^{(3)}$ values are much higher because the resonance frequency of nanoparticles is lower compared to bulk materials. The physics behind this phenomenon can be described by quantum mechanics and is related to the discretization of atomic energy levels for nanoparticles compared to a continuum of energy levels for bulk materials. When the energy levels are discrete, the restoring force becomes weaker, as a result the resonance frequency decreases. This leads to a higher nonlinear susceptibility. We can think of this as the accessibility of an electron by the nucleus. When the material is bulk the energy levels are continuous in the valence band and therefore the electron is "accessible", i.e, easier to restore to it's original position by the electrostatic binding force. When the material is in nanoparticle form, the energy levels become discrete and the nucleus has to exert a specific minimum amount of force to be able to restore the electron back to it's initial position. In some sense the electron is not as accessible as it is in the bulk material case.

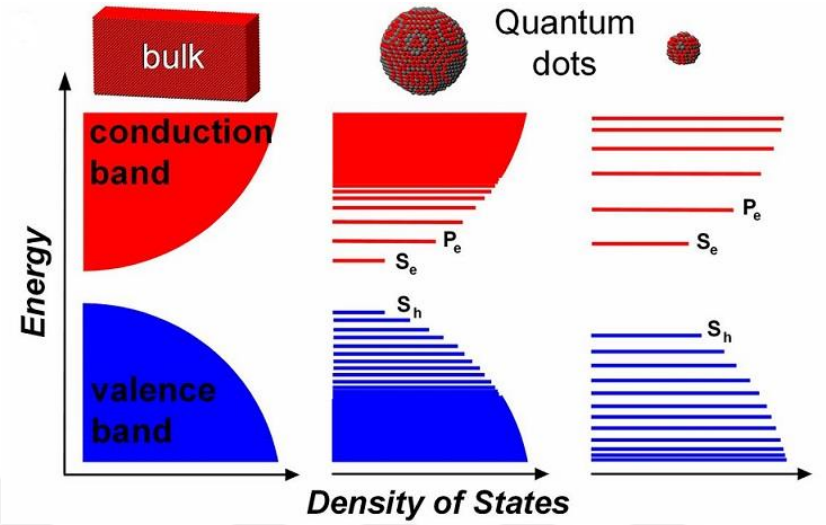

Figure 2.3 Energy level distributions of bulk materials and nanoparticles [22].

Gold nanoparticles for example have a 1000 times higher third order susceptibility compared to their bulk counterparts and can be doped in glass for applications in nonlinear optics. Also nanoparticles have lower conductivities compared to their bulk counterparts as the bandgap energy for a nanoparticle increases. Nanoparticles are also called quantum dots in literature and their production is known to be rather challenging.

To observe nonlinear effects on a laser beam, the required laser beam power must be on the order of gigawatts. This amount of power is not very straightforward to achieve. There are ways to produce very high intensity laser beams (usually in pulsed form), one of them is to use a mode locked laser which produces very short but very intense laser beams. Another way is to maximize the constructive interference inside a cavity. The simplest technique is to focus a medium power laser beam by a lens of high focusing ability.

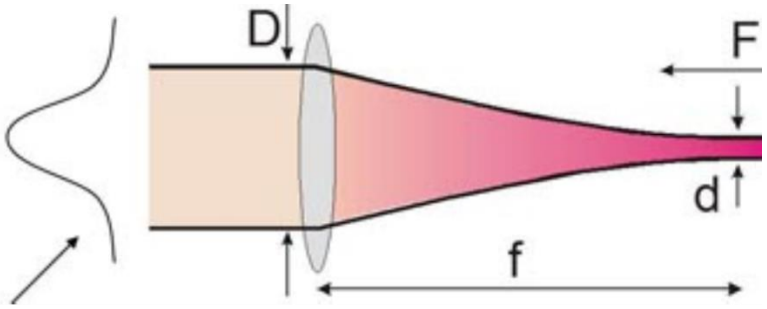

Figure 2.4 Focusing of a laser beam by a thin lens [6].

Observing nonlinear effects in optical frequencies is much easier than observing them in radio frequencies and microwave regions, as focusing a radio frequency electromagnetic wave is not very straightforward. This is one of the reasons that the field of nonlinear electromagnetics is concentrated on the optical frequency range. Another and a more important reason is that in the optical range of the spectrum, most solid materials exhibit a resonant nonlinear susceptibility. The nonlinear susceptibility of many solids can be greatly enhanced via plasmon resonance in the optical range. Current research on nonlinear materials is focused on creating artificial and composite materials that may show an unusually high second or third order susceptibility in optical frequencies. For example, nanoantennas of different shapes and sizes are modified by the addition of further nanoparticles to yield a boosted nonlinear response both in terms of second and third order susceptibility. It has been found that along with the size of a nanoparticle, it's shape also significantly affect it's nonlinear response. A triangular shaped nanomaterial as an example, can have a stronger nonlinear response than a square shaped nanomaterial in the optical frequency range. Just like the first order susceptibility, second and third order susceptibilities do not display any resonance in the microwave region of the electromagnetic spectrum. Though for some specially designed metamaterials, resonance in the microwave region may be possible.

The frequency response or the dispersion relation of the second and third order susceptibilities is not as precisely defined as it is for the first order susceptibility. However certain relations that relates the dispersion relation of the first order susceptibility to the second and the third orders exist. The frequency dispersion curve for the first order electric

susceptibility is as shown in Figure2.5. For many materials, resonances of the first order electric susceptibility exist in the infra-red or in the ultra-violet region, and some materials have strong resonances only in the visible range. A material might have more than one resonance frequency due to the electrons being in different positions or in different energy levels and the nucleus having different "spring constants" with "springs" of different strengths being attached to the electrons. This phenomena is included in the expression of the complex refractive index Λ. Each resonance frequency ω_{0j} with an oscillator strength f_j has a contribution to the overall value of the complex refractive index as given by Eq.23. As dictated by quantum mechanics, the sum of all oscillator strengths is equal to 1 [2,7].

$$\Lambda^2 = (\eta + i\kappa)^2 = 1 + \sum_{j=1}^{N} \frac{Ne^2}{m\varepsilon_0}\left[\frac{f_j}{{\omega_{0j}}^2 - \omega^2 - i\gamma_j\omega}\right] \quad (23)$$

$$\sum_{j=1}^{N} f_j = 1 \quad (24)$$

$$f_j: Oscillator\ strength$$

$$\gamma_j: Damping\ coefficient$$

The atom has an electron cloud around the nucleus and according to quantum mechanics the electron can be anywhere around the nucleus. As the distance from the nucleus decreases, the probability of finding an electron increases. And as the distance from the nucleus increases, the probability of finding an electron decreases. This is why we model the binding forces as different springs having different spring constants. Each spring resembles the electrostatic binding force whose strength depends on the relative position of the electron. As the total probability that an electron can be anywhere inside the whole atomic volume is 1, the integrated oscillation strength of all springs is equal to 1 as given by Eq.24.

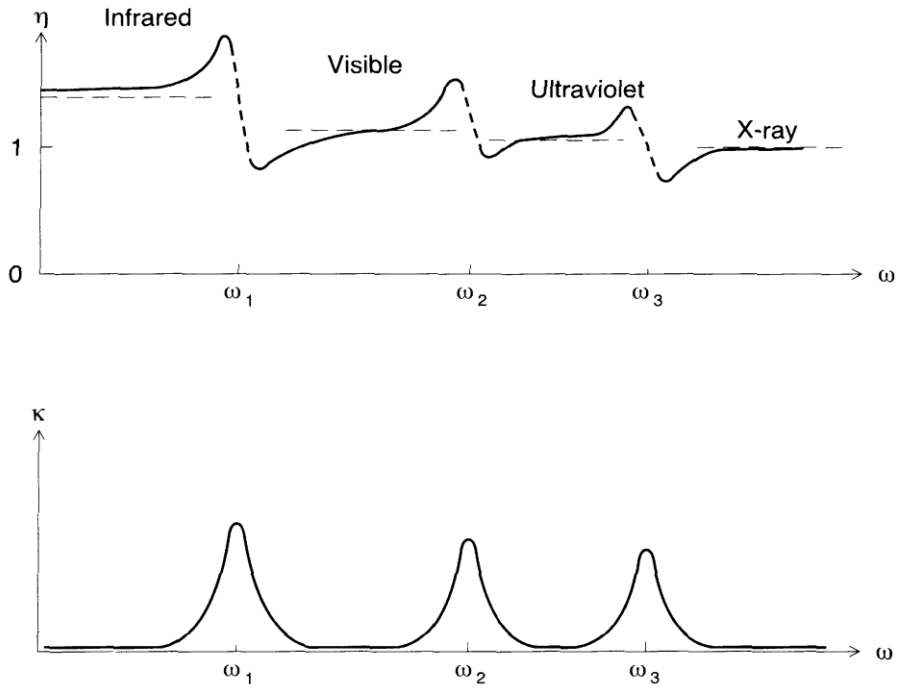

Figure 2.5 Resonance frequencies of an atom with multiple "springs" [2,7].

From the dispersion relation of the first order susceptibility, we can estimate the value of the second order susceptibility at a given frequency using the *Miller's rule*. This rule suggests that the expression [1]

$$\frac{\chi^{(2)}(\omega_2+\omega_1,\omega_1,\omega_2)}{\chi^{(1)}(\omega_2+\omega_1)\chi^{(1)}(\omega_1)\chi^{(1)}(\omega_2)} \qquad (25)$$

is almost constant for all non-centrosymmetric materials. From this relation we can conclude that in the radio frequency and in the microwave frequency regions of the spectrum, $\chi^{(2)}$ is almost constant. In the visible part of the spectrum this rule can help us estimate the resonance charactheristics of a material. Similarly for the third order susceptibility, we have the following relation [1]

$$\chi_{ijkl}{}^{(3)}(\omega_q,\omega_{m,}\omega_n,\omega_p) = \frac{bm{\varepsilon_0}^3}{3N^3e^4}[\chi^{(1)}(\omega_q)\chi^{(1)}(\omega_m)\chi^{(1)}(\omega_n)\chi^{(1)}(\omega_p)]$$
$$\times[\delta_{ij}\delta_{kl}+\delta_{ik}\delta_{jl}+\delta_{il}\delta_{jk}] \qquad (26)$$

From which we can conclude that in the radio frequency and in the microwave regions of the spectrum $\chi^{(3)}$ is almost constant.

At frequencies below the infra-red range, the first, second, and third order susceptibilities are nearly constant for all materials and any variation is negligible. However, especially in the optical frequency range, all three orders of susceptibilities are highly dispersive. In this case the electrical polarization is related to the susceptibility by the following relations [1,8-11]

$$P^{(1)}(t) = \varepsilon_0 \int_0^{\infty} \chi^{(1)}(\tau_1) E(t-\tau_1) d\tau_1 \qquad (27)$$

$$P^{(2)}(t) = \varepsilon_0 \int_0^{\infty} \int_0^{\infty} \chi^{(2)}(\tau_1, \tau_2) E(t-\tau_1) E(t-\tau_2) d\tau_1 d\tau_2 \qquad (28)$$

$$P^{(3)}(t) = \varepsilon_0 \int_0^{\infty} \int_0^{\infty} \int_0^{\infty} \chi^{(3)}(\tau_1, \tau_2, \tau_3) E(t-\tau_1) E(t-\tau_2) E(t - \tau_3) d\tau_1 d\tau_2 d\tau_3 \qquad (29)$$

At frequencies below the infra-red range, the susceptibilities can be expressed as

$$\chi^{(3)}(\tau_1, \tau_2, \tau_3) = {\chi_0}^{(3)} \delta(\tau_1, \tau_2, \tau_3) \qquad (30)$$

$$\chi^{(2)}(\tau_1, \tau_2) = {\chi_0}^{(2)} \delta(\tau_1, \tau_2) \qquad (31)$$

$$\chi^{(1)}(\tau_1) = {\chi_0}^{(1)} \delta(\tau_1) \qquad (32)$$

So that

$$P^{(3)}(t) = \varepsilon_0 {\chi_0}^{(3)} E^3(t), \quad P^{(2)}(t) = \varepsilon_0 {\chi_0}^{(2)} E^2(t), \quad P^{(1)}(t) = \varepsilon_0 {\chi_0}^{(1)} E(t) \qquad (33)$$

In the frequency domain Eq.27 can be expressed as

$$\zeta^{(1)}(\omega_1) = \varepsilon_0 \xi^{(1)}(\omega_1) \Phi(\omega_1) \qquad (34)$$

Where

$$\Phi(\omega_1) = \int_{-\infty}^{\infty} E(\tau_1) e^{-i\omega_1 \tau_1} d\tau_1 \qquad (35)$$

$$\xi^{(1)}(\omega_1) = \int_{-\infty}^{\infty} \chi^{(1)}(\tau_1) e^{-i\omega_1\tau_1} d\tau_1 \qquad (36)$$

$$\zeta^{(1)}(\omega_1) = \int_{-\infty}^{\infty} P^{(1)}(\tau_1) e^{-i\omega_1\tau_1} d\tau_1 \qquad (37)$$

Eq.28 is expressed in the frequency domain as follows

$$\zeta^{(2)}(\omega_1, \omega_2) = \varepsilon_0 \xi^{(2)}(\omega_1, \omega_2) \Phi(\omega_1, \omega_2) \qquad (38)$$

Where

$$\Phi(\omega_1, \omega_2) = \int_{-\infty}^{\infty}\int_{-\infty}^{\infty} E(\tau_1, \tau_2) e^{-i\omega_1\tau_1} e^{-i\omega_2\tau_2} d\tau_1 d\tau_2 \qquad (39)$$

$$\xi^{(2)}(\omega_1, \omega_2) = \int_{-\infty}^{\infty}\int_{-\infty}^{\infty} \chi^{(2)}(\tau_1, \tau_2) e^{-i\omega_1\tau_1} e^{-i\omega_2\tau_2} d\tau_1 d\tau_2 \qquad (40)$$

$$\zeta^{(2)}(\omega_1, \omega_2) = \int_{-\infty}^{\infty}\int_{-\infty}^{\infty} P^{(2)}(\tau_1, \tau_2) e^{-i\omega_1\tau_1} e^{-i\omega_2\tau_2} d\tau_1 d\tau_2 \qquad (41)$$

Similarly Eq.29 is expressed in the frequency domain as follows

$$\zeta^{(3)}(\omega_1, \omega_2, \omega_3) = \varepsilon_0 \xi^{(3)}(\omega_1, \omega_2, \omega_3) \Phi(\omega_1, \omega_2, \omega_3) \qquad (42)$$

$$\Phi(\omega_1, \omega_2, \omega_3) = \int_{-\infty}^{\infty}\int_{-\infty}^{\infty}\int_{-\infty}^{\infty} E(\tau_1, \tau_2, \tau_3) e^{-i\omega_1\tau_1} e^{-i\omega_2\tau_2} e^{-i\omega_3\tau_3} d\tau_1 d\tau_2\, d\tau_3 \qquad (43)$$

$$\xi^{(3)}(\omega_1, \omega_2, \omega_3) = \int_{-\infty}^{\infty}\int_{-\infty}^{\infty}\int_{-\infty}^{\infty} \chi^{(3)}(\tau_1, \tau_2, \tau_3) e^{-i\omega_1\tau_1} e^{-i\omega_2\tau_2} e^{-i\omega_3\tau_3} d\tau_1 d\tau_2\, d\tau_3 \qquad (44)$$

$$\zeta^{(3)}(\omega_1, \omega_2, \omega_3) = \int_{-\infty}^{\infty}\int_{-\infty}^{\infty}\int_{-\infty}^{\infty} P^{(3)}(\tau_1, \tau_2, \tau_3) e^{-i\omega_1\tau_1} e^{-i\omega_2\tau_2} e^{-i\omega_3\tau_3} d\tau_1 d\tau_2\, d\tau_3 \qquad (45)$$

These fourier transform relations and dispersion formulas are useful in the optical region of the spectrum, which includes the infra-red, visible, and the ultraviolet regions of the spectrum. Though special metamaterials may exhibit dispersion even in the microwave region of the spectrum.

2.2. Composite materials and nanocomposites for nonlinear electromagnetics

Using the latest advancements in production technology, we can design new artificial materials that are based on the composition of several materials, which are already found in nature. The purpose of creating composite materials is to utilize the unique features of all materials that are in the composition, by using a single artificial material. One example is the field of metamaterials, which usually aims to observe the negative refractive index phenomenon or to create artificial materials that yields to a zero reflection of electromagnetic waves when illuminated. Metamaterials are "meta" or artificial in the sense that while a classical or natural material forms a density of electric dipoles in its volume when excited by an electromagnetic wave, a metamaterial forms densities of both electric and magnetic dipoles in its volume when excited by an electromagnetic wave. Another example of a composite material is the doping of one material into another material. In such a case the one we dope is called the *dopant* material and the material that is being doped is called the *host* material. The resulting composite material carries the properties of both the dopant and the host materials and the charactheristics of the composite material can be changed by changing the doping concentration. An example is the doping of gold nanoparticles in glass.

A composite material has a conductivity, electrical and magnetic susceptibility, etc. The values of these parameters depend on the concentration of individual materials that form the composite material. If we dope a silicate glass with gold nanoparticles for example, the conductivity of the resulting composite material will be higher than undoped silicate glass. Or, if we dope silicon into a gallium-arsenide crystal, the resulting composite material will have a higher conductivity than the undoped gallium-arsenide crystal. Same thing is valid for the overall electric susceptibility of composite materials. Assume that we dope a silicate glass with germanium, since germanium has a higher electric susceptibility than the silicate glass, the resulting composite material will have a higher electric susceptibility than the undoped silicate glass. Composite materials of dopant/host type are mostly produced as thin films.

Recently the research has focused on nanocomposites, as nanoparticles have unique properties that are not observed with bulk materials. Especially in the field of nonlinear

optics, nanocomposites are found to be very promising for current and future research as they tend to display a higher nonlinear electric susceptibility, which can be modified by changing their shape and size. For example, a triangular shaped nanoparticle and an equal size circular shaped one exhibit different nonlinear electrical responses for the same excitation. Nanoparticles of materials that already have a high nonlinear susceptibility can be deposited on glass substrates to be used in applications of nonlinear optics. Structures of metal nanoparticles mounted on a glass substrate are called optical nano-antennas due to the effect of plasmon resonance. Since nanoparticles are very small, when a light beam is incident on them a very large locally enhanced electric near field is induced. This locally enhanced electric field can be utilized to generate a second or third order nonlinear response. Note that in the visible range of the spectrum, metals are less conductive compared to the microwave range. Therefore, instead of a complete scattering of the light beam, they absorb a portion of it and create a free electron density. This intense charge density produces a very strong electric field in the near field range. Intense locally enhanced electric near fields are used in microscopy to break the diffraction limit and to investigate the nanometer scale.

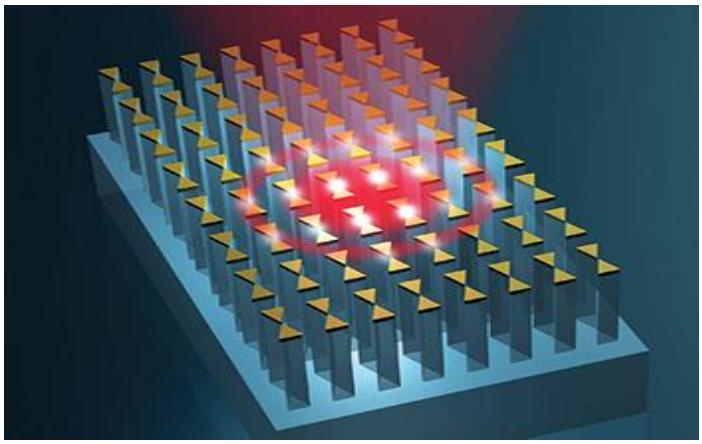

Figure 2.6 A light beam hits a gold bowtie nanoantenna array, forming plasmon resonances on the metal surfaces that create intense locally enhanced fields in the near field range [23].

Locally enhanced near fields can be better taken advantage of, if we mount highly nonlinear nanoparticles near the metal nanoparticles. Recall that metal nanoparticles are used to generate plasmon resonances, which yield to the intense locally enhanced electric near fields. To generate an efficient nonlinear electrical response, nanoparticles of highly nonlinear materials can be employed. As an example, highly nonlinear lithium-niobate nanoparticles can be mounted on a gold bowtie nanoantenna array structure to generate a second order nonlinear response as shown in Figure2.6.

When an incident light beam hits the surface of a metal structure, it induces electron stream oscillations (surface plasmons) inside the metal structure. Which is basically a plasma oscillation. Since the skin depth for an electromagnetic wave in the optical frequency range, is very small inside a metal structure (such as gold), plasma oscillations are concentrated on the surface of the metal. Hence the term surface plasmons. Recall that the skin depth for a good conductor is approximated by the following formula

$$\delta \approx \sqrt{\frac{2}{\omega\mu\sigma}} \qquad (46)$$

Assuming the following values are good approximations for our case, we calculate a typical skin depth value for a wave in the visible frequency range, that propagates inside a metal as

$$\sigma_{Gold} = 4.1 \times 10^{7}\ \frac{S}{m}\ , \qquad \omega = 2\pi \times 2.5 \times \frac{10^{14}\ rad}{s}, \qquad \mu = 4\pi \times 10^{-7}\ \frac{H}{m}$$

The resulting skin depth value is $\delta \approx 4\ nm$. Which indicates that the plasma oscillations are concentrated on the surface of the metal structure. The current density on the surface can be determined from the following simple relation

$$\boldsymbol{J} = \sigma \boldsymbol{E}_{light} \approx A_{\mathbf{0}} \sin(\omega t - \boldsymbol{k}.\boldsymbol{r}) \qquad \boldsymbol{k}: Wave\ vector, \quad \boldsymbol{r}: Position\ vector$$

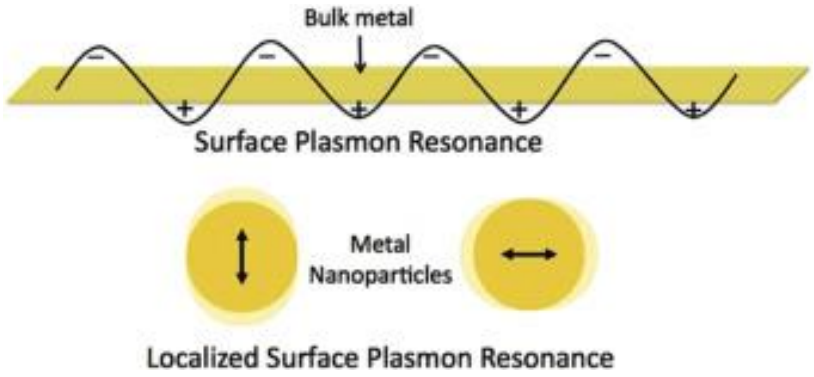

Figure 2.7 Surface plasmon resonance versus localized surface plasmon resonance [12].

When illuminated by an incident light beam, optical antennas such as gold nanostructures produce an enhanced scattered light in the near field range. This is not the case for example in the radio frequency range. The reason for that difference can be explained as follows:

On the metal surface where the current density forms

$$\boldsymbol{J} = \sigma \boldsymbol{E}_{light} \quad (47)$$

Due to this current density there is an associated magnetic vector potential

$$\boldsymbol{A} = \frac{\mu}{4\pi} \int_{-\infty}^{\infty} \int_{-\infty}^{\infty} \boldsymbol{J} \frac{e^{-jkR}}{R} dS' \quad (48)$$

From which the scattered electric field can be calculated as

$$\boldsymbol{E} = -j\omega \boldsymbol{A} - j \frac{1}{\omega \mu \varepsilon} \boldsymbol{\nabla}(\boldsymbol{\nabla}.\boldsymbol{A}) \quad (49)$$

In the optical frequency range we can approximate $\boldsymbol{E}$ as

$$\boldsymbol{E} \approx -j\omega A = -j\omega \frac{\mu}{4\pi} \int_{-\infty}^{\infty} \int_{-\infty}^{\infty} \boldsymbol{J} \frac{e^{-jkR}}{R} dS' \quad (50)$$

Which shows that the magnitude of the scattered electric field increases as the frequency of the incident electromagnetic wave increases. Since an electromagnetic wave in the optical region of the spectrum has a frequency that is typically a million times greater than an electromagnetic wave in the radio frequency range, the resulting scattered field is way much stronger. Note that the magnitude of the scattered field decreases with distance,

which gives a hint about why we have a locally enhanced field in the vicinity of the scatterer.

2.3. Plasma frequency and its effect on nonlinear susceptibility

The plasma frequency of a material is related to its atom density. Semiconductors such as silicon have a higher atom density and therefore a higher plasma frequency. We have already seen that as the resonance frequency of a material increases, it's second and third order nonlinear susceptibility decreases. The plasma frequency is related to the resonance frequency via plasmon resonance. Most solids have a plasma frequency in the visible or in the ultraviolet part of the spectrum due to their high atomic densities, therefore the electrical susceptibilities of these materials have a resonance behavior at these frequencies along with a much higher dielectric absorption loss. Apart from the resonance frequency, the behavior of the electrical susceptibility is mostly constant at the other parts of the spectrum. If we can somehow decrease the density of atoms in a material, it's resulting plasma frequency will decrease and this will lead to a lower plasmon resonance frequency and a higher nonlinear susceptibility. But how can we decrease the atom density of a material? We cannot! But we can mimic a decrease in the atom density of a material. We can do this by creating artificial atoms, which are known as nanoparticles or quantum dots. Let us consider a nanoparticle with a size of 30 nanometers. If we fill a material with such nanoparticles, each nanoparticle will act as an artificial atom and will form a local plasmon resonance when excited by an electric field, just like an ordinary atom. However, the "artificial atom" density is now lower compared to the case of ordinary atoms. This will cause a decrease in the plasma frequency (due to the existence of nanoparticles) and will yield a lower plasmon resonance frequency. Because of this decrease, the third and second order susceptibilities of this artificial material will increase. For example, gold has a third order susceptibility in the 10^{-19} scale in it's bulk form, however, gold nanoparticles embedded in a very thin glass slab, have a third order susceptibility that is in the 10^{-16} scale. Nanoparticles act like artificial atoms because they have discrete energy levels just like an ordinary atom. Though a perfectly discrete energy level density occurs only in an ordinary atom, nanoparticles have a much more discrete distribution of energy levels

compared to a bulk material, just like an ordinary atom. As the material gets bulkier, the distribution of energy levels has a more continuous structure. Nanoparticles are called quantum dots as they resemble a quantum equivalent of an ordinary atom in terms of energy level distribution.

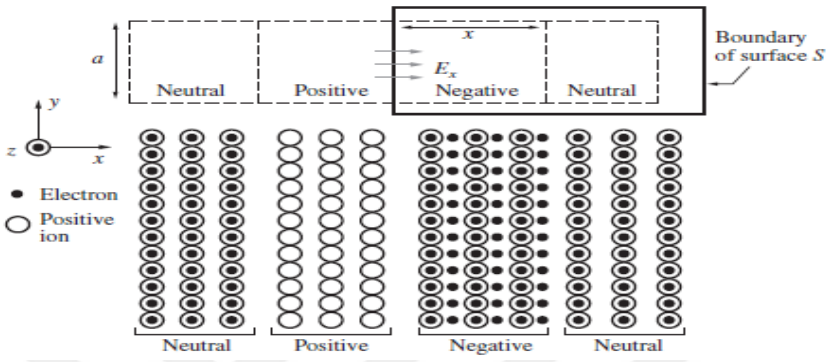

Figure 2.8 Electron movement between atoms inside a plasma slab [24].

Let us consider the plasma slab shown in Figure2.8 above. When the slab is excited or perturbed by an impulsive electric field **E**, that lasts a few picoseconds and then subsides, the electrons will move away from one atom towards the other leaving behind a "positively charged" atom and creating a new "negatively charged" atom. Due to this charge separation, a local, restoring, static electric field E_x will form [24]. This static electric field will try to restore the electrons back to their initial positions, but the electrons will displace further into the left and will create a negatively charged atom on the left, while the initially positively charged atom still remains positively charged. This time the static electric field E_x will pull the electrons to the right and try to restore them to their original positions, but the same cycle will continue, and the electrons will keep on oscillating this way. After the perturbing electric field subsides, the equation of motion for an electron is given by [24] (ignoring collusions)

$$m_{electron}\frac{d^2x}{dt^2} = q_e E_x \qquad (51)$$

Let us apply Gauss' law on the cross-sectional surface of figure8, assuming the thickness of the box is 'b' along the z direction.

$$\oint_S \boldsymbol{E}.\boldsymbol{ds} = \frac{Q}{\varepsilon_0} \qquad (52)$$

The cross-sectional area *S* is equal to *ab.* The total charge enclosed by the box volume within an electron displacement range *x* is

$$Q = N_e q_e abx \qquad (53)$$

Therefore, the restoring field can be found as

$$E_x = \frac{Q}{ab\varepsilon_0} = -\frac{N_e q_e abx}{ab\varepsilon_0} = -\frac{N_e q_e x}{\varepsilon_0} \qquad (54)$$

Substituting E_x back into Eq.51 gives out

$$\frac{d^2x}{dt^2} + \frac{N_e {q_e}^2}{m\varepsilon_0} x = 0 \qquad (55)$$

Which can be rewritten in a more compact form as

$$\frac{d^2x}{dt^2} + {\omega_p}^2 x = 0 \qquad (56)$$

$${\omega_p}^2 = \frac{N_e {q_e}^2}{m\varepsilon_0} \qquad (57)$$

Where ω_p is known as the plasma frequency and is related to the atom density of a material. The solutions to Eq.55 are steady oscillating functions with an oscillation frequency of ω_p, which can be either expressed as sines and cosines or complex exponential functions [24].

$$x(t) = Acos(\omega_p t) + Bsin(\omega_p t) \quad , \quad or$$

$$x(t) = Aexp(j\omega_p t) + Bexp(-j\omega_p t) \qquad (58)$$

Hence, we call these oscillations as plasma oscillations with the oscillation frequency being equal to the plasma frequency. Plasma oscillations are also called plasmons and a plasmon is considered a quanta of plasma oscillations. Just like a phonon, which is a quanta of lattice vibrations. In a collision-less plasma, these oscillations are undamped or steady, however, when we account for the collisions, these oscillations are damped and

will die out over time. Plasmas tend to stay neutral and they induce plasma oscillations as an effort to restore neutrality. Note that we have ignored the displacement of ions and treated them as stable in position since ions have a much greater mass compared to electrons. Recent research suggests that by using artificial materials made up of nanoparticles, we can create plasma oscillations of lower frequencies and change the frequency response of the first, second and third order nonlinear electrical susceptibilities.

CHAPTER 3

WAVE AMPLIFICATION VIA NONLINEAR COUPLING

3.1. Quality (Q) factor of a cavity: The quality factor indicates the maximum amount of energy that can be stored in a cavity. It is desirable to have a high Q factor for applications that require or utilize a high amount of stored energy density. The Q factor may be enhanced by increasing the length of the cavity, increasing the mean reflection coefficient by choosing the cavity walls as highly reflective, increasing the frequency of the wave that interacts with the cavity, decreasing the overall absorption coefficient of the interaction medium, and by minimizing any other kinds of losses that may result in a cavity. The formal definition of the Q factor can be expressed as

$$CAVITY\ QUALITY\ (Q) FACTOR = 2\pi \frac{Energy\ stored}{Energy\ dissipated\ per\ round\ trip} \qquad (59)$$

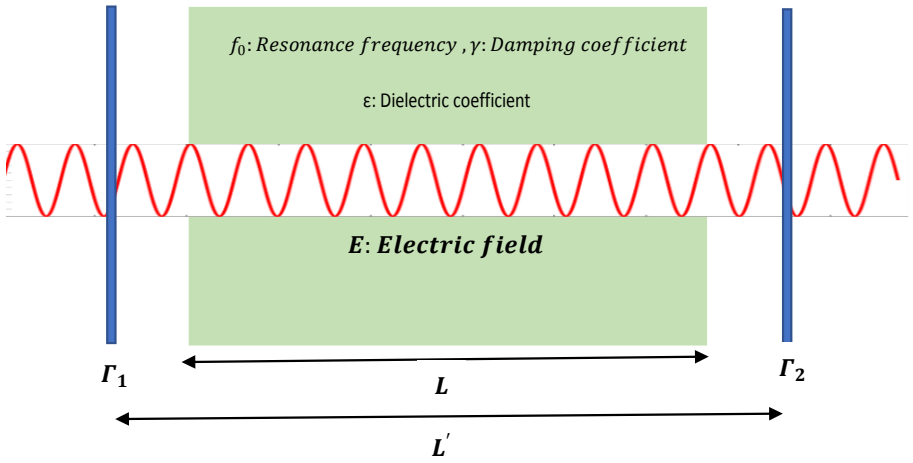

Figure 3.1 Configuration of an optical cavity

$$CAVITY\ QUALITY\ (Q)FACTOR = fT_{rt}\frac{2\pi}{\zeta} \qquad (60)$$

$$T_{rt}: Cavity\ round\ trip\ time \qquad f: Wave\ frequency$$

$$\zeta: Fractional\ power\ loss\ per\ round\ trip$$

The cavity round trip time is defined as

$$T_{rt} = \frac{2L'}{c} \qquad (61)$$

Where c is the speed of light. Therefore, the Q factor can be written as

$$CAVITY\ QUALITY\ (Q)FACTOR = \frac{4fL'\pi}{\zeta c} \qquad (62)$$

The accumulation of energy in a resonator is related to the amplitude of the intracavity electric field intensity and the resulting charge polarization in the interaction medium. It is feasible to store an enormous amount of energy in a resonator either by trapping a high amplitude wave pulse of long duration or by using a medium that has a high electric polarization density. In either case there must be an efficient trapping of the wave pulse in the cavity by using highly reflective cavity walls. Without highly reflective cavity walls, high energy cannot be stored.

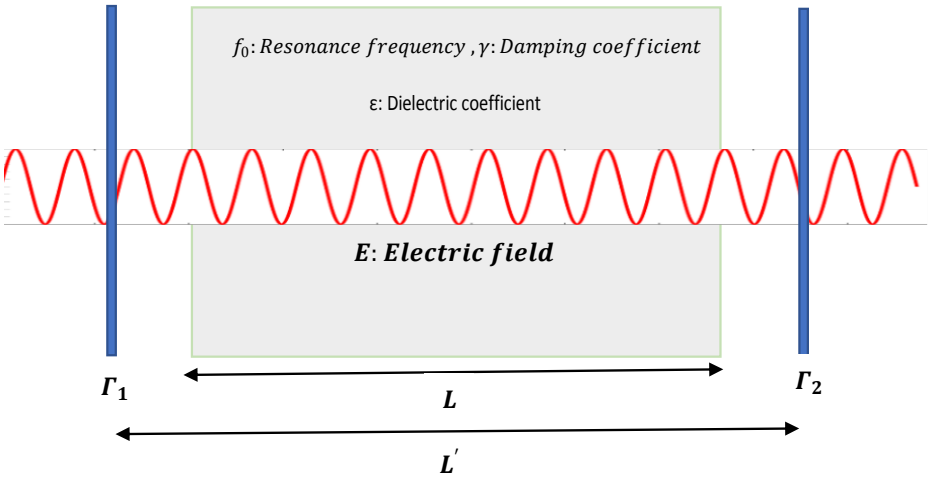

Figure 3.2 Configuration of an optical cavity

$$W_e = Stored\ energy\ density = \frac{1}{2}ED = \frac{1}{2}E(\varepsilon_0 E + P) = \frac{1}{2}\varepsilon_0 E^2 + \frac{1}{2}EP \qquad (63)$$

$$D: Electric\ flux\ density$$

$$P: Electric\ polarization\ density$$

$$E: Electric\ field\ intensity$$

For instance, high energy can be accumulated in a resonator with a highly polarizable interaction medium that has a resonance behavior displayed by its permittivity, which is expressed as

$$\varepsilon(\omega) = 1 + \chi + \frac{Ne^2}{m\varepsilon_0}\left[\frac{1}{\omega^2 - {\omega_0}^2 - i\gamma\omega}\right] \qquad (64)$$

Assume that $\omega\gamma \ll (\omega^2 - {\omega_0}^2)$, then we can write

$$\varepsilon(\omega) = 1 + \chi + \frac{Ne^2}{m\varepsilon_0}\left[\frac{1}{\omega^2 - {\omega_0}^2}\right] \qquad (65)$$

When the angular frequency ω of the monochromatic electromagnetic wave satisfies $\omega \approx \omega_0$ meaning that the wave frequency is around the polarization resonance of the interaction medium, then the intracavity electric energy density becomes quite large.

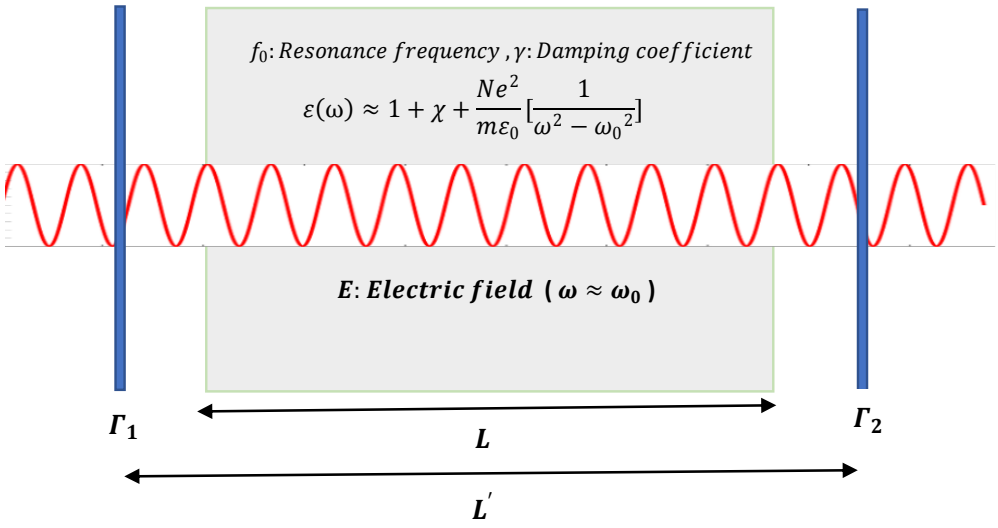

Figure 3.3 A cavity with maximized electric energy density due to polarization resonance.

If the damping coefficient (γ) is small, then the cavity would posess a very large electric energy as long as there is wave propagation inside. When γ is small and the cavity walls are highly reflective, wave propagation lasts for a long duration inside the cavity and electric energy can be stored for a longer time. But how can we make use of the high electric energy stored inside such a cavity? In order to transfer some of that huge energy, we need a coupling mechanism. Assume that we send another wave in the cavity whose frequency is not near the resonance frequency of the interaction medium, if this second wave does not have a nonlinearity inducing intensity, this second wave will not raise the intracavity energy significantly as it's frequency is different than the medium's resonance frequency. Moreover, although the accumulation of energy is high, the second wave cannot absorb any energy from the energized resonator as the intensities of the waves are not sufficiently high to induce any nonlinearity that is required for energy coupling.

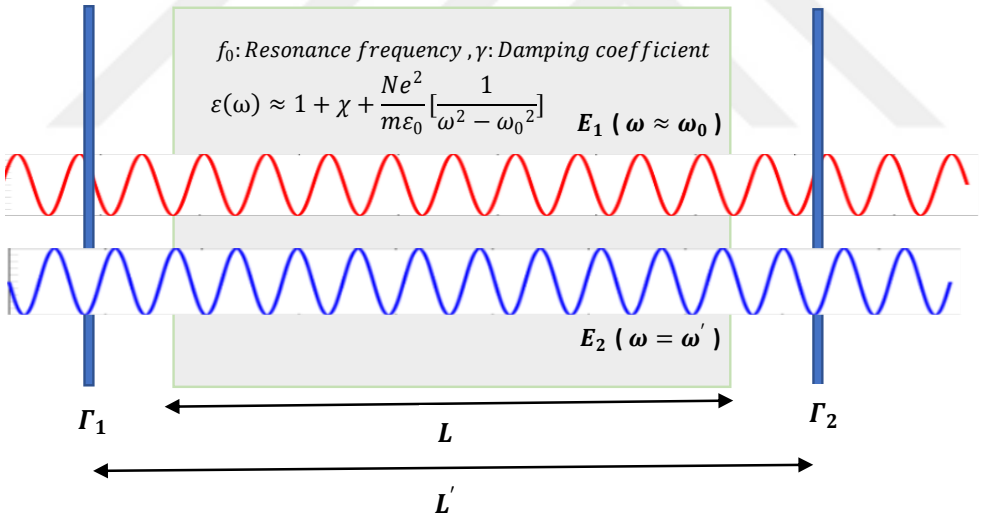

Figure 3.4 A cavity with maximized electric energy density and two propagating waves.

3.2. Wave analysis in dispersive cavities

The equation for wave analysis in a linear, isotropic, homogenous medium is stated as

$$\nabla^2 E - \mu_0 \varepsilon_0 \frac{\partial^2 E}{\partial t^2} = \mu_0 \sigma \frac{\partial E}{\partial t} + \mu_0 \varepsilon_0 \frac{\partial^2 P}{\partial t^2} \qquad (66)$$

When the medium is dispersive, the above equation can be rewritten as

$$\nabla^2 E - \mu_0 \varepsilon_0 \frac{\partial^2 E}{\partial t^2} = \mu_0 \sigma \frac{\partial E}{\partial t} + \mu_0 \varepsilon_0 \left(\frac{\partial^2 \left\{ \int_0^\infty \chi^{(1)}(\tau) E(t-\tau) d\tau \right\}}{\partial t^2} \right) \quad (67)$$

$$P = \varepsilon_0 \int_0^\infty \chi^{(1)}(\tau) E(t-\tau) d\tau \quad (68)$$

Where $\chi^{(1)}(t) = \chi_0 e^{-\gamma t} \sin(\omega_0 t)$ is the impulse polarization response of the dispersive medium. Obviously, the electric polarization in the medium lasts longer if the damping coefficient γ is lower. Eq.67 can be rewritten as

$$\nabla^2 E - \mu_0 \varepsilon_0 \frac{\partial^2 E}{\partial t^2} = \mu_0 \sigma \frac{\partial E}{\partial t} + \mu_0 \varepsilon_0 \left(\frac{\partial^2 \left\{ \int_0^\infty \chi_0 e^{-\gamma \tau} \sin(\omega_0 \tau) E(t-\tau) d\tau \right\}}{\partial t^2} \right) \quad (69)$$

Assume that we excite a high Q (low loss) cavity that houses a dispersive medium with a damping coefficient of $\gamma = 10^{10}$ Hz, by an ultrashort pulse of 300 femtosecond duration. In that case there will be wave propagation inside the cavity for a few ξ duration, where $\xi = \frac{1}{\gamma} = 10^{-10}\ s = 100\ ps$. The initially ultrashort pulse will expand in time to last around a few hundred picoseconds. In that sense γ and the choice of material is critical for energy storage inside a cavity.

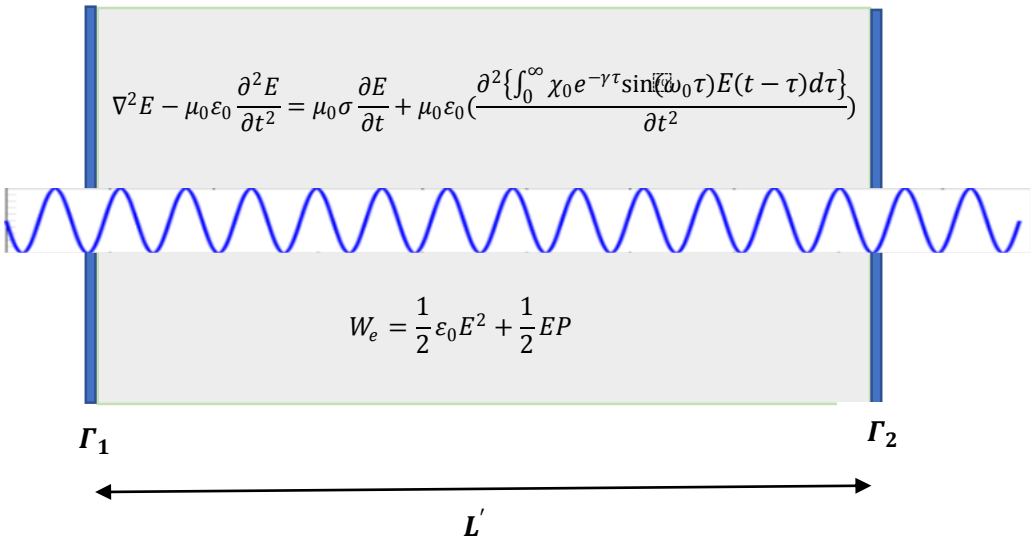

Figure 3.5 Dispersive medium placed in a cavity

3.3. Wave analysis in nonlinear dispersive cavities

The equation for wave analysis in a nonlinear, isotropic, homogenous, dispersive medium is expressed as

$$\nabla^2 E - \mu_0 \varepsilon_0 \frac{\partial^2 E}{\partial t^2} = \mu_0 \sigma \frac{\partial E}{\partial t} + \mu_0 \varepsilon_0 \frac{\partial^2 P}{\partial t^2} \quad (70)$$

Where

$$P(t) = P^{(1)}(t) + P^{(2)}(t) + P^{(3)}(t) \quad (71)$$

$$P^{(1)}(t) = \varepsilon_0 \int_0^\infty \chi^{(1)}(\tau_1) E(t-\tau_1) d\tau_1 \quad (72)$$

$$P^{(2)}(t) = \varepsilon_0 \int_0^\infty \int_0^\infty \chi^{(2)}(\tau_1, \tau_2) E(t-\tau_1) E(t-\tau_2) d\tau_1 d\tau_2 \quad (73)$$

$$P^{(3)}(t) = \varepsilon_0 \int_0^\infty \int_0^\infty \int_0^\infty \chi^{(3)}(\tau_1, \tau_2, \tau_3) E(t-\tau_1) E(t-\tau_2) E(t-\tau_3) d\tau_1 d\tau_2 d\tau_3 \quad (74)$$

The difficulty of analysis in such a media is the unavailability of the dispersion charactheristics of the terms $\chi^{(2)}$ and $\chi^{(3)}$. It is known that the nonlinear polarization impulse response is instantaneous (around 5 femtoseconds), however, the exact functions of $\chi^{(2)}$ and $\chi^{(3)}$ in time is unavailable for most materials.

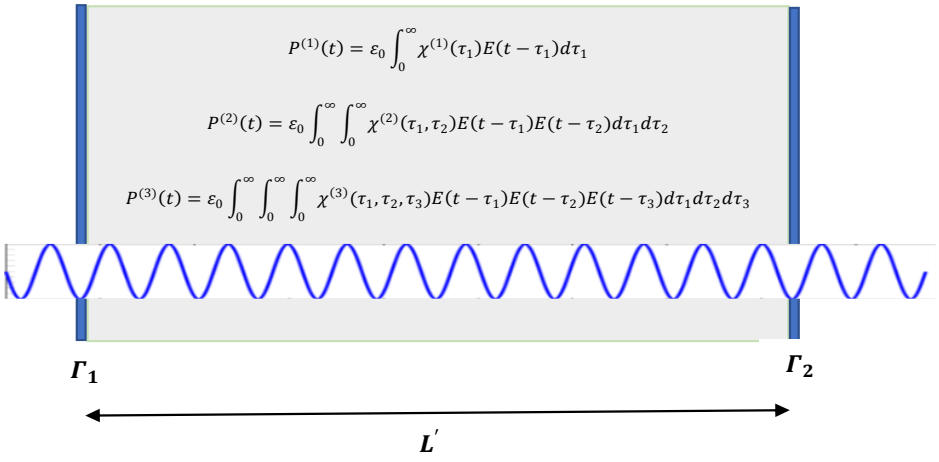

Figure 3.6 Nonlinear, dispersive interaction medium.

For a medium that is both dispersive and nonlinear, it is better to solve the wave equation in concurrence with the equation of nonlinear polarization density. Notice that these two equations are coupled to each other, the polarization density depends on the amplitude of the electric field and the electric field amplitude depends on the polarization density. Most resonator parameters have typical values (these parameters include the resonance frequency, the damping rate, and the atom density of the interaction medium), which allows the computational results to be more realistic. The set of equations to be solved for obtaining the variation of the electric field amplitude with respect to time in a nonlinear and a dispersive cavity is expressed as [1]

$$\nabla^2 E - \mu_0 \varepsilon_0 \frac{d^2 E}{dt^2} = \mu_0 \sigma \frac{dE}{\partial t} + \mu_0 \varepsilon_0 \frac{d^2 P}{dt^2} \quad (75)$$

$$\frac{d^2 P}{dt^2} + \gamma \frac{dP}{dt} + {\omega_0}^2 P - \frac{{\omega_0}^2}{Ned} P^2 + \frac{{\omega_0}^2}{N^2 e^2 d^2} P^3 = \frac{Ne^2}{m} E \quad (76)$$

$$Resonance\ frequency\ of\ the\ nonlinear\ medium:\ f_0 = 1 \times 10^{15}\ Hz$$

$$Damping\ rate\ of\ the\ nonlinear\ medium:\ \gamma = 1 \times 10^{10}\ Hz$$

$$Electron\ density\ of\ the\ nonlinear\ medium:\ N = 3.5 \times 10^{28}/m^3$$

$$Atomic\ or\ molecular\ diameter: d = 0.3\ nanometers$$

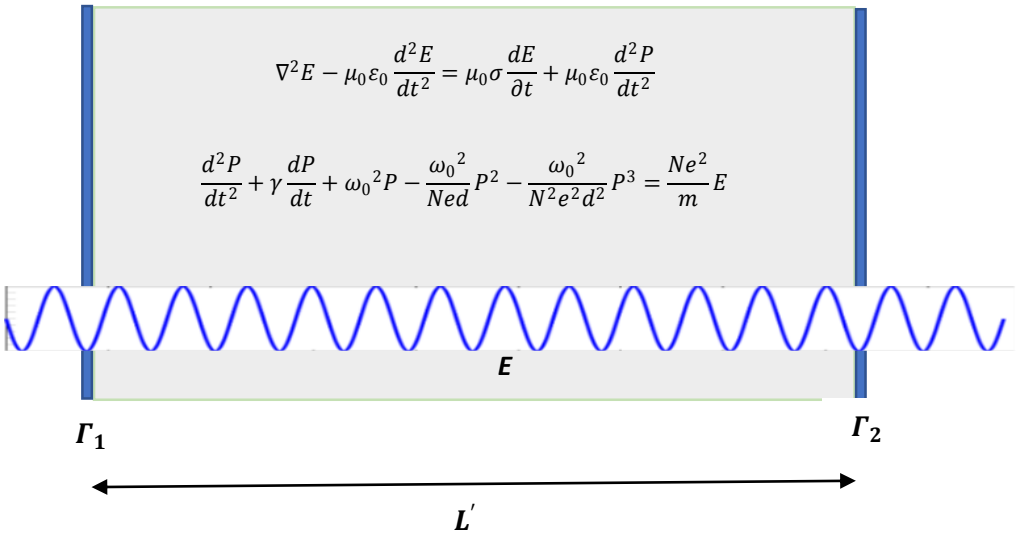

Figure 3.7 Nonlinear, dispersive medium placed in a cavity.

Now let us presume that two waves are simultaneously present in a nonlinear dispersive interaction medium and their electric fields are called E_1 and E_2, then the set of equations that model the total electric field amplitude in this medium is stated as

$$\nabla^2(E_1+E_2)-\mu_0\varepsilon_0\frac{d^2(E_1+E_2)}{dt^2}=\mu_0\sigma\frac{d(E_1+E_2)}{\partial t}+\mu_0\varepsilon_0\frac{d^2(P')}{dt^2} \quad (77)$$

$$\frac{d^2(P')}{dt^2}+\gamma\frac{d(P')}{dt}+{\omega_0}^2(P')-\frac{{\omega_0}^2}{Ned}(P')^2+\frac{{\omega_0}^2}{N^2e^2d^2}(P')^3=\frac{Ne^2}{m}(E_1+E_2) \quad (78)$$

Assume that we want to determine the time variation of the low amplitude field E_1 in the presence of the high amplitude field E_2, i.e. we want to obtain the time variation of E_1 while there is an electric energy transfer from E_2. In order to do that, we first write the pair of equations for E_2 assuming that E_1 is not present in the medium [30-32]

$$\nabla^2(E_2)-\mu_0\varepsilon_0\frac{d^2(E_2)}{dt^2}=\mu_0\sigma\frac{d(E_2)}{\partial t}+\mu_0\varepsilon_0\frac{d^2P}{dt^2} \quad (79)$$

$$\frac{d^2P}{dt^2}+\gamma\frac{dP}{dt}+{\omega_0}^2(P)-\frac{{\omega_0}^2}{Ned}(P)^2+\frac{{\omega_0}^2}{N^2e^2d^2}(P)^3=\frac{Ne^2}{m}(E_2) \quad (80)$$

Subtracting Eq 79 and 80 from Eq 77 and 78 respectively, we get

$$\nabla^2(E_1)-\mu_0\varepsilon_0\frac{d^2(E_1)}{dt^2}=\mu_0\sigma\frac{d(E_1)}{\partial t}+\mu_0\varepsilon_0\frac{d^2(P'-P)}{dt^2} \quad (81)$$

$$\frac{d^2(P'-P)}{dt^2}+\gamma\frac{d(P'-P)}{dt}+{\omega_0}^2(P'-P)-\frac{{\omega_0}^2}{Ned}\{(P')^2-(P)^2\}+\frac{{\omega_0}^2}{N^2e^2d^2}\{(P')^3-(P)^3\}=\frac{Ne^2}{m}(E_1) \quad (82)$$

If we call $P'=P_1+P_2$, and $P=P_2$, then we have

$$\nabla^2(E_1)-\mu_0\varepsilon_0\frac{d^2(E_1)}{dt^2}=\mu_0\sigma\frac{d(E_1)}{\partial t}+\mu_0\varepsilon_0\frac{d^2(P_1)}{dt^2} \quad (83)$$

$$\frac{d^2(P_1)}{dt^2}+\gamma\frac{d(P_1)}{dt}+{\omega_0}^2(P_1)-\frac{{\omega_0}^2}{Ned}\{{P_1}^2+2P_1P_2\}+\frac{{\omega_0}^2}{N^2e^2d^2}\{{P_1}^3+3{P_1}^2P_2+3P_1{P_2}^2\}=\frac{Ne^2}{m}(E_1) \quad (84)$$

Eq 83 and 84 represent the propagation of E_1 under the presence of E_2. As we can easily notice, in this nonlinear medium, E_2 acts as a source for E_1.

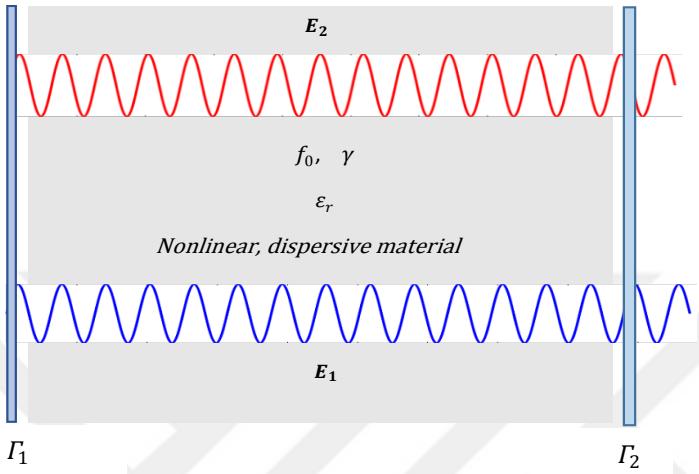

Figure 3.8 Simultaneous propagation of two waves in a resonator.

Similarly, E_1 acts as a source for E_2, going back to the wave equation for the total wave $E = E_1 + E_2$, we have

$$\nabla^2(E_1 + E_2) - \mu_0\varepsilon_0\frac{d^2(E_1 + E_2)}{dt^2} = \mu_0\sigma\frac{d(E_1 + E_2)}{\partial t} + \mu_0\varepsilon_0\frac{d^2(P_1 + P_2)}{dt^2} \quad (85)$$

$$\frac{d^2(P_1 + P_2)}{dt^2} + \gamma\frac{d(P_1 + P_2)}{dt} + {\omega_0}^2(P_1 + P_2) - \frac{{\omega_0}^2}{Ned}(P_1 + P_2)^2 + \frac{{\omega_0}^2}{N^2e^2d^2}(P_1 + P_2)^3 = \frac{Ne^2}{m}(E_1 + E_2) \quad (86)$$

Assume that we want to determine the propagation of E_2 in the presence of E_1, i.e. our goal is to obtain the time variation of E_2 while there is an electric energy transfer from E_1. In order to do that we write the pair of equations for E_1 assuming E_2 is not present in the medium

$$\nabla^2(E_1) - \mu_0\varepsilon_0\frac{d^2(E_1)}{dt^2} = \mu_0\sigma\frac{d(E_1)}{\partial t} + \mu_0\varepsilon_0\frac{d^2P_1}{dt^2} \quad (87)$$

$$\frac{d^2P_1}{dt^2} + \gamma\frac{dP_1}{dt} + {\omega_0}^2(P_1) - \frac{{\omega_0}^2}{Ned}(P_1)^2 + \frac{{\omega_0}^2}{N^2e^2d^2}(P_1)^3 = \frac{Ne^2}{m}(E_1) \quad (88)$$

Subtracting Eqs 87 and 88 from Eqs 85 and 86 respectively, we get the pair of equations that represents the propagation of E_2 under the presence of E_1:

$$\nabla^2(E_2) - \mu_0\varepsilon_0\frac{d^2(E_2)}{dt^2} = \mu_0\sigma\frac{d(E_2)}{\partial t} + \mu_0\varepsilon_0\frac{d^2P_2}{dt^2} \qquad (89)$$

$$\frac{d^2P_2}{dt^2} + \gamma\frac{dP_2}{dt} + {\omega_0}^2(P_2) - \frac{{\omega_0}^2}{Ned}\{{P_2}^2 + 2P_2P_1\} + \frac{{\omega_0}^2}{N^2e^2d^2}\{{P_2}^3 + 3{P_2}^2P_1 + 3P_2{P_1}^2\} = \frac{Ne^2}{m}(E_2) \qquad (90)$$

Ex: The low amplitude wave with an electric field $\boldsymbol{E_1}$ and the high amplitude wave with an electric field $\boldsymbol{E_2}$ are concurrently propagating in a simple Fabry-Perot type resonator. The low amplitude field $\boldsymbol{E_1}$ has an amplitude of 1 V/m and a frequency of 160 THz. The nonlinearity inducing high amplitude field $\boldsymbol{E_2}$ has an amplitude of 1.5×10^9 V/m and a frequency of 240 THz. $\boldsymbol{E_2}$ is an ultrashort pulse with a pulse width of 300 femtoseconds and $\boldsymbol{E_1}$ has a pulse width of 30 picoseconds. The parameters that are related to the medium are given in Figure 3.9.

$$\boldsymbol{E_1}(x = 2.5\,\mu m, t) = 1 \times \frac{\sin(2\pi(1.6 \times 10^{14})t)\ \ V}{m},\ \ for\ \ 0 \le t \le 30\ ps$$

$$\boldsymbol{E_2}(x = 2.5\,\mu m, t) = 1.5 \times 10^9 \times \frac{\sin(2\pi(2.4 \times 10^{14})t)\ \ V}{m},\ \ for\ \ 0 \le t \le 300\ fs$$

In such a case, $\boldsymbol{E_2}$ will act as a source for $\boldsymbol{E_1}$ because $\boldsymbol{E_2}$ is the wave that creates the nonlinearity in the medium and enables power coupling. Since the damping coefficient inside the medium is relatively low, $\boldsymbol{E_2}$ will yield a high amplitude wave propagation inside the cavity for at least a few hundred picoseconds.

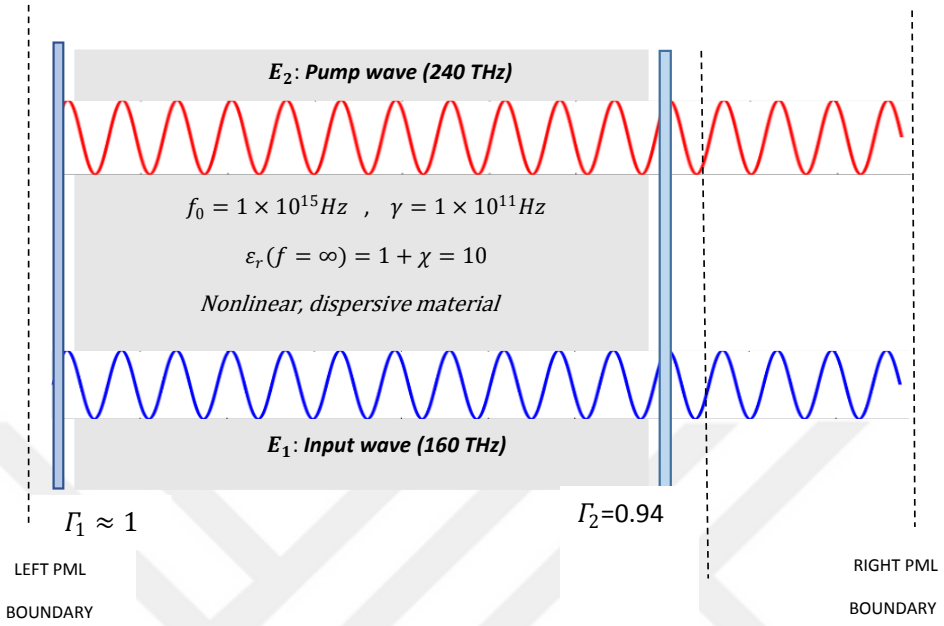

Figure 3.9 The cavity described in the example along with the given parameters.

Assume that we want to determine the time variation of $\boldsymbol{E_1}$ at any given point inside the cavity. There are four differential equations to be solved. The first two of them is to determine the amplitude of the pump wave and its associated polarization density at any given time instant at any point inside the cavity, and then substituting their values in the pair of differential equations for $\boldsymbol{E_1}$. These four equations are respectively as follows

$$\nabla^2(E_2) - \mu_0\varepsilon_0\frac{d^2(E_2)}{dt^2} = \mu_0\sigma\frac{d(E_2)}{\partial t} + \mu_0\varepsilon_0\frac{d^2P_2}{dt^2} \quad (91-94)$$

$$\frac{d^2P_2}{dt^2} + \gamma\frac{dP_2}{dt} + {\omega_0}^2(P_2) - \frac{{\omega_0}^2}{Ned}(P_2)^2 + \frac{{\omega_0}^2}{N^2e^2d^2}(P_2)^3 = \frac{Ne^2}{m}(E_2)$$

$$\nabla^2(E_1) - \mu_0\varepsilon_0\frac{d^2(E_1)}{dt^2} = \mu_0\sigma\frac{d(E_1)}{\partial t} + \mu_0\varepsilon_0\frac{d^2(P_1)}{dt^2}$$

$$\frac{d^2(P_1)}{dt^2} + \gamma\frac{d(P_1)}{dt} + {\omega_0}^2(P_1) - \frac{{\omega_0}^2}{Ned}\{{P_1}^2 + 2P_1P_2\} + \frac{{\omega_0}^2}{N^2e^2d^2}\{{P_1}^3 + 3{P_1}^2P_2 + 3P_1{P_2}^2\} = \frac{Ne^2}{m}(E_1)$$

The degree of nonlinearity depends on the amplitude of the pump wave $\boldsymbol{E_2}$. If the peak amplitude of $\boldsymbol{E_2}$ is very high, the resulting nonlinear coupling will be stronger. On the other hand, if the amplitude of $\boldsymbol{E_2}$ is not sufficiently high, nonlinear coupling of the two waves will be negligible. The pulse duration of the pump wave in this case is ultrashort but since the medium is highly dispersive, once the electrons in the medium are excited by a stimulus, they tend to keep on oscillating and this oscillation damps very slowly if the damping coefficient of the medium is low. This causes a much longer duration of high amplitude wave propagation inside the cavity and in turn a very high electric energy density stored for a much longer duration. This allows energy coupling from the cavity to the low amplitude input wave. Therefore, the high amplitude ultrashort pulse is used to create an accumulation of energy inside the low loss cavity. Similarly, we can use the other set of four equations to determine the time variation of $\boldsymbol{E_2}$ at any given point inside the cavity. As stated previously, these are

$$\nabla^2(E_1) - \mu_0\varepsilon_0\frac{d^2(E_1)}{dt^2} = \mu_0\sigma\frac{d(E_1)}{\partial t} + \mu_0\varepsilon_0\frac{d^2P_1}{dt^2}$$

$$\frac{d^2P_1}{dt^2} + \gamma\frac{dP_1}{dt} + {\omega_0}^2(P_1) - \frac{{\omega_0}^2}{Ned}(P_1)^2 + \frac{{\omega_0}^2}{N^2e^2d^2}(P_1)^3 = \frac{Ne^2}{m}(E_1)$$

$$\nabla^2(E_2) - \mu_0\varepsilon_0\frac{d^2(E_2)}{dt^2} = \mu_0\sigma\frac{d(E_2)}{\partial t} + \mu_0\varepsilon_0\frac{d^2P_2}{dt^2}$$

$$\frac{d^2P_2}{dt^2} + \gamma\frac{dP_2}{dt} + {\omega_0}^2(P_2) - \frac{{\omega_0}^2}{Ned}\{{P_2}^2 + 2P_2P_1\} + \frac{{\omega_0}^2}{N^2e^2d^2}\{{P_2}^3 + 3{P_2}^2P_1 + 3P_2{P_1}^2\} = \frac{Ne^2}{m}(E_2)$$

Though since $\boldsymbol{E_2}$ has a very high amplitude and $\boldsymbol{E_1}$ is low in amplitude, $\boldsymbol{E_1}$ will be a negligibly small source for $\boldsymbol{E_2}$. And the propagation of $\boldsymbol{E_2}$ will not be affected by the presence of $\boldsymbol{E_1}$ until $\boldsymbol{E_1}$ has been significantly amplified. Note that for now we do not know whether $\boldsymbol{E_1}$ will be amplified due to nonlinear coupling or not. As of yet the amplification of $\boldsymbol{E_1}$ is just an assumption. We will investigate the time variation of $\boldsymbol{E_1}$ at any given point in a specified cavity via finite difference time domain analysis.

3.4. Finite difference time domain analysis of nonlinear coupling in a resonator

Assume that E_2 is the electric field of the intense wave that induces the nonlinear coupling and E_1 is the electric field of the low intensity wave that absorbs energy from the resonator that is energized by E_2. First we write the set of equations that needs to be discretized in time and space

$$\nabla^2(E_2) - \mu_0\varepsilon_0\frac{d^2(E_2)}{dt^2} = \mu_0\sigma\frac{d(E_2)}{\partial t} + \mu_0\varepsilon_0\frac{d^2P_2}{dt^2} \qquad (95-98)$$

$$\frac{d^2P_2}{dt^2} + \gamma\frac{dP_2}{dt} + {\omega_0}^2(P_2) - \frac{{\omega_0}^2}{Ned}(P_2)^2 + \frac{{\omega_0}^2}{N^2e^2d^2}(P_2)^3 = \frac{Ne^2}{m}(E_2)$$

$$\nabla^2(E_1) - \mu_0\varepsilon_0\frac{d^2(E_1)}{dt^2} = \mu_0\sigma\frac{d(E_1)}{\partial t} + \mu_0\varepsilon_0\frac{d^2(P_1)}{dt^2}$$

$$\frac{d^2(P_1)}{dt^2} + \gamma\frac{d(P_1)}{dt} + {\omega_0}^2(P_1) - \frac{{\omega_0}^2}{Ned}\{{P_1}^2 + 2P_1P_2\} + \frac{{\omega_0}^2}{N^2e^2d^2}\{{P_1}^3 + 3{P_1}^2P_2 + 3P_1{P_2}^2\} = \frac{Ne^2}{m}(E_1)$$

Assume a single dimensional analysis (x direction) so that we can write

$$\nabla^2(E_2) = \frac{d^2(E_2)}{dx^2} \quad , \quad \nabla^2(E_1) = \frac{d^2(E_1)}{dx^2}$$

We discretize the set of four equations as follows; first let us discretize equations (95) and (96)

$$\frac{E_2(i+1,j) - 2E_2(i,j) + E_2(i-1,j)}{\Delta x^2} - \mu_0\varepsilon_0\frac{E_2(i,j+1) - 2E_2(i,j) + E_2(i,j-1)}{\Delta t^2} = \mu_0\sigma\frac{E_2(i,j) - E_2(i,j-1)}{\Delta t} + \mu_0\varepsilon_0\frac{P_2(i,j+1) - 2P_2(i,j) + P_2(i,j-1)}{\Delta t} \qquad (99)$$

$$\frac{P_2(i,j+1) - 2P_2(i,j) + P_2(i,j-1)}{\Delta t^2} + \gamma\frac{P_2(i,j) + P_2(i,j-1)}{\Delta t} + {\omega_0}^2\big(P_2(i,j)\big) - \frac{{\omega_0}^2}{Ned}\big(P_2(i,j)\big)^2 + \frac{{\omega_0}^2}{N^2e^2d^2}\big(P_2(i,j)\big)^3 = \frac{Ne^2}{m}\big(E_2(i,j)\big) \qquad (100)$$

Our aim is to solve for $E_2(i,j+1)$ i.e the amplitude of E_2 at a certain point at the adjacent time step. As E_2 and P_2 are coupled to each other, we initially solve for $P_2(i,j+1)$ and then insert its value into the equation for $E_2(i,j+1)$. We repeat this procedure for all instances and all coordinates in the solution domain of a given problem. For an accurate solution, one should select Δt and Δx as narrow as one can.

Similarly, we discretize equations (97) and (98) as

$$\frac{E_1(i+1,j)-2E_1(i,j)+E_1(i-1,j)}{\Delta x^2}-\mu_0\varepsilon_0\frac{E_1(i,j+1)-2E_1(i,j)+E_1(i,j-1)}{\Delta t^2} \quad (101)$$
$$=\mu_0\sigma\frac{E_1(i,j)-E_1(i,j-1)}{\Delta t}+\mu_0\varepsilon_0\frac{P_1(i,j+1)-2P_1(i,j)+P_1(i,j-1)}{\Delta t}$$

$$\frac{P_1(i,j+1)-2P_1(i,j)+P_1(i,j-1)}{\Delta t^2}+\gamma\frac{P_1(i,j)+P_1(i,j-1)}{\Delta t}+{\omega_0}^2\big(P_1(i,j)\big)$$
$$-\frac{{\omega_0}^2}{Ned}\Big\{\big(P_1(i,j)\big)^2+2P_1(i,j)P_2(i,j)\Big\}+\frac{{\omega_0}^2}{N^2e^2d^2}\{\big(P_1(i,j)\big)^3$$
$$+3\big(P_1(i,j)\big)^2P_2(i,j)+3P_1(i,j)\big(P_2(i,j)\big)^2\}=\frac{Ne^2}{m}(E_1(i,j)) \quad (102)$$

By solving these 4 equations, one can solve for the fields E_1 and E_2 at any given point in a single dimensional solution domain for a given instance.

The total wave in the medium is $E=E_1+E_2$, we can get the time variation of the total wave by solving the following equations

$$\nabla^2(E)-\mu_0\varepsilon_0\frac{d^2(E)}{dt^2}=\mu_0\sigma\frac{d(E)}{\partial t}+\mu_0\varepsilon_0\frac{d^2P}{dt^2} \quad (103)$$

$$\frac{d^2P}{dt^2}+\gamma\frac{dP}{dt}+{\omega_0}^2(P)-\frac{{\omega_0}^2}{Ned}(P)^2+\frac{{\omega_0}^2}{N^2e^2d^2}(P)^3=\frac{Ne^2}{m}(E) \quad (104)$$

These equations are discretized as

$$\frac{E(i+1,j)-2E(i,j)+E(i-1,j)}{\Delta x^2}-\mu_0\varepsilon_0\frac{E(i,j+1)-2E(i,j)+E(i,j-1)}{\Delta t^2} \quad (105)$$
$$=\mu_0\sigma\frac{E(i,j)-E(i,j-1)}{\Delta t}+\mu_0\varepsilon_0\frac{P(i,j+1)-2P(i,j)+P(i,j-1)}{\Delta t}$$

$$\frac{P(i,j+1)-2P(i,j)+P(i,j-1)}{\Delta t^2}+\gamma\frac{P(i,j)+P(i,j-1)}{\Delta t}+{\omega_0}^2\big(P(i,j)\big)$$
$$-\frac{{\omega_0}^2}{Ned}\big(P(i,j)\big)^2+\frac{{\omega_0}^2}{N^2e^2d^2}\big(P(i,j)\big)^3=\frac{Ne^2}{m}\big(E(i,j)\big) \quad (106)$$

Note that Δt and Δx must be chosen as small as possible. This drastically increases the computational cost; however, it is necessary as the problem is nonlinear. The stability condition $\Delta t<\Delta x/\mathrm{c}$ is not always valid in the nonlinear case, as a result Δt must be chosen to be much smaller than $\Delta x/c$.

3.5. Simulations of wave amplification via nonlinear coupling

Simulation 3.1:

The input wave $\boldsymbol{E_1}$ to be amplified and the intense pump wave $\boldsymbol{E_2}$ are simultaneously present in a simple Fabry-Perot type resonator. The reflectance of the left and right walls of the resonator are Γ_1 and Γ_2 respectively. Both waves are generated at x=2.5 μm inside the cavity at time t=0. The amplitude of the electric field ($\boldsymbol{E_1}$) of the input wave is 1 V/m and its frequency is 30 THz. The electric field ($\boldsymbol{E_2}$) of the pump wave has a large amplitude of 2×10^9 V/m and its frequency is 50 THz.

$$\boldsymbol{E_1}(x = 2.5\ \mu m, t) = 1 \times \sin(2\pi(3 \times 10^{13})t + \varphi_1)\ \ V/m$$

$$For\ simplicity, assume\ that\ \varphi_1 = 0$$

$$\boldsymbol{E_2}(x = 2.5\ \mu m, t) = 2 \times 10^9 \times \sin(2\pi(5 \times 10^{13})t + \varphi_2)\ \ V/m$$

$$For\ simplicity, assume\ that\ \varphi_2 = 0$$

$$Time\ interval\ and\ duration\ of\ simulation\colon\ 0 \le t \le 50\ ps$$

$$Spatial\ range\ of\ the\ simulation\ domain\colon\ 0 \le x \le 10\ \mu m$$

$$Resonance\ frequency\ of\ the\ nonlinear\ medium\colon\ f_0 = 8 \times 10^{14}\ Hz$$

$$Damping\ rate\ of\ the\ nonlinear\ medium\colon\ \gamma = 5 \times 10^{10}\ Hz$$

$$Dielectric\ constant\ of\ the\ nonlinear\ material\ (\varepsilon_r) = 10 \quad (\mu_r = 1)$$

$$Left\ perfectly\ matched\ layer\ is\ from\ x = 0\ to\ x = 2.25\ \mu m$$

$$Right\ perfectly\ matched\ layer\ is\ from\ x = 7.75\ \mu m\ to\ x = 10\ \mu m$$

$$Nonlinear\ dielectric\ material\ spatial\ range\colon 3.33\ \mu m < x < 6.66\ \mu m$$

$$Left\ cavity\ wall\ reflection\ coefficient\colon\ \Gamma_1 = 0.87\ for - \infty < \omega < \infty$$

$$Right\ cavity\ wall\ reflection\ coefficient\colon\ \Gamma_2 = 0.87\ \ for - \infty < \omega < \infty$$

$$Electron\ density\ of\ the\ nonlinear\ medium\colon\ N = 3.5 \times 10^{28}/m^3$$

$$Atomic\ or\ molecular\ diameter : d = 0.3\ nanometers$$

After the interaction with the pump wave inside the cavity, the input wave $\boldsymbol{E_1}$ is recorded over time at x=7.06 μm inside the cavity. Both waves' amplitude variations are plotted with respect to time in figures 3.10 and 3.11.

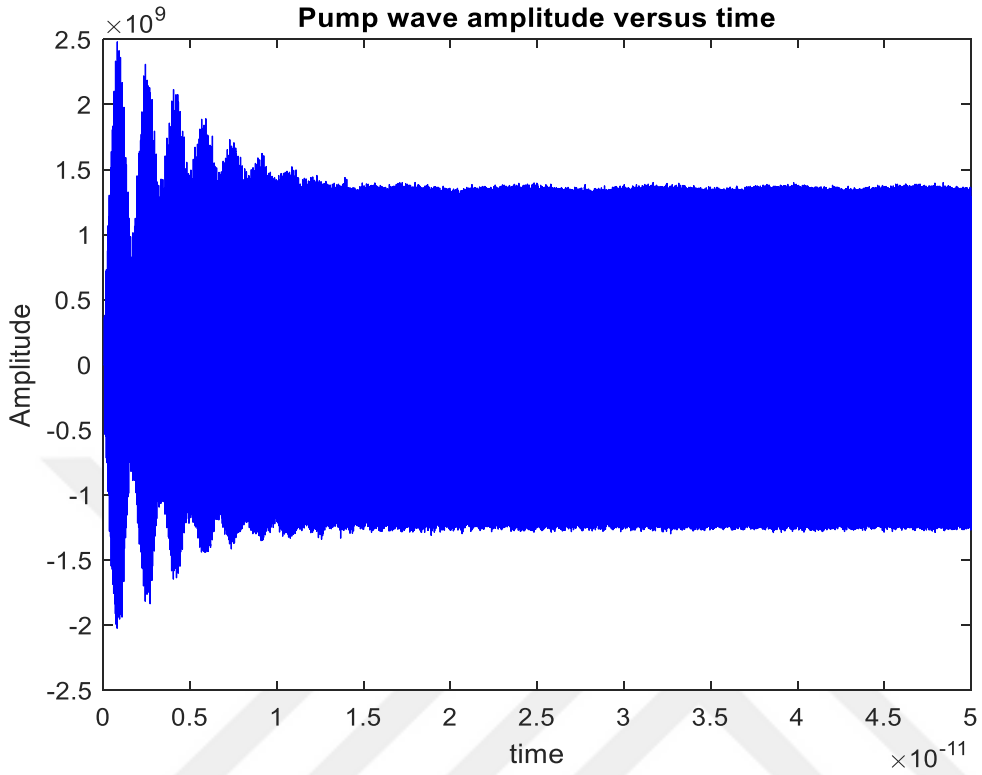

Figure 3.10 Pump wave amplitude versus time at x=7.06 µm (inside the cavity).

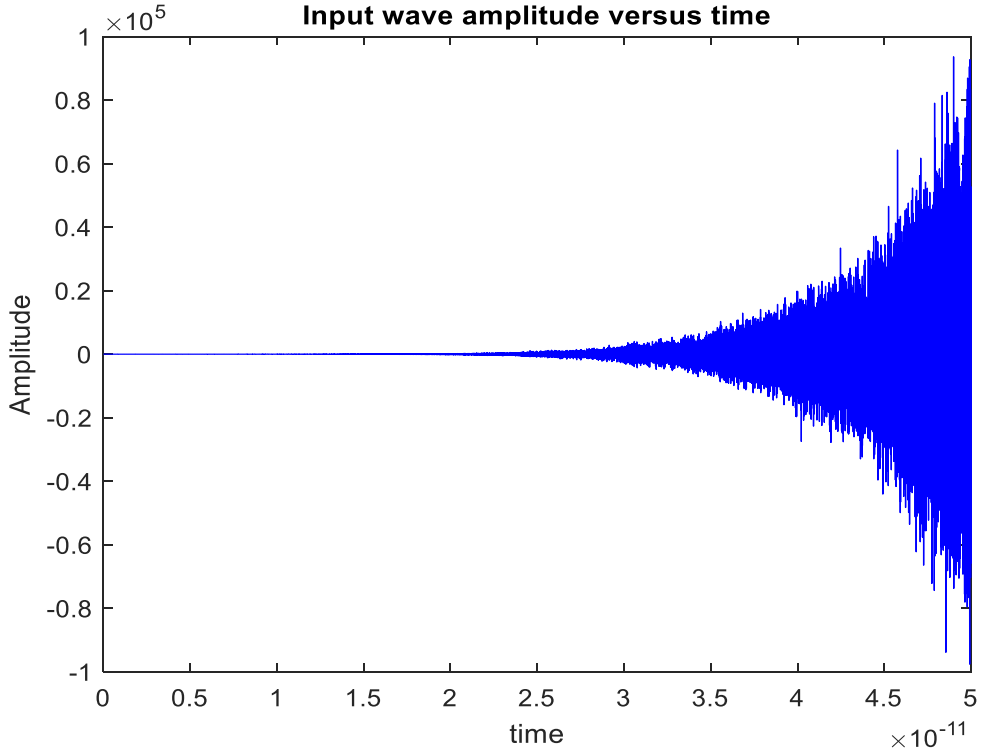

Figure 3.11 Input wave amplitude versus time at x=7.06 µm (inside the cavity).

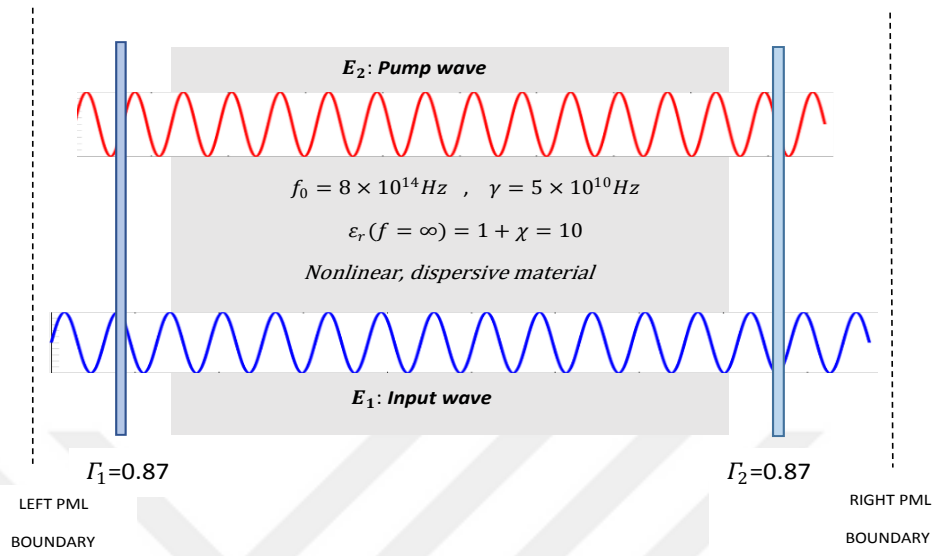

Figure 3.12 The cavity that is simulated in Simulation 3.1 along with the given parameters.

The input wave gets amplified, but over time it becomes highly polychromatic, having frequency components from the infra-red to the ultraviolet region of the spectrum. Since the initial input wave was monochromatic with a frequency of 30 THz, we want to see how much the 30 THz frequency component of the wave is amplified. Using a band-stop filter with a central frequency of 30 THz and a bandwidth of 0.5 THz, we get the 30 THz component of the polychromatic amplified wave. It is clear via Figure 3.13 that the 30 THz component of the input wave, which initially had a 1 V/m amplitude has been amplified by a factor of approximately κ=3000.

The amplification of the input wave depends on the value of the resonance frequency f_0, the value of the decay rate γ and the reflectance of the resonator walls. If the values of the reflection coefficients are high, the damping rate is low, and the resonance frequency is not too large, then the amplification of the input wave is usually more efficient. Though amplification also depends on other factors such as the length of the nonlinear material, the permittivity of the interaction medium, the length of the cavity, and the pulse duration of both waves. The existence of so many variables makes the determination of the required values of different parameters for efficient amplification extremely complex.

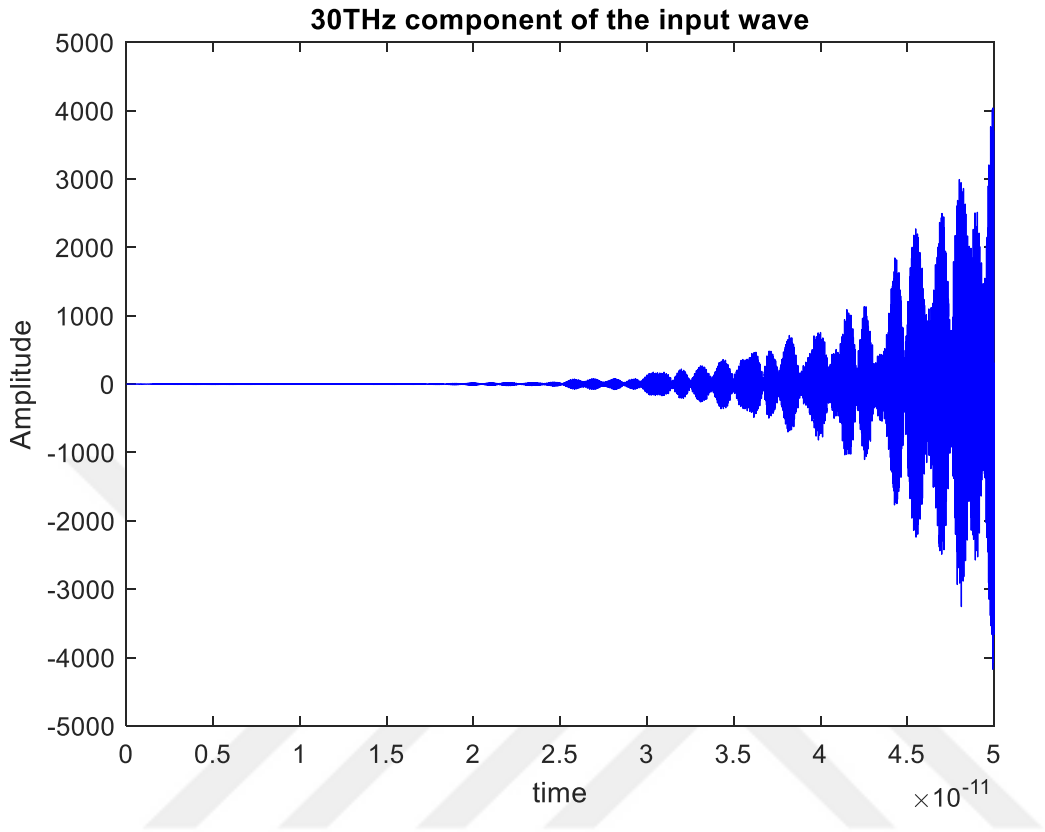

Figure 3.13 Amplification of the input wave at the frequency of 30 THz.

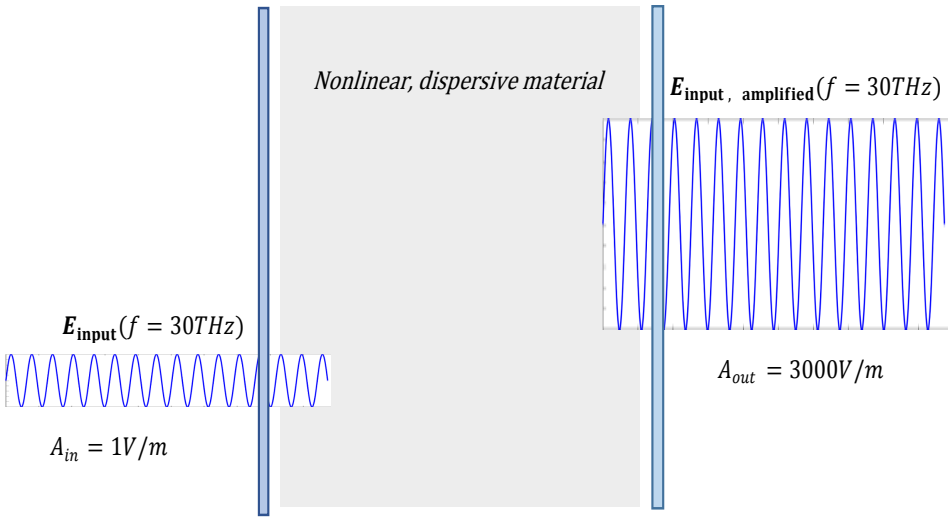

Figure 3.14 Monochromatic wave amplification at f=30 THz

CHAPTER 4

ENHANCEMENT OF NONLINEAR WAVE AMPLIFICATION EFFICIENCY IN MICRORESONATORS VIA PARAMETER TUNING

This chapter focuses on the performance enhancement of nonlinear wave amplification. Our aim is to examine the influence of the polarization damping coefficient (γ), and the dominant resonance frequency (f_0) on wave amplification via nonlinear coupling in an optical microcavity. The optimal range of values for the damping rate and the dominant resonance frequency will be determined for a high-gain amplification of the stimulus wave. An interaction medium with a large damping rate will attenuate the intensity of the pump wave, and thereby will cause a lower rate of stimulus wave amplification. Our aim is to identify a critical or a threshold value of the polarization damping coefficient, beyond which the gain factor of the amplified stimulus wave will drastically reduce to an insignificant level. If this could be shown, this would mean that the influence of the damping rate (or polarization damping coefficient) is much stronger when nonlinearity is involved. An identical threshold-value investigation will also be carried out for the dominant resonance frequency.

The effect of the polarization damping rate and the dominant resonance frequency can be disregarded for a single pass gain factor analysis (without the cavity walls). However, when an interaction medium is placed inside a cavity, electric energy is accumulated, and a much higher gain factor can be attained. This energy accumulation is strongly dependent on the values of the damping rate and the resonance frequency of the interaction medium. Assuming an interaction medium with a single (dominant) resonance, three example simulations based on arbitrary parameters will be investigated via finite difference time domain analysis and the obtained gain factor versus damping rate/resonance frequency functions are plotted and tabulated to illustrate the drastic gain sensitivity. Finally, the

effect of the reflectance of the cavity walls will be examined and incorporated in the performance enhancement analysis.

Simulation7: The input wave to be amplified and the high intensity pump wave are simultaneously present in a simple Fabry-Perot resonator. The reflectance of the left and right resonator wall is Γ_1 and Γ_2 respectively. The waves are originated at x=2.5 μm inside the resonator at time t=0. The amplitude of the input wave electric field ($\boldsymbol{E_1}$) is 1 V/m its frequency is 10 THz. The amplitude of the pump wave electric field ($\boldsymbol{E_2}$) is 1×10^9 V/m its frequency is 300 THz.

$$\boldsymbol{E_1}(x = 2.5\ \mu m, t) = 1 \times \frac{\sin(2\pi(1 \times 10^{13})t + \varphi_1)\ \ V}{m}\ ,\ \ for\ \ 0 \le t \le 50\ ps$$

$$\boldsymbol{E_2}(x = 2.5\ \mu m, t) = 1 \times 10^9 \times \frac{\sin(2\pi(3 \times 10^{14})t + \varphi_2)\ \ V}{m},\ \ for\ \ 0 \le t \le 500\ fs$$

$$Time\ interval\ and\ duration\ of\ simulation\colon\ 0 \le t \le 50\ ps$$

$$Spatial\ range\ of\ the\ simulation\ domain\colon\ 0 \le x \le 10\ \mu m$$

$$Resonance\ frequency\ of\ the\ gain\ medium\colon\ f_0 = 600\ THz$$

$$Polarization\ decay\ rate\ of\ the\ gain\ medium\colon\ \gamma = 5 \times 10^7\ Hz$$

$$Dielectric\ constant\ of\ the\ gain\ medium\ \ (\varepsilon_\infty) = 12 \quad (\mu_\infty = 1)$$

$$Left\ perfectly\ matched\ layer\ (pml) is\ from\ x = 0\ to\ x = 2.40\ \mu m$$

$$Right\ perfectly\ matched\ layer\ (pml) is\ from\ x = 7.6\ \mu m\ to\ x = 10\ \mu m$$

$$Gain\ medium\ spatial\ range\colon 3.33\ \mu m < x < 6.66\ \mu m$$

$$Left\ cavity\ wall\ reflection\ coefficient\colon\ \Gamma_1 = 0.96$$

$$Right\ cavity\ wall\ reflection\ coefficient\colon\ \Gamma_2 = 0.96$$

$$Left\ cavity\ wall\ location\colon\ x = 2.53\ \mu m;\ Right\ cavity\ wall\ location\colon\ x = 7.3\ \mu m$$

$$Electron\ density\ of\ the\ gain\ medium\colon\ N = 3.5 \times 10^{28}/m^3$$

$$Atomic\ diameter : d = 0.3\ nanometers$$

The electric field of the input wave ($\boldsymbol{E_1}$) is computed for all instances at x=5.73 μm in the micro-resonator. Since the pump wave is very intense, there is a nonlinear coupling of the pump wave and the input wave. The pump wave energizes the cavity via accumulation of the polarization density, and this enables high-gain nonlinear wave amplification.

The time variation of the amplitude of the input wave with respect to the damping coefficient (γ) is illustrated in Figures (4.2-4.5). These figures show that the gain factor sharply decreases beyond the threshold value of the damping coefficient due to insufficient stored energy. Good dielectric media usually has a lower damping coefficient and therefore can be preferred for wave amplification via nonlinear mixing.

As previously pointed out, the time variation of the electric fields (E_1 and E_2) can be obtained by solving the following set of equations.

$$\nabla^2(E_2) - \mu_0\varepsilon_0\frac{d^2(E_2)}{dt^2} = \mu_0\sigma\frac{d(E_2)}{\partial t} + \mu_0\varepsilon_0\frac{d^2P_2}{dt^2}$$

$$\frac{d^2P_2}{dt^2} + \gamma\frac{dP_2}{dt} + {\omega_0}^2(P_2) - \frac{{\omega_0}^2}{Ned}(P_2)^2 + \frac{{\omega_0}^2}{N^2e^2d^2}(P_2)^3 = \frac{Ne^2}{m}(E_2)$$

$$\nabla^2(E_1) - \mu_0\varepsilon_0\frac{d^2(E_1)}{dt^2} = \mu_0\sigma\frac{d(E_1)}{\partial t} + \mu_0\varepsilon_0\frac{d^2(P_1)}{dt^2}$$

$$\frac{d^2(P_1)}{dt^2} + \gamma\frac{d(P_1)}{dt} + {\omega_0}^2(P_1) - \frac{{\omega_0}^2}{Ned}\{{P_1}^2 + 2P_1P_2\} + \frac{{\omega_0}^2}{N^2e^2d^2}\{{P_1}^3 + 3{P_1}^2P_2 + 3P_1{P_2}^2\} = \frac{Ne^2}{m}(E_1)$$

The initial, excitation, and boundary conditions are

$P_1(x,0) = {P_1}'(x,0) = 0,\ P_2(x,0) = {P_2}'(x,0) = 0,\ E_1(x,0) = {E_1}'(x,0) = 0,$
$E_2(x,0) = {E_2}'(x,0) = 0$

$E_1(x = 0\ \mu m, t) = E_1(x = 10\ \mu m, t) = E_2(x = 0\ \mu m, t) = E_2(x = 10\ \mu m, t) = 0\ V/m$

$$E_1(x = 2.5\ \mu m, t) = 1 \times \frac{\sin(2\pi(1 \times 10^{13})t)\ \ V}{m}$$

$$E_2(x = 2.5\ \mu m, t) = 1 \times 10^9 \times \sin(2\pi(3 \times 10^{14})t)\ \ V/m$$

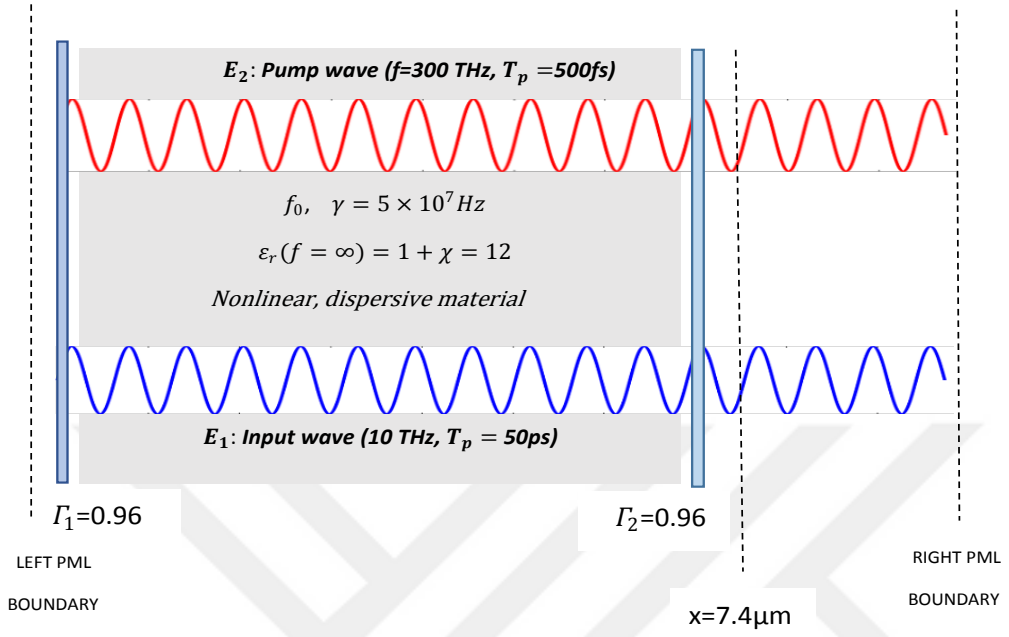

Figure 4.1 The configuration of the resonator given in Simulation 7.

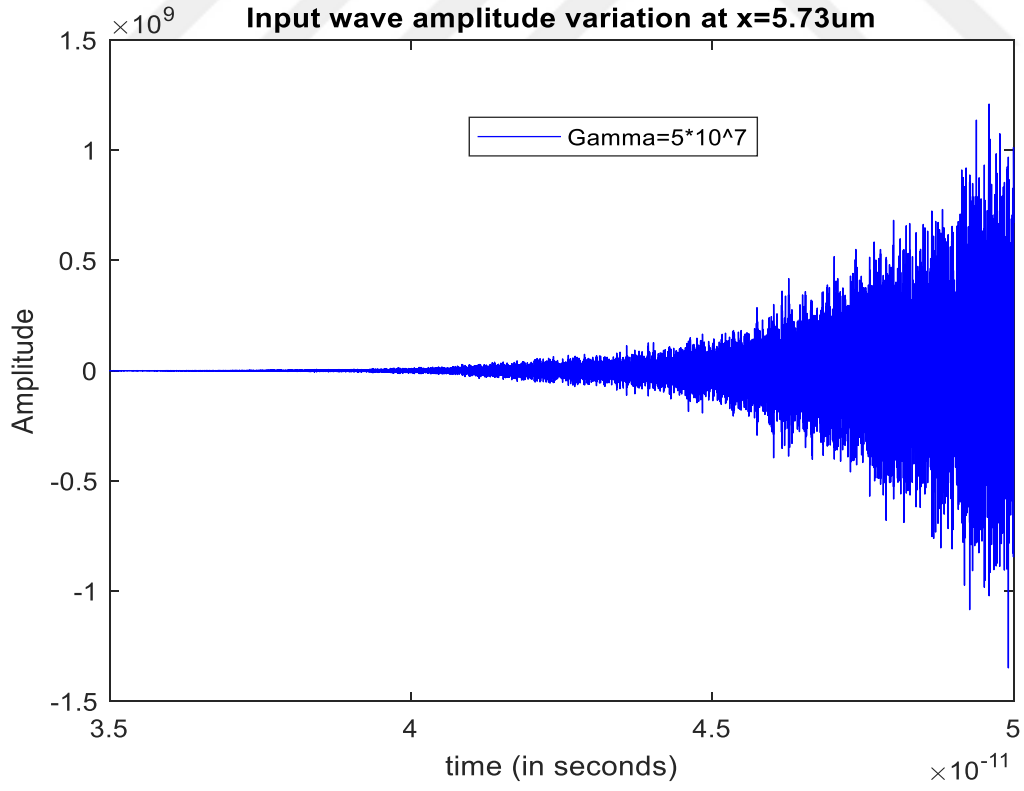

Figure 4.2 Amplitude variation of the input wave (E_1) as computed in the resonator at x=5.73 µm with respect to time for an original pump wave amplitude of $1 \times 10^9\ V/m$ for $f_0 = 6 \times 10^{14}\ Hz$ and for $\gamma = 5 \times 10^7\ Hz$.

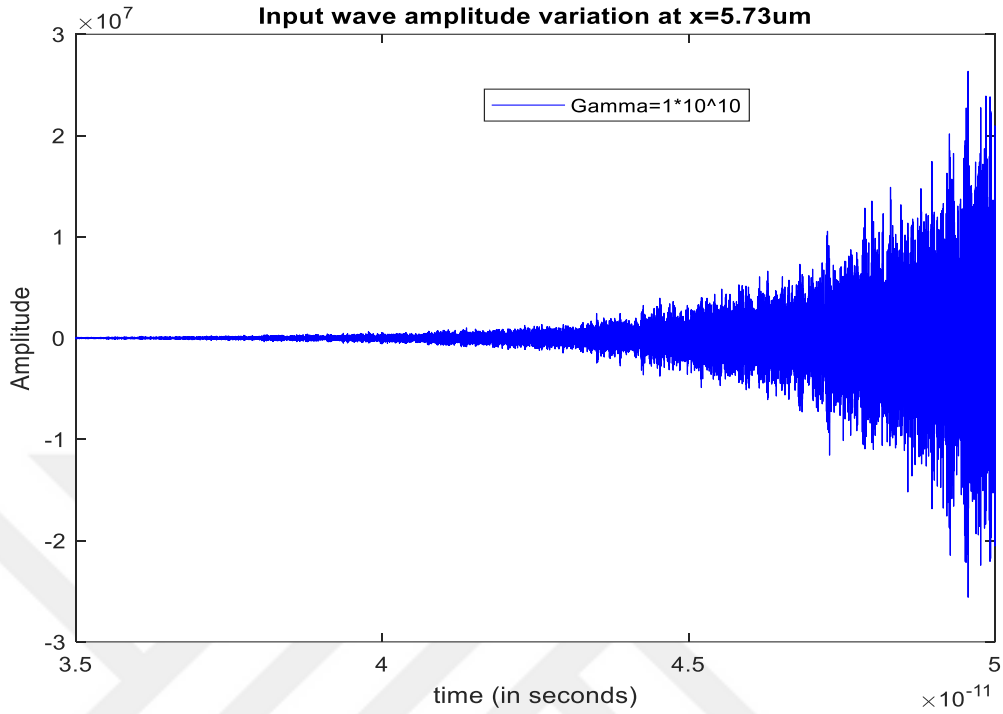

Figure 4.3 Amplitude variation of the input wave (E_1) as computed in the resonator at x=5.73 μm with respect to time for an original pump wave amplitude of $1 \times 10^9\ V/m$ for $f_0 = 6 \times 10^{14}\ Hz$ and for γ=$1 \times 10^{10}\ Hz$.

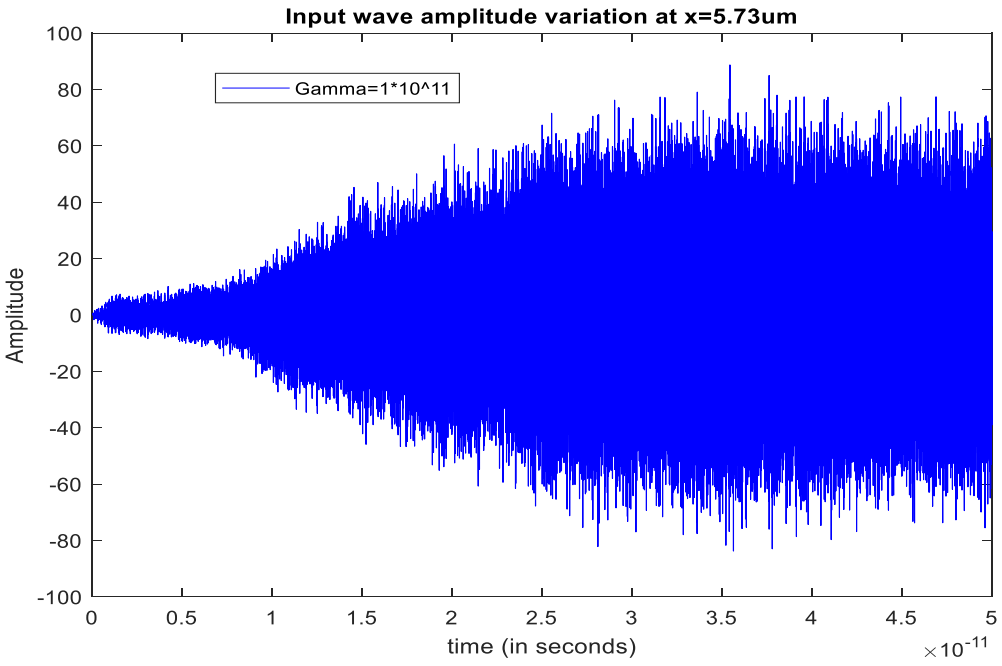

Figure 4.4 Amplitude variation of the input wave (E_1) as computed in the resonator at x=5.73 μm with respect to time for an original pump wave amplitude of $1 \times 10^9\ V/m$ for $f_0 = 6 \times 10^{14}\ Hz$ and for γ=$1 \times 10^{11}\ Hz$.

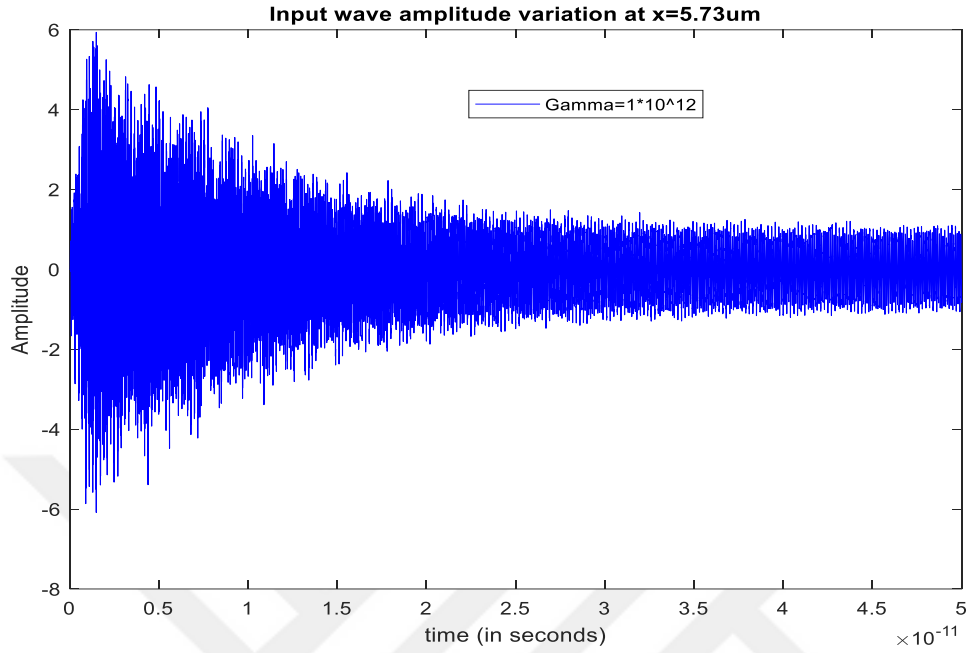

Figure 4.5 Amplitude variation of the input wave (E_1) as computed in the resonator at x=5.73 µm with respect to time for an original pump wave amplitude of $1 \times 10^9\, V/m$ for $f_0 = 6 \times 10^{14}\, Hz$ and for γ=$1 \times 10^{12}\, Hz$.

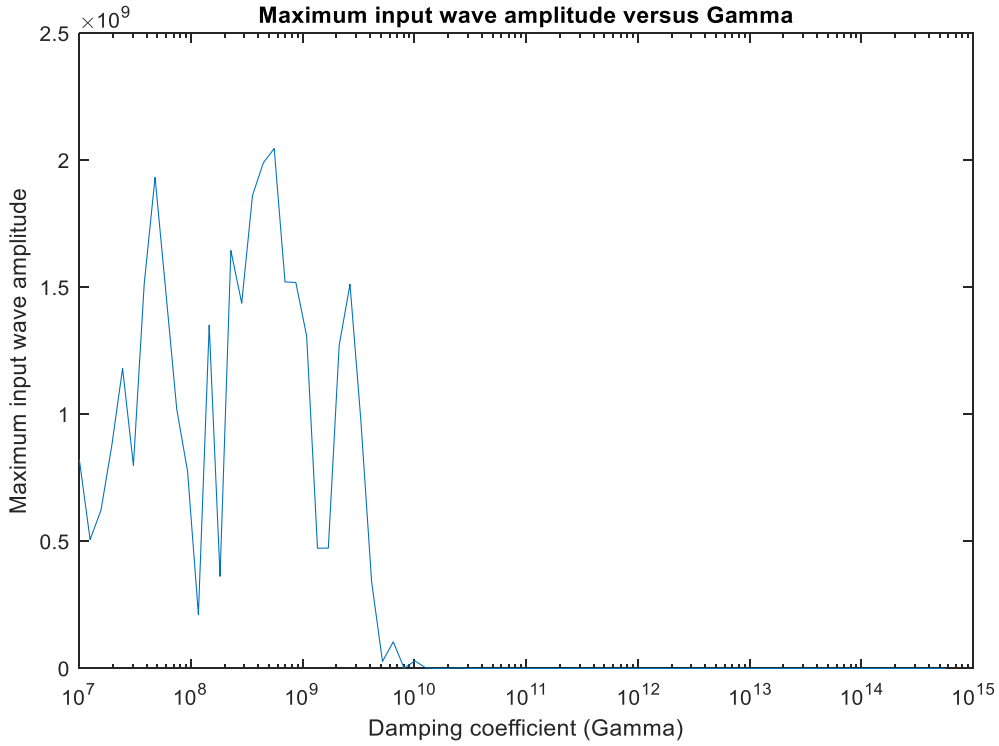

Figure 4.6 Maximum amplitude of the input wave (gain factor) computed at x=5.73 µm versus the damping rate of the interaction medium (gamma (γ)).

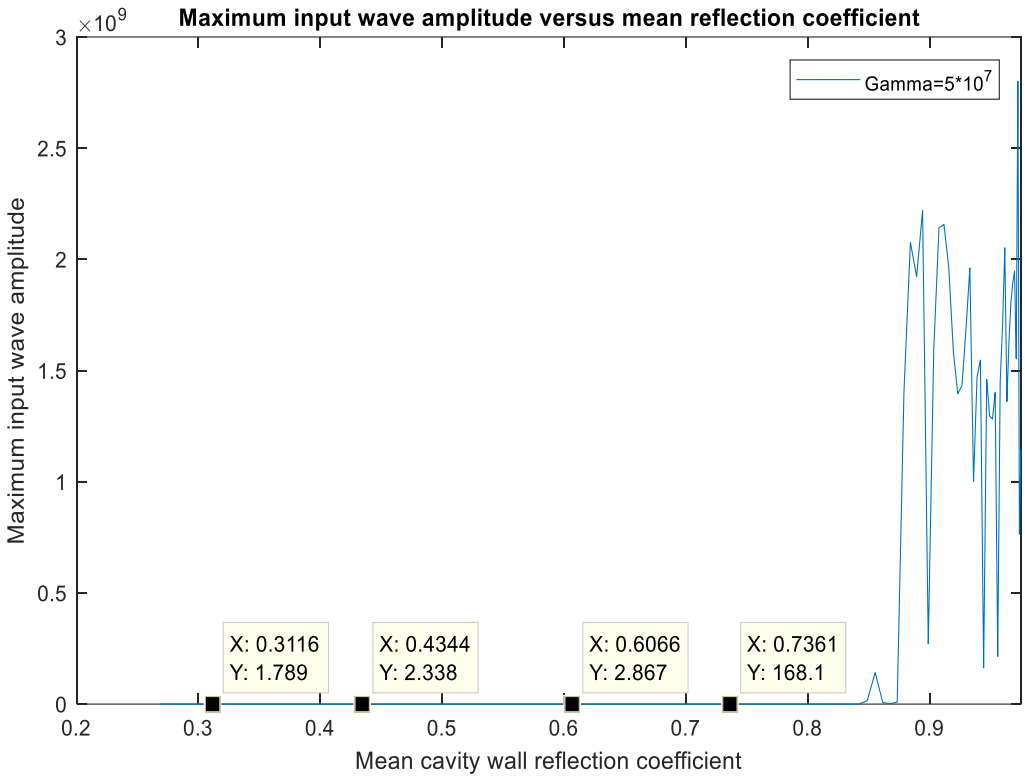

Figure 4.7 Maximum amplitude of the input wave (gain factor) computed at x=5.73 μm with respect to the mean cavity wall reflectance for an original pump wave amplitude of $1 \times 10^9\, V/m$ for $f_0 = 6 \times 10^{14}\, Hz$ and for $\gamma = 5 \times 10^7\, Hz$.

Figures 4.6 and 4.7 indicate that an interaction material with a low damping coefficient and cavity walls with high reflectance may strongly enhance the gain factor of the input wave as more electric energy can be stored. Notice that both parameters have critical/threshold values for gain factor enhancement.

Figures 4.6 and 4.7 are illustrated for a dominant resonance frequency of $f_0 = 6 \times 10^{14}\, Hz$. If we use an interaction medium with a higher resonance frequency, the threshold pump wave amplitude that is necessary for an enhanced input wave amplification gets higher and the resulting gain is lower. This is tabulated in Table 4.1.

The gain factor of the input wave is also dependent on the permittivity of the interaction medium. A resonator medium with a lower permittivity can store less energy and yields a lower gain factor. This is tabulated in Table 4.2.

As a result, the gain factor of a non-linear electromagnetic wave amplification process can be strongly increased by doing the followings

1) Using a resonator medium with a lower dominant resonance frequency.
2) Using a resonator medium with a low polarization damping rate.
3) Choosing cavity walls with high reflectance.
4) Using a resonator medium with a high permittivity.

$$f_0: Resonance\ frequency\ of\ the\ interaction\ medium$$

$$\gamma: Damping\ \ coefficient\ of\ the\ interaction\ medium$$

$$\varepsilon_\infty: Dielectric\ constant\ of\ the\ interaction\ medium$$

$$Gain_{max}: Maximum\ gain\ that\ has\ been\ achieved\ in\ the\ cavity\ for\ 0 < t < 30ps$$

$$E_{hp,min}: Minimum\ pump\ wave\ amplitude\ required\ to\ produce\ a\ gain\ factor\ that\ is\ greater\ than\ 10^7.$$

Table 4.1: Maximum attainable gain $Gain_{max}$ versus resonance frequency f_0.

f_0	$\gamma(THz)$	ε_∞	$Gain_{max}$	$E_{hp,min}$ (V/m)
400THz	5×10^7	12	1.6×10^9	1.3×10^8
500THz	5×10^7	12	1.4×10^9	1.5×10^8
600THz	5×10^7	12	1.3×10^9	1.8×10^8
700THz	5×10^7	12	1.1×10^9	2×10^8
800THz	5×10^7	12	9×10^8	2.3×10^8
900THz	5×10^7	12	8×10^8	2.7×10^8
1000THz	5×10^7	12	6×10^8	3.3×10^8
1100THz	5×10^7	12	4×10^8	3.9×10^8
1200THz	5×10^7	12	2×10^8	4.6×10^8
1300THz	5×10^7	12	1×10^8	5.4×10^8
1400THz	5×10^7	12	8×10^7	6.3×10^8
1500THz	5×10^7	12	7×10^7	7.3×10^8
1600THz	5×10^7	12	5×10^7	8.5×10^8
1700THz	5×10^7	12	4×10^7	9.9×10^8

Table 4.2: Maximum attainable gain $Gain_{max}$ versus material permittivity.

f_0	$\gamma(THz)$	ε_∞	$Gain_{max}$
600THz	5×10^7	2	59.48
600THz	5×10^7	4	3134
600THz	5×10^7	6	82450
600THz	5×10^7	8	1.67×10^6
600THz	5×10^7	10	3.06×10^7
600THz	5×10^7	12	1.4×10^9
600THz	5×10^7	14	1.3×10^9
600THz	5×10^7	16	1.5×10^9
600THz	5×10^7	18	1.2×10^9
600THz	5×10^7	20	1.4×10^9

Simulation8: The input wave ($\boldsymbol{E_1}$) and the pump wave ($\boldsymbol{E_2}$) are simultaneously present in a simple Fabry-Perot resonator. The left resonator wall has a reflectance of Γ_1 and the right one has a reflectance of Γ_2. The waves are originated at x=2.5 μm in the resonator at time t=0 s. The amplitude of the electric field of the input wave ($\boldsymbol{E_1}$) is 1 V/m and its frequency is 300 THz. The amplitude of the electric field of the pump wave ($\boldsymbol{E_2}$) is 2.75×10^8 V/m and its frequency is 200 THz.

$$\boldsymbol{E_1}(x = 2.5\ \mu m, t) = 1 \times \frac{\sin(2\pi(3 \times 10^{14})t + \varphi_1)\ \ V}{m}\ ,\ \ for\ \ 0 \le t \le 50\ ps$$

$$For\ simplicity, assume\ that\ \varphi_1 = 0$$

$$\boldsymbol{E_2}(x = 2.5\ \mu m, t) = 2.75 \times 10^8 \times \frac{\sin(2\pi(2 \times 10^{14})t + \varphi_2)\ \ V}{m},\ \ \ 0 \le t \le 300\ fs$$

$$For\ simplicity, assume\ that\ \varphi_2 = 0$$

$$Time\ interval\ and\ duration\ of\ simulation\colon\ 0 \le t \le 50\ ps$$

$$Spatial\ range\ of\ the\ simulation\ domain\colon\ 0 \le x \le 10\ \mu m$$

$$Resonance\ frequency\ of\ the\ gain\ medium\colon\ f_0 = 400\ THz$$

$$Damping\ coefficient\ of\ the\ gain\ medium\colon\ \gamma = 5 \times 10^9\ Hz$$

$$Dielectric\ constant\ of\ the\ gain\ medium\ (\varepsilon_\infty) = 10 \quad (\mu_\infty = 1)$$

$$Left\ perfectly\ matched\ layer\ is\ from\ x = 0\ to\ x = 2.40\ \mu m$$

$$Right\ perfectly\ matched\ layer\ is\ from\ x = 7.6\ \mu m\ to\ x = 10\ \mu m$$

$$Gain\ medium\ spatial\ range: 3\ \mu m < x < 7\ \mu m$$

$$Left\ cavity\ wall\ reflection\ coefficient:\ \Gamma_1 = 0.96$$

$$Right\ cavity\ wall\ reflection\ coefficient:\ \Gamma_2 = 0.94$$

$$Right\ cavity\ wall\ location:\ x = 7.3\ \mu m$$

$$Left\ cavity\ wall\ location:\ x = 2.53\ \mu m$$

$$Electron\ density\ of\ the\ gain\ medium:\ N = 3.5 \times 10^{28}/m^3$$

$$Atomic\ diameter: d = 0.3\ nanometers$$

While interacting with the high intensity (pump) wave, the electric field of the input wave ($\boldsymbol{E_1}$) is computed for every instance at x=5.73 μm in the micro-resonator. The time variation of the input wave electric field amplitude is illustrated in Figure4.9 with respect to time (t) and decay rate (γ). It is clear from Figures 4.9 and 4.10 that the gain factor decreases as the polarization decay rate is increased. These results indicate that the damping coefficient (polarization decay rate (γ)) is an important parameter to take into account in the amplification of the low intensity input (stimulus) wave. Since an interaction medium with a low polarization decay rate enables the charge polarization density in the micro-resonator to accumulate for a longer duration, the stored energy in the resonator increases. A high stored electric energy allows the pump wave to maintain its high intensity for a longer time in the resonator and this yields to a high gain factor.

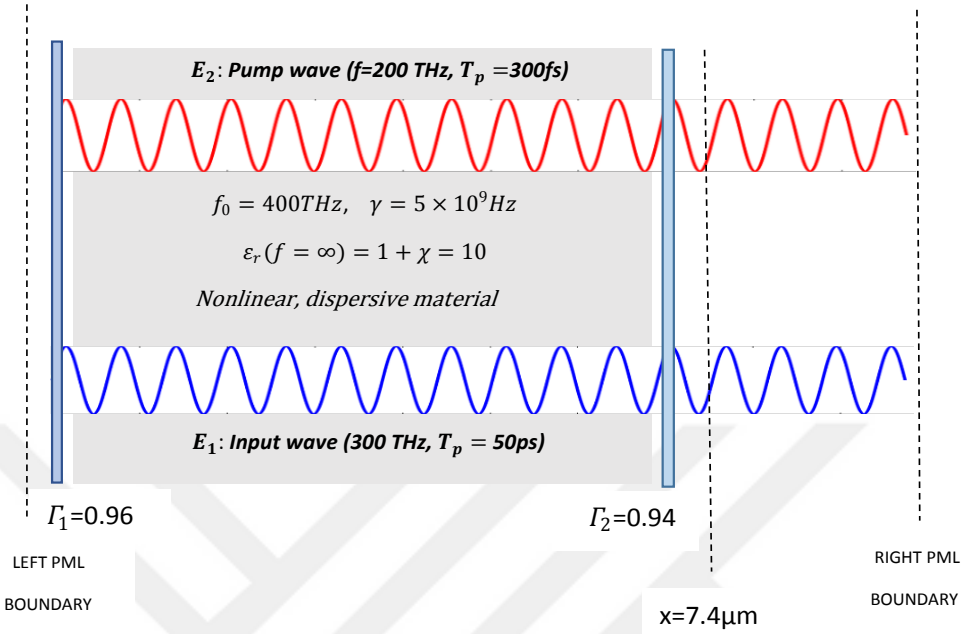

Figure 4.8 The configuration of the resonator given in Simulation 8.

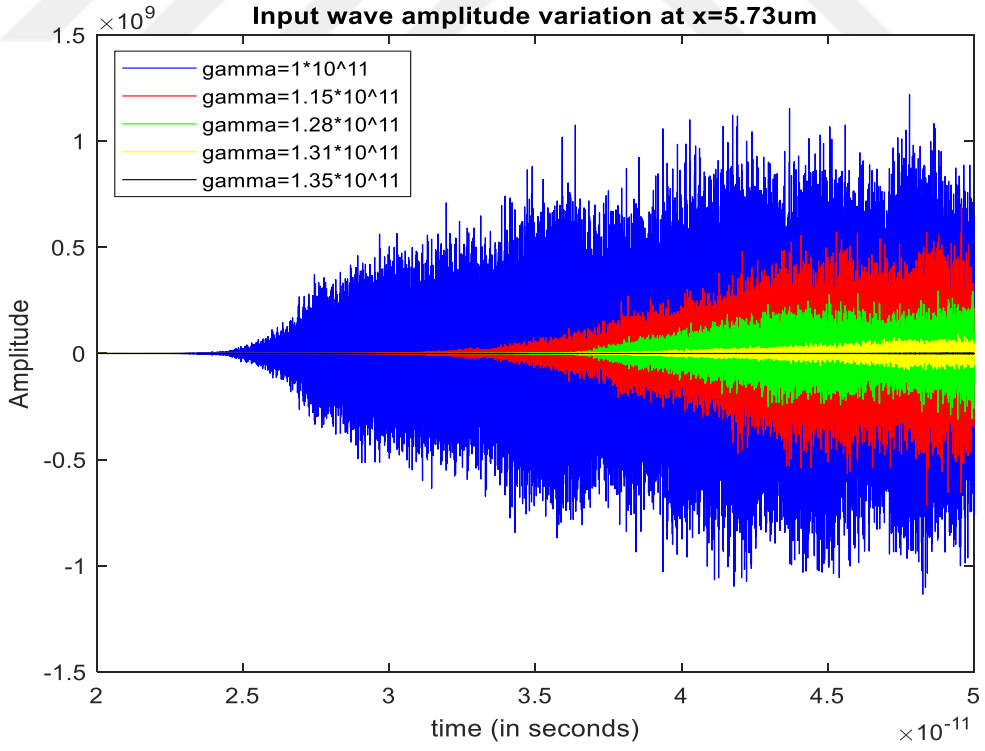

Figure 4.9 Amplitude of the input wave (V/m) at x=5.73 μm vs the decay rate (γ).

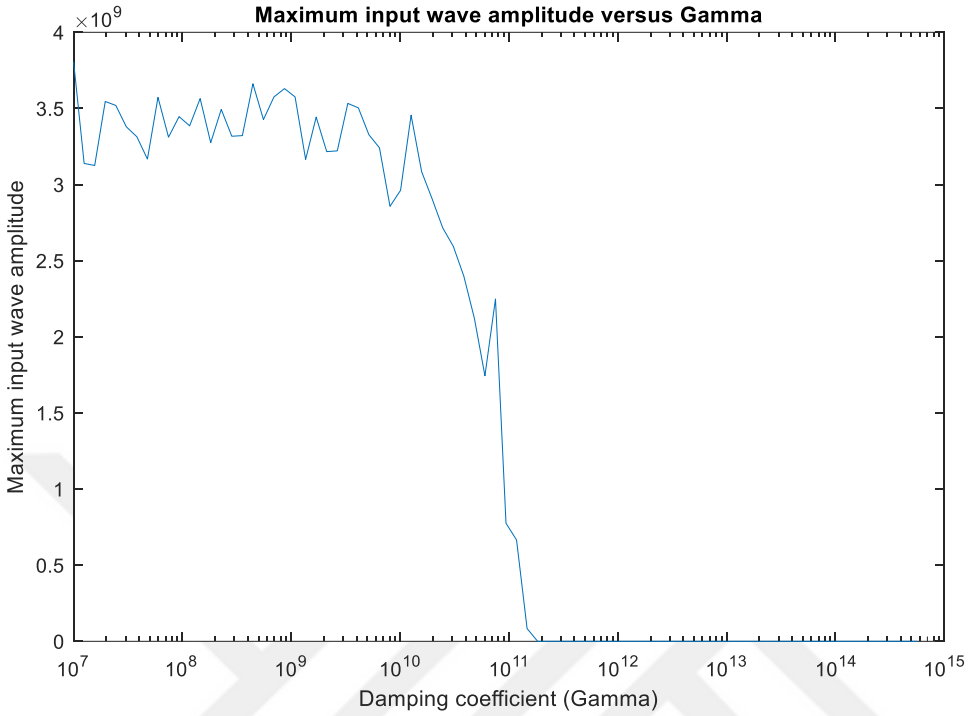

Figure 4.10 Highest input wave amplitude (V/m) recorded at x=5.73 µm with respect to the damping coefficient (γ).

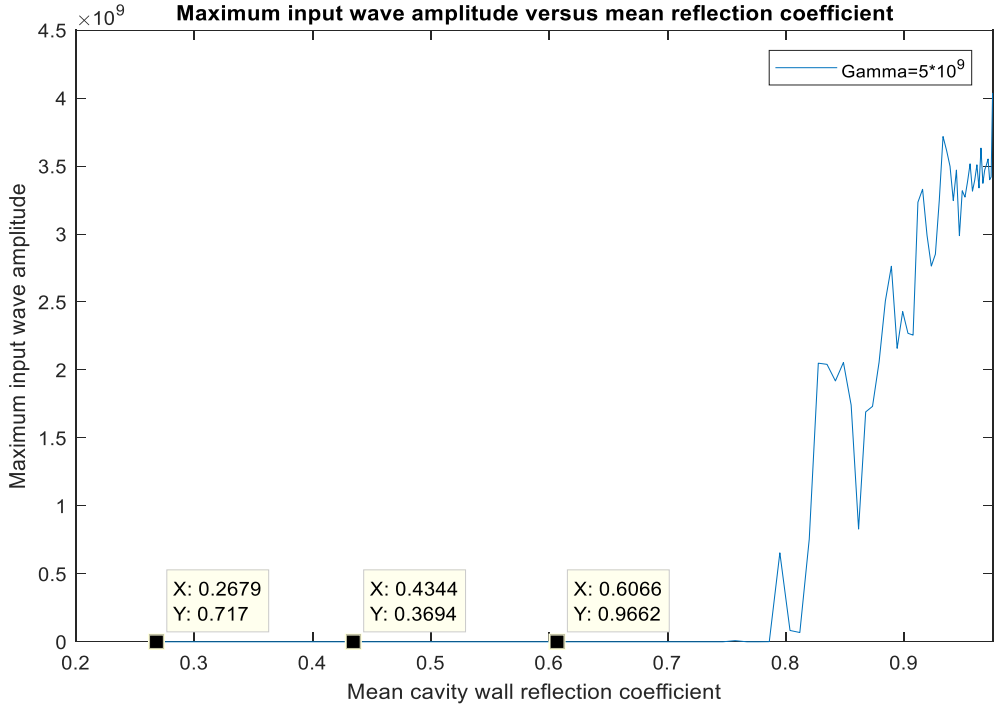

Figure 4.11 Highest input wave amplitude (gain factor) recorded at x=5.73 µm plotted with respect to the mean cavity wall reflectance for an original pump wave amplitude of $2.75 \times 10^8\ V/m$ for $f_0 = 4 \times 10^{14}\ Hz$ and for $\gamma = 5 \times 10^9\ Hz$.

Figures 4.10 and 4.11 summarize that choosing an interaction material with a low polarization decay rate and using resonator walls with a high reflectance significantly improves the gain factor of the input wave, since the accumulated electric energy density can be increased further via these preferences. Both variables (reflectance, decay rate) have critical values for gain factor improvement. Figures 4.10 and 4.11 are illustrated for a dominant resonance frequency of $f_0 = 4 \times 10^{14}\ Hz$. Since the dominant resonance frequency is in the infra-red spectral range, the required pump wave amplitude for nonlinear coupling is lower and consequently the input wave gain factor is higher. For interaction media with higher resonance frequencies, the maximum attainable gain factor is lower for the same pump wave amplitude. This relation is tabulated in Table 4.3.

$$f_0 : Resonance\ frequency\ of\ the\ interaction\ medium$$

$$\gamma : Damping\ \ coefficient\ of\ the\ interaction\ medium$$

$$\varepsilon_\infty : Dielectric\ constant\ of\ the\ interaction\ medium$$

$$Gain_{max} : Maximum\ gain\ that\ has\ been\ achieved\ in\ the\ cavity\ for\ 0 < t < 30\ ps$$

$$E_{hp,min} : Minimum\ pump\ wave\ amplitude\ required\ to\ produce\ a\ gain\ factor\ that\ is\ greater\ than\ 10^7.$$

Table 4.3: Maximum gain factor $Gain_{max}$ versus resonance frequency f_0 (Simulation 8)

f_0	$\gamma(THz)$	ε_∞	$Gain_{max}$	$E_{hp,min}$ (V/m)
400THz	5×10^9	10	1.1×10^9	1.6×10^8
500THz	5×10^9	10	1.0×10^9	1.8×10^8
600THz	5×10^9	10	8×10^8	2.0×10^8
700THz	5×10^9	10	6×10^8	2.2×10^8
800THz	5×10^9	10	5×10^8	2.5×10^8
900THz	5×10^9	10	3×10^8	2.9×10^8
1000THz	5×10^9	10	3×10^8	3.4×10^8
1100THz	5×10^9	10	2×10^8	3.9×10^8
1200THz	5×10^9	10	1×10^8	4.6×10^8
1300THz	5×10^9	10	5×10^7	5.5×10^8
1400THz	5×10^9	10	3×10^7	6.5×10^8
1500THz	5×10^9	10	2×10^7	7.6×10^8
1600THz	5×10^9	10	1.5×10^7	8.8×10^8
1700THz	5×10^9	10	1.1×10^7	1.0×10^9

Table 4.4: Maximum attainable gain factor $Gain_{max}$ versus medium permittivity (Simulation8)

f_0	$\gamma(THz)$	ε_∞	$Gain_{max}$
400THz	5×10^9	2	49.7
400THz	5×10^9	4	2857
400THz	5×10^9	6	79676
400THz	5×10^9	8	1.81×10^6
400THz	5×10^9	10	2.99×10^7
400THz	5×10^9	12	1.3×10^9
400THz	5×10^9	14	1.4×10^9
400THz	5×10^9	16	1.5×10^9
400THz	5×10^9	18	1.5×10^9
400THz	5×10^9	20	1.4×10^9

Simulation9:

The low intensity input wave ($\boldsymbol{E_1}$) and the high intensity pump wave ($\boldsymbol{E_2}$) are simultaneously present in a two-port Fabry-Perot resonator. The waves are originated at the point x=0 μm and at the instance t=0 sec. The configuration is as stated below

$$\boldsymbol{E_1}(x = 0\ \mu m, t) = 1 \times \frac{\sin(2\pi(2.5 \times 10^{14})t)\ \ V}{m}\ ,\ \ for\ \ 0 \le t \le 50\ ps$$

$$\boldsymbol{E_2}(x = 0\ \mu m, t) = 3.75 \times 10^8 \times \frac{\sin(2\pi(1 \times 10^{14})t)\ \ V}{m}\ ,\ \ for\ \ 0 \le t \le 1\ ps$$

$$Resonance\ frequency\ of\ the\ gain\ medium:\ f_0 = 800\ THz$$

$$Damping\ rate\ of\ the\ gain\ medium:\ \gamma = 1 \times 10^9\ Hz$$

$$Dielectric\ constant\ of\ the\ gain\ medium\ (\varepsilon_\infty) = 10 \quad (\mu_\infty = 1)$$

$$Spatial\ range\ of\ the\ simulation\ domain:\ 0 \le x \le 15\ \mu m$$

$$Gain\ medium\ spatial\ range: 0\mu m < x < 10\ \mu m$$

$$Left\ \ wall\ reflection\ coefficient:\ \Gamma_1 = 0.96$$

$$Right\ wall\ reflection\ coefficient:\ \Gamma_2 = 0.96$$

$Electron\ density\ of\ the\ gain\ medium: N = 3.5 \times \frac{10^{28}}{m^3},\ Atomic\ diameter: d = 0.3\ nm$

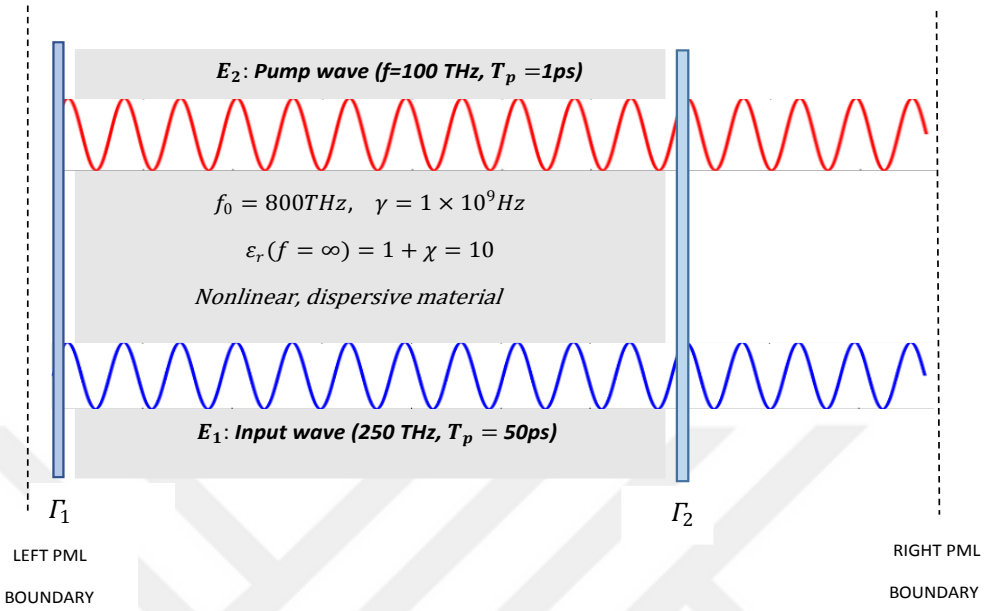

Figure 4.12 The configuration of the described resonator in Simulation 4

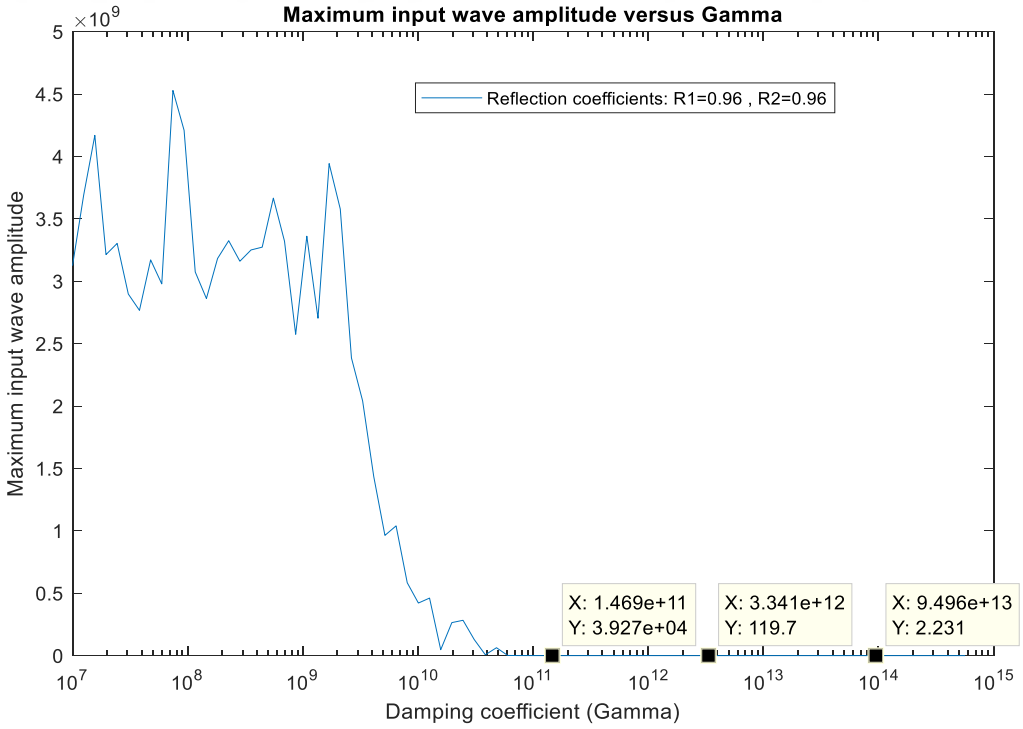

Figure 4.13 Max. amplitude of the input wave (V/m) at x=5.73 µm vs the damping coefficient.

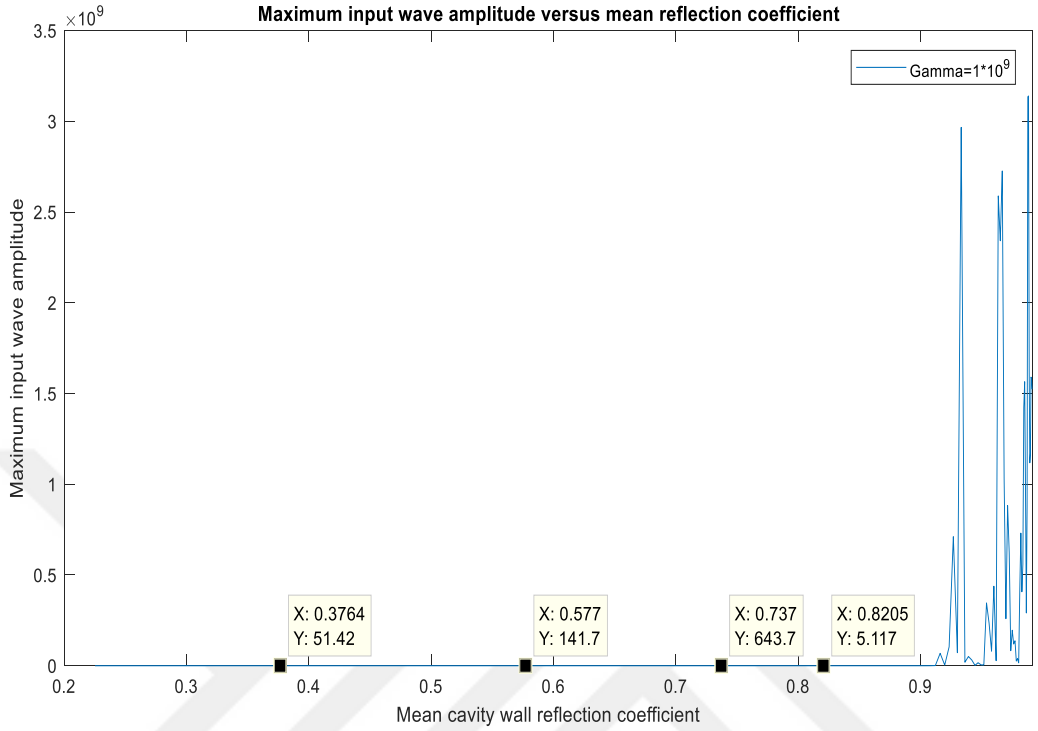

Figure 4.14 Max. amplitude of the input wave (gain factor) at x=5.73 μm vs mean resonator wall reflectance for an original pump wave amplitude of $3.75 \times 10^8\ V/m$ for a resonance frequency of $f_0 = 8 \times 10^{14}\ Hz$ and for a damping rate of $\gamma = 1 \times 10^9\ Hz$.

From Figures 4.13 and 4.14, one can deduce that by choosing an interaction material with a low polarization decay rate (damping coefficient) and by adjusting the resonator walls to be highly reflective, one can significantly improve the gain factor of the input wave. Both the polarization decay rate and the mean resonator reflectance have threshold/critical values for gain factor improvement, below which the amplification is insignificant. Both figures (4.13 and 4.14) are illustrated for a dominant resonance frequency of $f_0 = 8 \times 10^{14}\ Hz$. For interaction mediums with higher resonance frequencies, the critical pump wave intensity that is necessary for nonlinear coupling is larger and the attained gain factor is smaller, this relation is tabulated in Table 4.5.

$$f_0 : Resonance\ frequency\ of\ the\ gain\ medium$$

$$\gamma : Damping\ \ coefficient\ of\ the\ gain\ medium$$

$$\varepsilon_\infty : Dielectric\ constant\ of\ the\ gain\ medium$$

$Gain_{max}$: *Maximum gain that has been achieved in the cavity for* $0 < t < 30\ ps$

$E_{hp,min}$: *Minimum pump wave amplitude required to produce a gain factor that is greater than* 10^7.

Table 4.5: Max. attainable gain factor $Gain_{max}$ versus the dominant resonance frequency f_0.

f_0	$\gamma(THz)$	ε_∞	$Gain_{max}$	$E_{hp,min}$ (V/m)
400THz	1×10^9	10	2.2×10^9	1.6×10^8
500THz	1×10^9	10	2.1×10^9	1.8×10^8
600THz	1×10^9	10	2×10^9	2.1×10^8
700THz	1×10^9	10	1.9×10^9	2.5×10^8
800THz	1×10^9	10	1.7×10^9	3.0×10^8
900THz	1×10^9	10	1.5×10^9	3.6×10^8
1000THz	1×10^9	10	1.2×10^9	4.4×10^8
1100THz	1×10^9	10	1×10^9	5.4×10^8
1200THz	1×10^9	10	7×10^8	6.5×10^8
1300THz	1×10^9	10	4×10^8	7.7×10^8
1400THz	1×10^9	10	2×10^8	8.8×10^8
1500THz	1×10^9	10	9×10^7	1×10^9
1600THz	1×10^9	10	4×10^7	1.1×10^9
1700THz	1×10^9	10	1.5×10^7	1.2×10^9

Table 4.6: Maximum attainable gain factor $Gain_{max}$ versus interaction medium permittivity. The gain factor increases with the medium permittivity as the stored energy is proportional to the permittivity value.

f_0	$\gamma(THz)$	ε_∞	$Gain_{max}$
800THz	1×10^9	2	69.7
800THz	1×10^9	4	3301
800THz	1×10^9	6	62575
800THz	1×10^9	8	1.57×10^6
800THz	1×10^9	10	3.08×10^7
800THz	1×10^9	12	1.2×10^9
800THz	1×10^9	14	1.3×10^9
800THz	1×10^9	16	1.3×10^9
800THz	1×10^9	18	1.4×10^9
800THz	1×10^9	20	1.5×10^9

Simulation 4.10 – part 1: Choosing the optimum pump wave frequency

A 300 THz infra-red stimulus (input) wave E_{st} and a high-intensity pump wave E_{hp} are simultaneously present in a Fabry-Perot resonator. The left wall of the resonator is an optical isolator with an amplitude reflectance of $\Gamma_1 \approx 1$, and the right wall is a shutter equipped bandpass filter with a frequency selective reflectance of $\Gamma(f)$. The waves are originated at x=0 μm at the instance t=0s. The configuration of the resonator is as stated below:

$E_{hp}(x = 0\ \mu m, t) = 5 \times 10^8 \times \sin(2\pi(f_p)t)\ \ V/m,\ \ for\ \ 0 \le t \le 1\ ps$

$E_{st}(x = 0\ \mu m, t) = 1 \times \sin(2\pi(3 \times 10^{14})t)\ \ V/m,\ \ for\ \ 0 \le t \le 10\ ps$

$Dielectric\ constant\ of\ the\ gain\ medium\ (\varepsilon_\infty) = 10 \quad (\mu_r = 1)$

$Resonance\ frequency\ of\ the\ gain\ medium = \ f_0 = 800\ THz$

$Damping\ coefficient\ of\ the\ gain\ medium:\ \gamma = 1 \times 10^7\ Hz$

$Time\ interval\ and\ duration\ of\ simulation:\ 0 \le t \le 10\ ps$

$Spatial\ range\ of\ the\ gain\ medium: 0\mu m < x < 10\ \mu m$

$Right\ wall\ location:\ x = 10\ \mu m\ \ ;\ \ Left\ wall\ location:\ x = 0\ \mu m$

$Electron\ density:\ N = 3.5 \times 10^{28}/m^3\ \ ;\ \ Atomic\ diameter: d = 0.3\ nm$

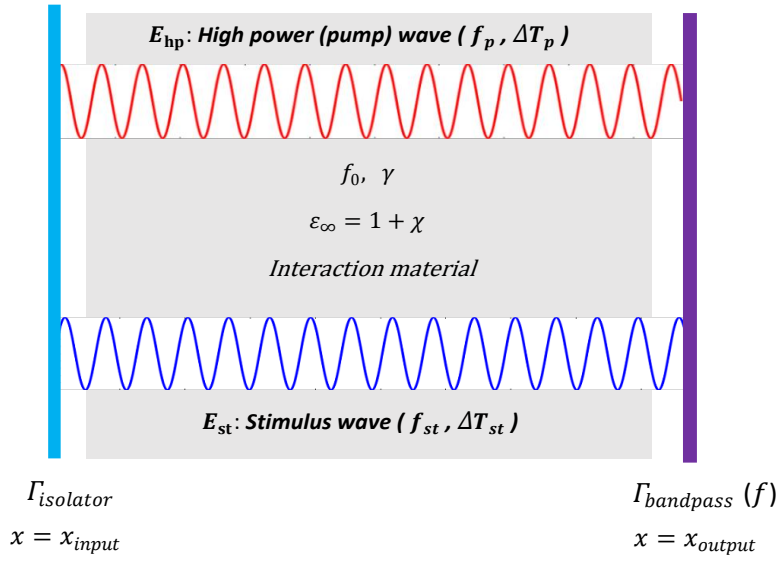

Figure 4.15 Configuration of the cavity and the parameters of the simulation.

Aim: Identifying the pump (source) wave frequency f_p that yields the maximum stimulus wave magnitude ($|E_{st}|$) inside the resonator, in the spectral range 10 THz $< f_p <$ 1000 THz, for $0\ \mu m < x < 10\ \mu m,\ 0 \le t \le 10\ ps$, given that

$$\nabla^2 E_{hp}(f_p) - \mu_0 \varepsilon_\infty \frac{\partial^2 E_{hp}(f_p)}{\partial t^2} = \mu_0 \sigma \frac{\partial E_{hp}(f_p)}{\partial t} + \mu_0 \frac{\partial^2 P_{hp}}{\partial t^2}.$$

$$\frac{\partial^2 P_{hp}}{\partial t^2} + \gamma \frac{\partial P_{hp}}{\partial t} + {\omega_0}^2 (P_{hp}) - \frac{{\omega_0}^2}{Ned} (P_{hp})^2 + \frac{{\omega_0}^2}{N^2 e^2 d^2} (P_{hp})^3 = \frac{Ne^2}{m} E_{hp}(f_p).$$

$$\nabla^2 E_{st}(f_p) - \mu_0 \varepsilon_\infty \frac{\partial^2 E_{st}(f_p)}{\partial t^2} = \mu_0 \sigma \frac{\partial E_{st}(f_p)}{\partial t} + \mu_0 \frac{\partial^2 E_{st}(f_p)}{\partial t^2}.$$

$$\frac{\partial^2 (P_{st})}{\partial t^2} + \gamma \frac{\partial (P_{st})}{\partial t} + {\omega_0}^2 (P_{st}) - \frac{{\omega_0}^2}{Ned} \{ {P_{st}}^2 + 2 P_{st} P_{hp} \} + \frac{{\omega_0}^2}{N^2 e^2 d^2} \{ {P_{st}}^3 + 3 {P_{st}}^2 P_{hp} + 3 P_{st} {P_{hp}}^2 \} = \frac{Ne^2}{m} E_{st}(f_p)$$

Initial values:

$$P_{hp}(x,0) = {P_{hp}}'(x,0) = E_{hp}(x,0) = {E_{hp}}'(x,0) = P_{st}(x,0) = {P_{st}}'(x,0) = E_{st}(x,0) = {E_{st}}'(x,0) = 0$$

Excitation conditions:

$$E_{hp}(x = 0\ \mu m, t) = 5 \times 10^8 \times \sin\left(2\pi (f_p) t\right)\ \ V/m,\ \ for\ \ 0 \le t \le 1\ ps$$

$$E_{st}(x = 0\ \mu m, t) = 1 \times \sin(2\pi (3 \times 10^{14}) t)\ \ V/m,\ \ for\ \ 0 \le t \le 10\ ps$$

$$E_{hp}(x = 15\ \mu m, t) = E_{st}(x = 15\ \mu m, t) = 0 \qquad for\ 0 < t < 10\ ps$$

Absorbing layer for computational domain termination:

$$\sigma(x) = \{ (x - (L - \Delta))\sigma_0\ ,\ \ (L - \Delta) \le x < L \qquad \}, for\ L = 15\ \mu m,\ \Delta = 2.5\ \mu m,\ \sigma_0 = 4.5 \times 10^8\ S/m$$

Optical isolator: Perfect reflection at x = 0 μm

$$\Gamma(x = 0\ \mu m, t) = 1\ \ (Reflection\ coefficient\ is\ equal\ to\ 1)$$

Shutter equipped band-pass filter: Located at $x = 10\ \mu m$. Perfect reflection for t≤10 ps, frequency selective reflection for t>10 ps.

$$|\Gamma(f')| = \begin{cases} 1 \qquad for\ all\ f'\ , \quad for\ \ x = 10\ \mu m,\ \ 0 \le t \le 10\ ps \\ 1 - e^{-(\frac{(f'-f)}{\sqrt{2}\ THz})^2} \quad , \quad for\ \ x = 10\ \mu m,\ \ t > 10\ ps \end{cases}$$

To identify the optimal pump wave frequency that maximizes the magnitude of the stimulus wave electric field in the resonator (for 0<t<10ps), at each step of the optimization we use a simple recursive equation derived from Newton's update formula. Accordingly, the frequency of the pump wave and the optimal step length are stated as

$$f_{p,k+1} = f_{p,k} - \rho_k \frac{\left|E_{st}(f_{p,k})\right|}{\left|E_{st}(f_{p,k})\right| - \left|E_{st}(f_{p,k-1})\right|}\left(f_{p,k} - f_{p,k-1}\right)\ , \qquad k = 1,2,\dots$$

$$\rho_k = 1.467^{\left(\log\left|\frac{|E_{st}(f_{p,k})|}{|E_{st}(f_{p,k})|-|E_{st}(f_{p,k-1})|}\right|\right)/\left(\left|\frac{|E_{st}(f_{p,k})|}{|E_{st}(f_{p,k})|-|E_{st}(f_{p,k-1})|}\right|\right)}$$

After 60 updates (at the iteration k=61), the highest stimulus wave amplitude that is attained in the resonator for 0<t<10ps is found as $Gain_{max} = |E_{st}|_{max} = 7.74 \times 10^6\ V/m$. This amplitude is reached at a pump wave frequency of $f_p = 349.5\ THz$. The optimization process is shown in Table 4.7.

Table4.7: Updating the pump wave frequency for gain factor maximization.

f_0	$\gamma(THz)$	ε_∞	$Gain_{max}$	f_p	k (iteration #)
800THz	1×10^7	10	3.48	500THz	1
800THz	1×10^7	10	7.13	488THz	4
800THz	1×10^7	10	6.22	441THz	7
800THz	1×10^7	10	18.61	402THz	10
800THz	1×10^7	10	26.59	317THz	13
800THz	1×10^7	10	21.42	393THz	16
800THz	1×10^7	10	53.38	322THz	19
800THz	1×10^7	10	151.4	294THz	22
800THz	1×10^7	10	137.7	265THz	25
800THz	1×10^7	10	28.81	282THz	28
800THz	1×10^7	10	4.97	289THz	31
800THz	1×10^7	10	3.75×10^2	377THz	34
800THz	1×10^7	10	69.07	386THz	37
800THz	1×10^7	10	2.34×10^3	365THz	40

Table4.7: (Continued)

800THz	1×10^7	10	4.18×10^3	364THz	43
800THz	1×10^7	10	7.92×10^4	353THz	46
800THz	1×10^7	10	5.53×10^3	340THz	49
800THz	1×10^7	10	1.68×10^6	348.5THz	52
800THz	1×10^7	10	5.37×10^6	349.1THz	55
800THz	1×10^7	10	7.02×10^6	349.4THz	58
800THz	1×10^7	10	7.74×10^6	349.5THz	61

To uncover the physical phenomena behind the super-gain at this specific pump wave frequency, the frequency of the pump wave is varied from 10 THz to 1000 THz in 10 THz increments, so that we can observe the gain factor in a wide spectral range. The density of intracavity electric energy (W_e) and the intracavity polarization density (P_{hp}) induced by the high intensity of the pump wave are illustrated against the pump wave frequency in Figures 4.16 and 4.17. It is clear from Figure 4.16 that the stored electric energy density is the highest near $f_p = 350\,THz$, and our optimization problem essentially determines the optimal excitation frequency of the pump wave that yields the highest electric energy in the cavity. If we investigate the highest gain peak which occurs at $f_p = 350\,THz$, we can see that the intracavity polarization density (P_{hp}) induced by the pump wave (which enables the energy transfer) is the highest for this excitation frequency. The pump wave induced electric energy density W_e also has its maximum value around $f_p = 350\,THz$. Consequently, we have the strongest gain factor peak around $f_p = 350\,THz$. As tabulated in Table4.8, when the stored electric energy density and the intracavity polarization density induced by the pump wave are simultaneously high, the stimulus wave amplification is stronger. As the pump wave frequency of $f_p = 350\,THz$ yields the major peak in the electric energy density and amplifies the electric field of the stimulus wave, this frequency is selected as the pump wave excitation frequency for the computation of the gain spectrum of the stimulus wave. After its amplification, the stimulus wave becomes slightly polychromatic as a consequence of the spectral broadening in the resonator. For this reason, it is necessary to perform another investigation to attain the amplification spectrum of the stimulus wave using a 350 THz (optimal) pump wave excitation.

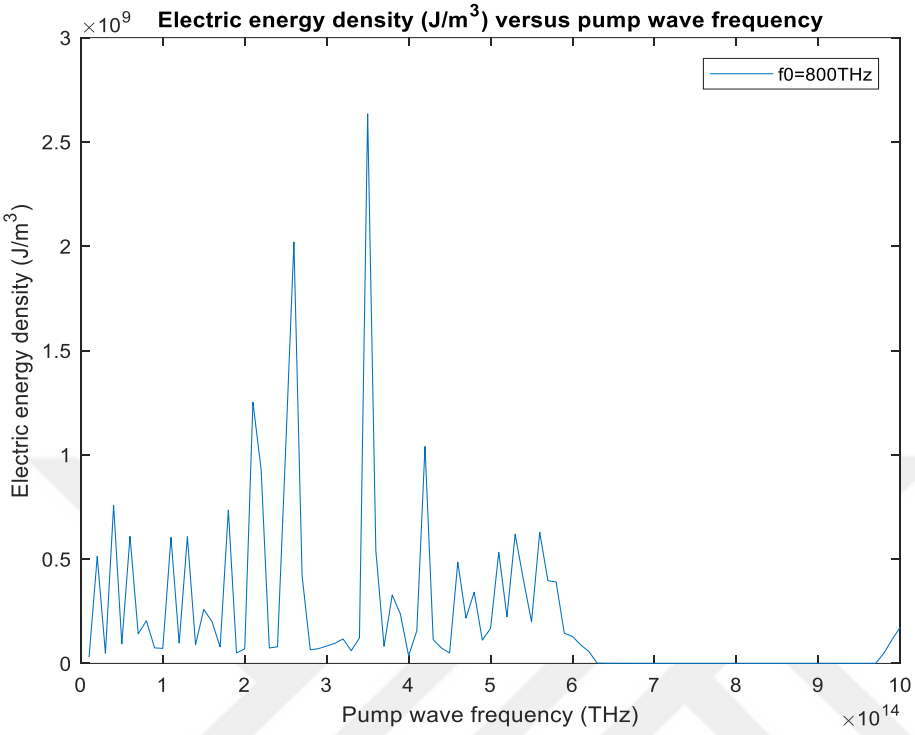

Figure 4.16 Pump wave induced electric energy density (0<t<10ps) as computed in the resonator (at x=5.73 μm) versus the pump wave frequency.

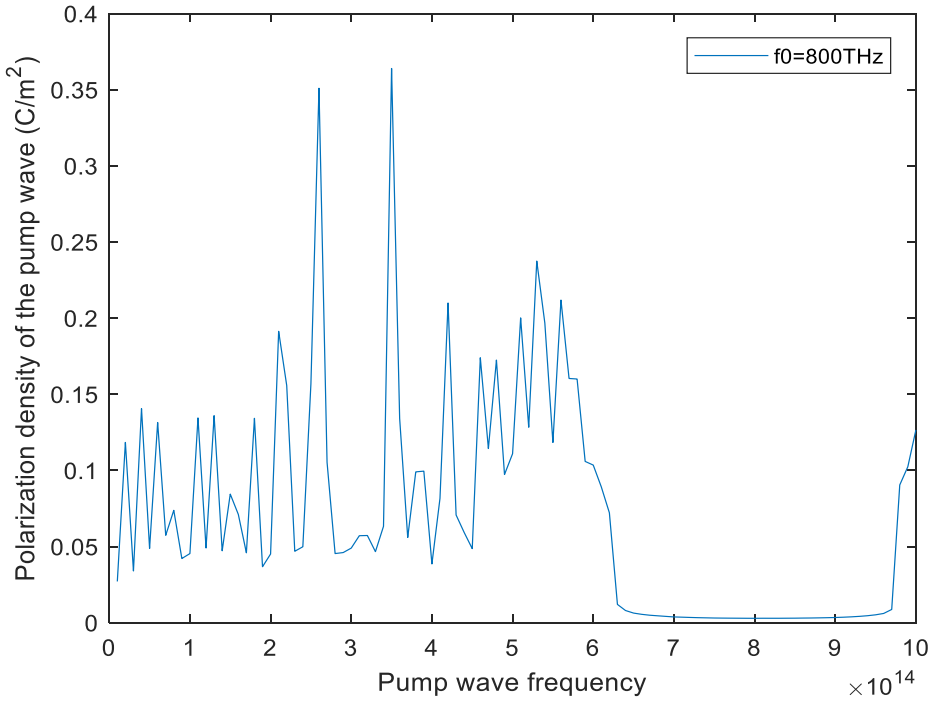

Figure 4.17 Pump wave induced polarization density (highest value in the range 0<t<10ps) as computed in the resonator (computation coordinate: x=5.73 μm) versus pump wave frequency.

W_e: *Maximum electric energy density created by the pump wave in the cavity*
P_{hp}: *Maximum charge polarization density created by the pump wave in the cavity*
$A_{st,max}$: *Maximum stimulus wave amplitude in the cavity*

Table4.8: Pump wave frequency, highest amplitude of the stimulus wave (gain factor), highest electric energy density induced via pump wave, highest polarization density induced via pump wave

f_p(THz)	$A_{st,max}$	W_e	P_{hp}
10	5.883986	29699657	0.027091
20	13.42542	5.13E+08	0.118397
30	12.99005	48849682	0.033976
40	9.096766	7.58E+08	0.14055
50	17.10611	93371276	0.048789
60	4.474521	6.09E+08	0.131476
70	5.069646	1.42E+08	0.057396
80	3.561172	2.05E+08	0.073801
90	2.641755	74279614	0.042153
100	4.077828	72125541	0.045394
110	8.999627	6.04E+08	0.13448
120	2.613823	97309728	0.049051
130	3.933646	6.07E+08	0.135959
140	2.685399	89828810	0.047224
150	2.446767	2.58E+08	0.08447
160	2.277283	2.01E+08	0.071119
170	2.568835	78977510	0.045889
180	3.640279	7.35E+08	0.134221
190	3.496944	50155368	0.036736
200	5.209949	69704490	0.045108
210	39.38512	1.25E+09	0.19136
220	17.4777	9.3E+08	0.155742
230	3.781144	73950854	0.046904
240	6.847807	79718064	0.049873
250	66.4612	1.03E+09	0.156807
260	1354.073	2.03E+09	0.350968
270	14.35446	4.2E+08	0.105385
280	13.4472	65372520	0.045401
290	6.311408	70860412	0.046055
300	2.760757	83057212	0.048992
310	2.27222	96378435	0.057127
320	2.685882	1.17E+08	0.057266
330	2.403513	60937048	0.046658
340	1.907491	1.22E+08	0.06329
350	**6835947**	**2.65E+09**	**0.36398**
360	51.09379	5.4E+08	0.134201
370	2.244881	82294755	0.055986
380	4.045674	3.28E+08	0.099051
390	2.385328	2.36E+08	0.099527
400	1.914928	36407088	0.038589
410	2.245768	1.57E+08	0.081641
420	60.8144	1.04E+09	0.209959
430	2.316941	1.14E+08	0.070736
440	2.424293	74048560	0.059251
450	1.903607	50132227	0.048627
460	22.94166	4.85E+08	0.173972
470	2.353593	2.17E+08	0.114367
480	11.76979	3.42E+08	0.172466
490	7.203818	1.12E+08	0.097311
500	7.889092	1.68E+08	0.110958

f_p (THz)	$A_{st,max}$	W_e	P_{hp}
510	1211.665	5.33E+08	0.200157
520	12.03636	2.24E+08	0.128374
530	6380.668	6.2E+08	0.237481
540	197.2572	4.04E+08	0.196768
550	2.228608	2E+08	0.118366
560	3341.632	6.28E+08	0.211868
570	50526.02	3.97E+08	0.160384
580	1.952741	3.91E+08	0.160039
590	1.836473	1.45E+08	0.105914
600	2.067759	1.29E+08	0.103506
610	2.159113	88756343	0.089169
620	7.876075	56936698	0.072166
630	2.014397	1719389	0.012014
640	2.002486	867505.3	0.008003
650	1.99723	594922.3	0.006319
660	1.992377	454115.5	0.005502
670	1.992079	380584.9	0.004912
680	1.99609	327444.1	0.004525
690	1.992056	281248.6	0.004147
700	1.994624	254086.5	0.003786
710	2.003631	239090.8	0.003631
720	2.008237	224470.1	0.003453
730	2.014686	212223.1	0.003299
740	2.08819	194997.7	0.00319
750	2.020707	189412.7	0.003079
760	2.026132	182209.2	0.003019
770	2.031172	171364.8	0.002977
780	2.106717	167320.3	0.002944
790	2.062642	160819.4	0.002907
800	2.123964	154567	0.00289
810	2.074114	150234.4	0.002923
820	2.043318	146722.7	0.002912
830	2.033978	142738.8	0.00291
840	2.02517	137337.5	0.002947
850	2.07065	135352.4	0.002973
860	2.042151	133736	0.003041
870	2.013683	130354.1	0.003091
880	2.048405	129162.4	0.003179
890	1.986717	133554.1	0.003284
900	2.000912	135280.2	0.003413
910	1.981226	141468.3	0.003604
920	2.02185	150727.1	0.003847
930	2.017607	161806.4	0.004165
940	2.009308	175362.1	0.004584
950	2.004022	198713	0.005175
960	2.00816	238825.9	0.006067
970	2.008864	307733	0.008694
980	122.4469	48819069	0.090452
990	404.8945	1.14E+08	0.10242
1000	34391.77	1.74E+08	0.126597

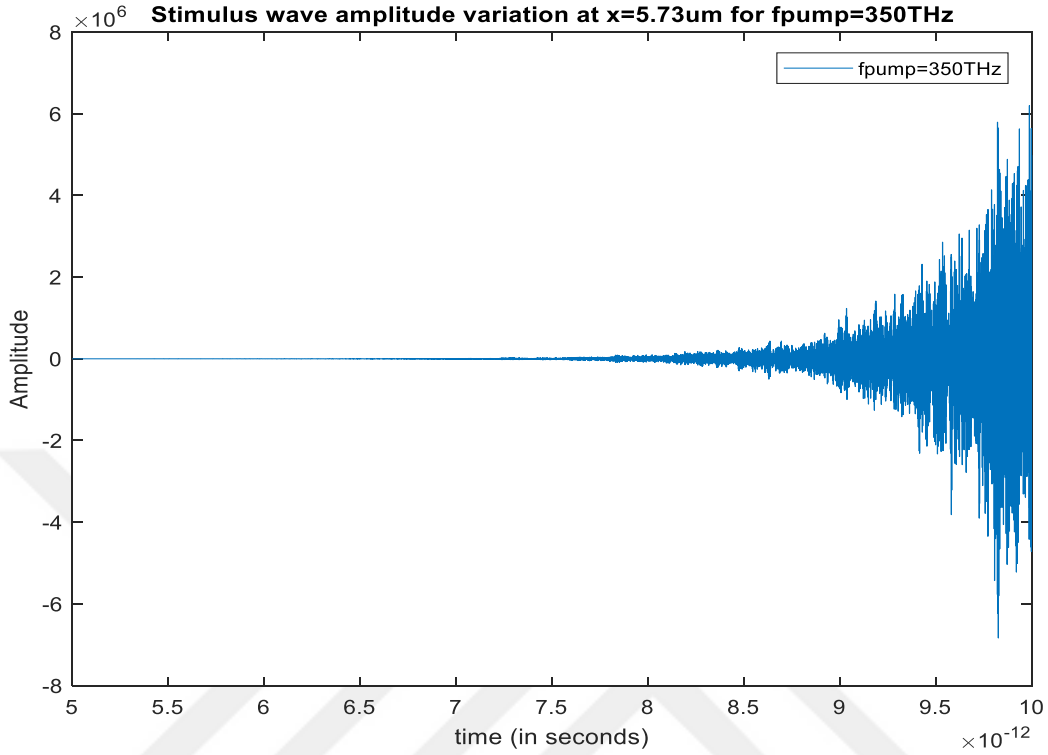

Figure 4.18 Amplitude of the stimulus wave versus time as computed at x=5.73 μm for a pump wave excitation at $f_p = 350$ THz.

Simulation 10 - Part2: Amplification (gain) spectrum of the stimulus wave under the optimal pump wave excitation frequency of $f_p = 350\ THz$

Aim: For the optimal ($f_p = 350\ THz$) pump wave frequency, determine the stimulus wave gain factor $|E_{st}|_{max}$ in the micro-resonator for every stimulus frequency f_s in the interval 10 THz $< f_s < 1000\ THz$ ($0\ \mu m < x < 10\ \mu m,\ 0 \le t \le 10\ ps$), given the following equations

$$\nabla^2(E_{hp}) - \mu_0\varepsilon_\infty \frac{\partial^2(E_{hp})}{\partial t^2} = \mu_0\sigma \frac{\partial(E_{hp})}{\partial t} + \mu_0 \frac{\partial^2 P_{hp}}{\partial t^2}. \qquad (107a)$$

$$\frac{\partial^2 P_{hp}}{\partial t^2} + \gamma \frac{\partial P_{hp}}{\partial t} + {\omega_0}^2(P_{hp}) - \frac{{\omega_0}^2}{Ned}(P_{hp})^2 + \frac{{\omega_0}^2}{N^2e^2d^2}(P_{hp})^3 = \frac{Ne^2}{m}(E_{hp}). \qquad (107b)$$

$$\nabla^2(E_{st}) - \mu_0\varepsilon_\infty \frac{\partial^2(E_{st})}{\partial t^2} = \mu_0\sigma \frac{\partial(E_{st})}{\partial t} + \mu_0 \frac{\partial^2(P_{st})}{\partial t^2}. \qquad (108a)$$

$$\frac{\partial^2(P_{st})}{\partial t^2} + \gamma \frac{\partial(P_{st})}{\partial t} + {\omega_0}^2(P_{st}) - \frac{{\omega_0}^2}{Ned}\{{P_{st}}^2 + 2P_{st}P_{hp}\} + \frac{{\omega_0}^2}{N^2e^2d^2}\{{P_{st}}^3 + 3{P_{st}}^2P_{hp} + 3P_{st}{P_{hp}}^2\} = \frac{Ne^2(E_{st})}{m} \quad (108b)$$

Initial values:

$$P_{hp}(x,0) = {P_{hp}}'(x,0) = E_{hp}(x,0) = {E_{hp}}'(x,0) = P_{st}(x,0) = {P_{st}}'(x,0) = E_{st}(x,0) = {E_{st}}'(x,0) = 0$$

Excitation conditions:

$$E_{hp}(x = 0\,\mu m, t) = 5 \times 10^8 \times \sin(2\pi(3.5 \times 10^{14})t)\ \ V/m,\ \ for\ \ 0 \le t \le 1\,ps$$

$$E_{st}(x = 0\,\mu m, t) = 1 \times \sin(2\pi(f_s)t)\ \ V/m,\ \ for\ \ 0 \le t \le 10\,ps$$

$$E_{hp}(x = 15\,\mu m, t) = E_{st}(x = 15\,\mu m, t) = 0 \quad for\ 0 < t < 10ps$$

Absorbing layer for computational domain termination:

$$\sigma(x) = \{\,(x - (L - \Delta))\sigma_0\,,\ \ (L - \Delta) \le x < L\ \ \},\ for\ L = 15\,\mu m,\ \ \Delta = 2.5\,\mu m,\ \sigma_0 = 4.5 \times 10^8\ S/m$$

Optical isolator: Displays perfect reflection at the location x = 0 μm

$$\Gamma(x = 0\,\mu m, t) = 1\ \ (Reflection\ coefficient\ is\ equal\ to\ 1)$$

Shutter equipped band-pass filter: Displays perfect reflection at x = 10 μm before t=10 ps, displays frequency selective reflection at x = 10 μm after t=10 ps. For a stimulus frequency (*f*), the spectral response of the band-pass filter is adjusted to be

$$|\Gamma(f')| = \begin{cases} 1 & for\ all\ f'\ , \quad for\ \ x = 10\,\mu m,\ \ 0 \le t \le 10\,ps \\ 1 - e^{-(\frac{(f'-f)}{\sqrt{2}THz})^2} & ,\ \ for\ \ x = 10\,\mu m,\ \ t > 10\,ps \end{cases}$$

The gain response of the stimulus wave for 10 THz < $f_s < 1000\,THz$, $f_{pump} = 350\,THz$ is illustrated in Figure 4.19. The stimulus wave is fed to the resonator at t=0 s as a

semi-monochromatic wave. For an original (for t=0 s) stimulus wave frequency, the central frequency of the bandpass filter is selected to be the same frequency with the original stimulus wave frequency. This allows us to examine the maximum gain that can be achieved from the resonator for each stimulus wave excitation frequency. We select the pump wave excitation frequency as $f = 350\ THz$ as it enables the highest gain factor to be achieved and we vary the stimulus wave frequency from 10 THz to 1000 THz by 10 THz at each step.

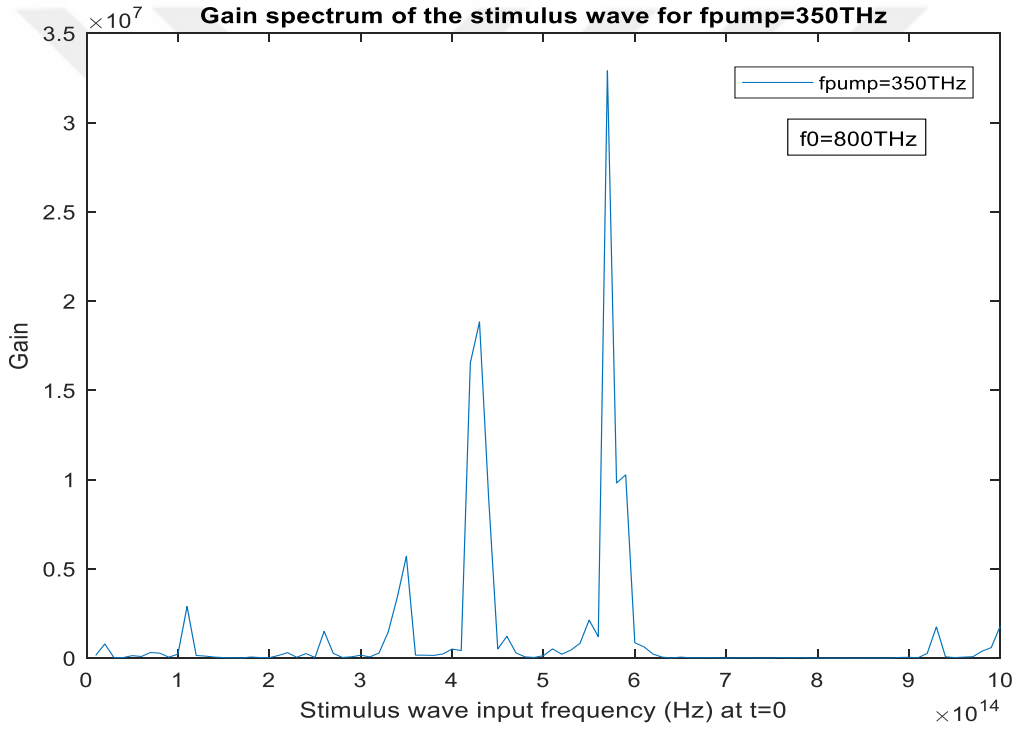

Figure 4.19 Variation of the stimulus wave gain factor with respect to the stimulus wave excitation frequency for $f_{pump} = 350\ THz$ and $f_0 = 800\ THz$.

Simulation 11: A stimulus wave with an electric field E_{st} and a high-intensity pump wave with an electric field E_{hp} are simultaneously present in a high-Q Fabry-Perot resonator. The left wall is an optical isolator and has a reflectance of $\Gamma_1 \approx 1$. The right one is a band-pass filter with a frequency selective reflectance $\Gamma(f)$. The waves are originated at the point x=0.1 μm (interior to the resonator), and at the instance t=0 s.

$$E_{hp}(x = 0.1\ \mu m, t) = 7 \times 10^8 \times \sin(2\pi(2.82 \times 10^{14})t)\ \ V/m,\ \ for\ \ 0 \le t \le 500\ fs$$

$$E_{st}(x = 0.1\ \mu m, t) = 1 \times \sin(2\pi(4.4 \times 10^{14})t)\ \ V/m\ ,\ \ for\ \ 0 \le t \le 30\ ps$$

$$Dielectric\ constant\ of\ the\ nonlinear\ material\ (\varepsilon_{f=\infty}) = 12 \quad (\mu_r = 1)$$

$$Resonance\ frequency\ of\ the\ dispersive\ material = f_0$$

$$Time\ interval\ and\ duration\ of\ simulation:\ 0 \le t \le 30\ ps$$

$$Strongly\ nonlinear\ dielectric\ material\ spatial\ range: 0.15\ \mu m < x < 9.85\ \mu m$$

$$Right\ cavity\ wall\ location:\ x = 0\ \mu m\ \ ,\ \ Left\ cavity\ wall\ location:\ x = 10\ \mu m$$

$$Electron\ density\ of\ the\ nonlinear\ medium:\ N = 3.5 \times 10^{28}/m^3$$

$$Atomic\ diameter: d = 0.3\ nanometers$$

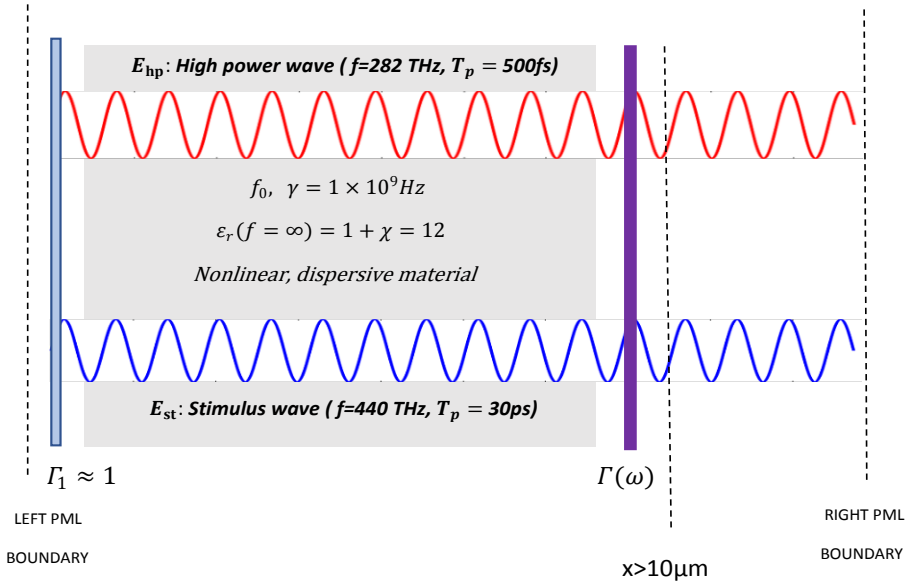

Figure 4.20 The micro-resonator described in Simulation 11.

Ideally, the magnitude spectral response of the band-pass filter should be

$$\Gamma(\omega) = \begin{cases} 1 & for\ all\ \omega\ , \quad 0 < t < 30\ ps \\ 1 & for\ \omega < 437.5\ THz\ and\ \omega > 442.5\ THz \quad , \quad t > 30\ ps \\ 0 & for\ 437.5\ THz < \omega < 442.5\ THz \quad , \quad t > 30\ ps \end{cases}$$

Evidently, during the computation $\Gamma(\omega) = 1$ for all ω. The filter is used for post-processing of the simulation results. In order to solve for the pump wave E_{hp} at each point in the computation domain and at every instance, the equations that need to be solved are

$$\nabla^2(E_{hp}) - \mu_0\varepsilon_\infty \frac{d^2(E_{hp})}{dt^2} = \mu_0\sigma\frac{d(E_{hp})}{\partial t} + \mu_0\frac{d^2P_{hp}}{dt^2}$$

$$\frac{d^2P_{hp}}{dt^2} + \gamma\frac{dP_{hp}}{dt} + {\omega_0}^2(P_{hp}) - \frac{{\omega_0}^2}{Ned}(P_{hp})^2 + \frac{{\omega_0}^2}{N^2e^2d^2}(P_{hp})^3 = \frac{Ne^2}{m}(E_{hp})$$

After solving for P_{hp}, we substitute it in the equations below to solve for E_{st}.

$$\nabla^2(E_{st}) - \mu_0\varepsilon_\infty \frac{d^2(E_{st})}{dt^2} = \mu_0\sigma\frac{d(E_{st})}{\partial t} + \mu_0\frac{d^2(P_{st})}{dt^2}$$

$$\frac{d^2(P_{st})}{dt^2} + \gamma\frac{d(P_{st})}{dt} + {\omega_0}^2(P_{st}) - \frac{{\omega_0}^2}{Ned}\{{P_{st}}^2 + 2P_{st}P_{hp}\} + \frac{{\omega_0}^2}{N^2e^2d^2}\{{P_{st}}^3 + 3{P_{st}}^2P_{hp} + 3P_{st}{P_{hp}}^2\} = \frac{Ne^2}{m}(E_{st})$$

The initial values and excitation conditions are as follows

$$P_{hp}(x,0) = {P_{hp}}'(x,0) = 0\ , \quad P_{st}(x,0) = {P_{st}}'(x,0) = 0$$

$$E_{hp}(x,0) = {E_{hp}}'(x,0) = 0\ , \quad E_{st}(x,0) = {E_{st}}'(x,0) = 0$$

$$E_{hp}(x = 0.1\mu m, t) = 7 \times 10^8 \times \sin(2\pi(2.82 \times 10^{14})t + \varphi_1)\ \ V/m,\ \ 0 < t < 500\ fs$$

$$E_{st}(x = 0.1\mu m, t) = 1 \times \sin(2\pi(4.4 \times 10^{14})t + \varphi_1)\ \ V/m\ \ ,\ \ 0 < t < 30\ ps$$

$$E_{hp}(x = 10\mu m, t) = E_{hp}(x = 0\mu m, t) = 0\ \ ,\ \ 0 < t < 30\ ps$$

$$E_{st}(x = 10\mu m, t) = E_{st}(x = 0\mu m, t) = 0\ \ ,\ \ 0 < t < 30\ ps$$

$Where\quad {P_{hp}}' = \frac{dP_{hp}}{dt}\quad ,\quad {E_{hp}}' = \frac{dE_{hp}}{dt}\quad ,\quad {P_{st}}' = \frac{dP_{st}}{dt}\quad ,\quad {E_{st}}' = \frac{dE_{st}}{dt}$

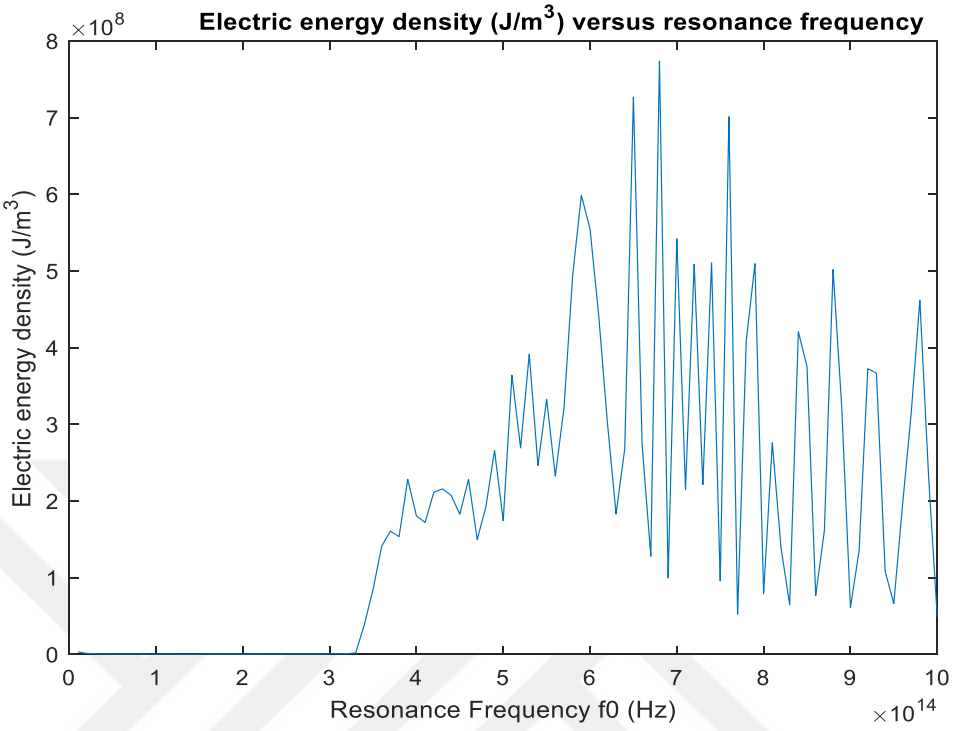

Figure 4.21 Intracavity electric energy density induced by the pump wave at x=5.73 µm vs f_0.

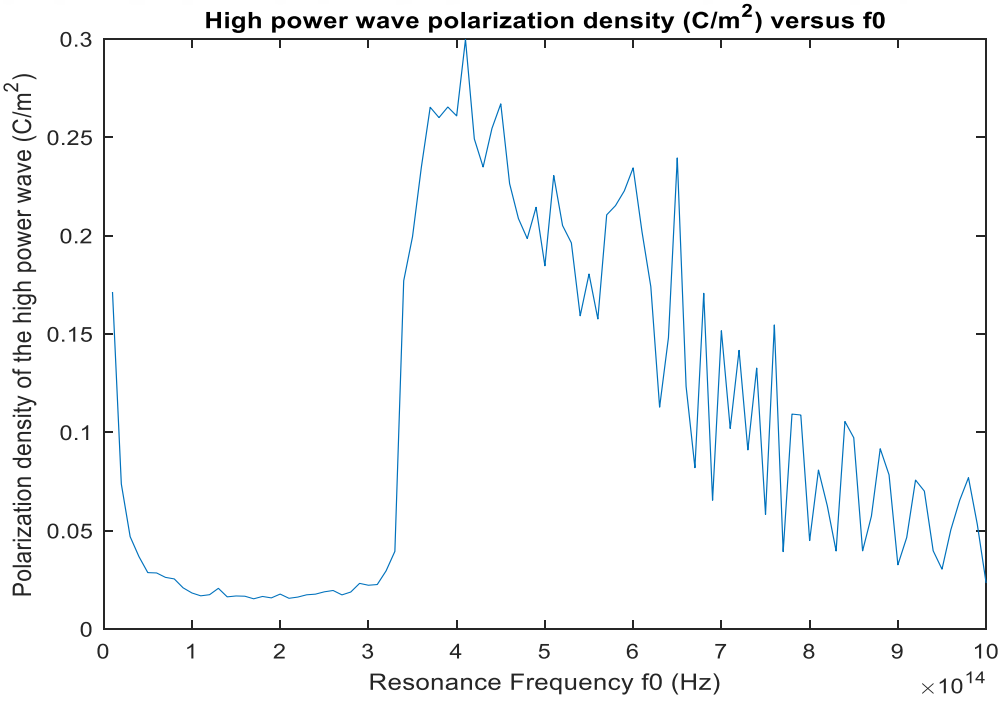

Figure 4.22 Intracavity polarization density induced by the pump wave at x=5.73 µm vs f_0.

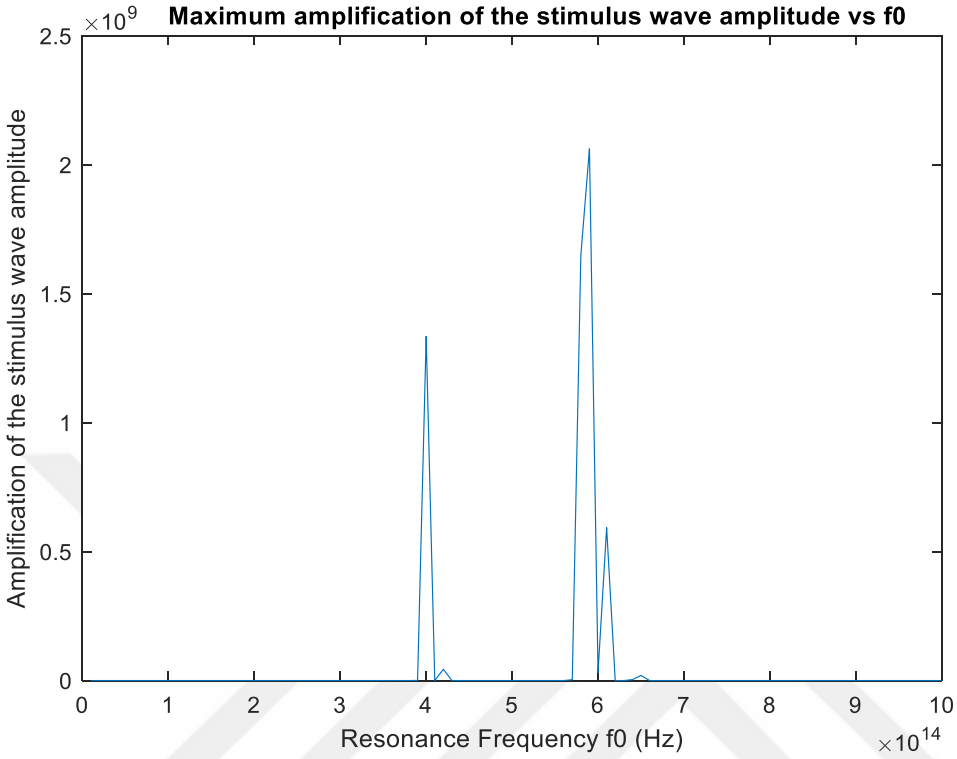

Figure 4.23 Highest intracavity stimulus wave amplitude computed at x=5.73 μm (t<30ps) vs f_0.

Identifying the optimal dominant resonance frequency values that enable a large gain factor for the stimulus wave is a challenging issue. Nevertheless, it is clear that high-gain amplification of an input wave requires a large amount of stored energy [29-32] and a large intracavity polarization density (P_{hp}) in the resonator. If we check the plots of the stored energy density W_e and the polarization density P_{hp} induced by the pump wave, versus the dominant resonance frequency of the interaction medium, we notice that amplifying the stimulus wave requires either the electric energy density or the polarization density induced by the pump wave to be high (ideally both should be high).

If we examine the gain peaks, one of the main peaks occurs at $f_0 = 400\ THz$ and it is clear from Figure 4.22 that the energy coupling coefficient i.e. the polarization density P_{hp} induced by the high-intensity pump wave is quite large (highest in the examined range) at this resonance frequency. The stored electric energy is also high at $f_0 = 400\ THz$ ($W_e = 1.78 \times 10^8\ J/m^3$). Consequently, there is a gain peak at $f_0 = 400\ THz$.

The major peak is located at $f_0 = 590\ THz$, where the stored energy density has the fourth highest peak along the examined frequency range ($W_e = 6 \times 10^8\ J/m^3$). The polarization density induced by the ultra-short pump wave is also quite high at $f_0 = 590\ THz$. For this reason, as W_e and P_{hp} are both very high at $f_0 = 590\ THz$, strongest amplification of the stimulus wave corresponds to this resonance frequency. Ideally, W_e and P_{hp} should be concurrently high for super-gain amplification.

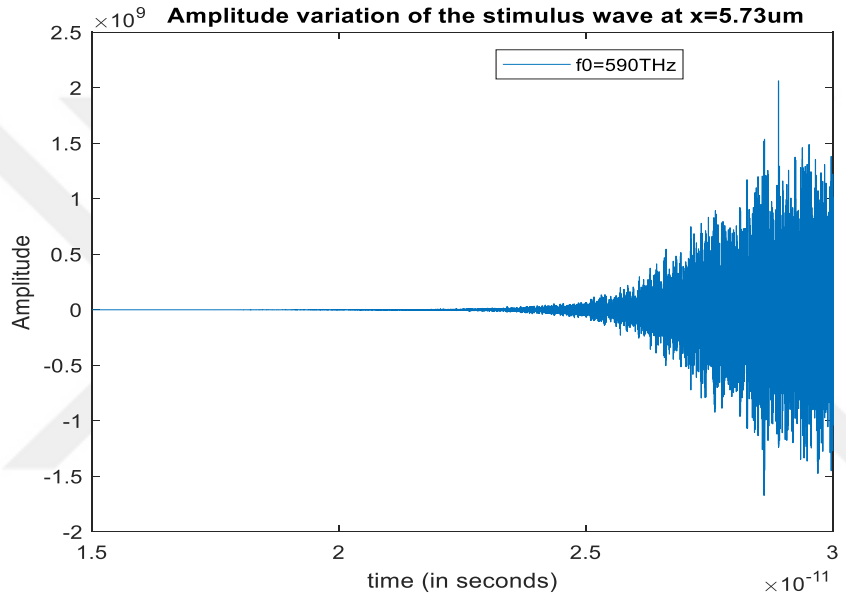

Figure 4.24 Stimulus wave amplitude vs time (computed at x=5.73 μm) for $f_0 = 590\ THz$.

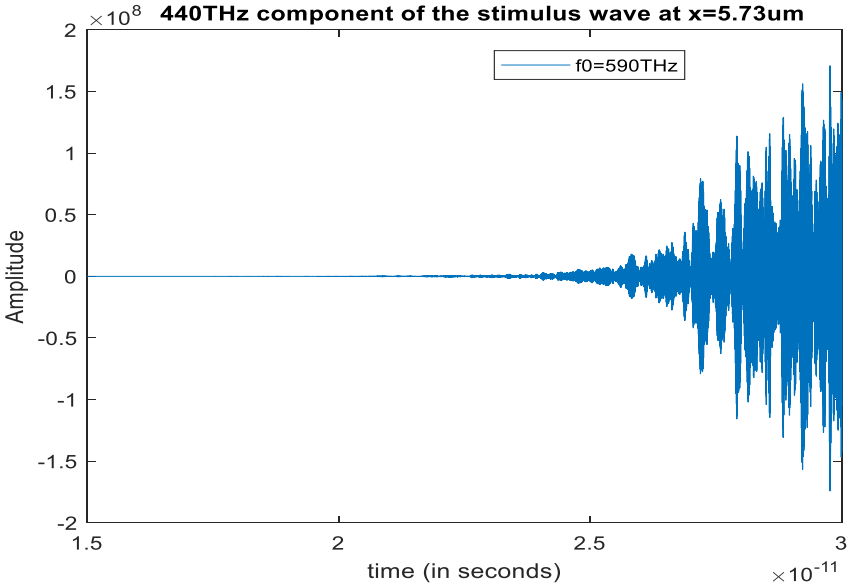

Figure 4.25 Stimulus wave filtered at 440 THz (computed at x=5.73 μm) for $f_0 = 590\ THz$

The gain spectrum of the amplified stimulus wave as computed inside the resonator illustrated in Figure 4.26 for f_0=590 THz is shown in Figure 4.27. The original stimulus wave is fed to the resonator (at t=0 s) as a single (pure) harmonic. For each stimulus wave excitation (initial) frequency, the center frequency of the ideal band-pass filter is selected to be the same with the stimulus frequency. This way we can examine the maximum attainable gain factor for each stimulus wave excitation frequency. The dominant resonance frequency is selected as $f_0 = 590\ THz$ as the gain factor is the highest at this frequency of the interaction medium. For a particular stimulus wave excitation frequency (*f*), the magnitude spectral response of the bandpass filter is adjusted as

$$\Gamma(\omega) = \begin{cases} 1 & for\ all\ \omega\ ,\quad 0 < t < 30\ ps \\ 1 & for\ \omega < (f - 2.5)\ THz \quad and \quad \omega > (f + 2.5)\ THz \quad ,\quad t > 30\ ps \\ 0 & for\ (f - 2.5)\ THz < \omega < (f + 2.5)\ THz \quad ,\quad t > 30\ ps \end{cases}$$

The bandwidth of the ideal band-pass filter is 5 THz. During the computation (t<30ps) $\Gamma(\omega) = 1$ for every ω. The bandpass filter is applied for postprocessing of the computed output data. The obtained gain spectrum for this configuration is illustrated in Figure 4.27.

$$E_{hp}(x = 0.1\ \mu m, t) = 7 \times 10^8 \times \sin(2\pi(2.82 \times 10^{14})t)\ \ V/m,\ \ for\ \ 0 \le t \le 500\ fs$$

$$E_{st}(x = 0.1\ \mu m, t) = 1 \times \sin(2\pi(f)t)\ \ V/m\ ,\ \ for\ \ 0 \le t \le 30\ ps$$

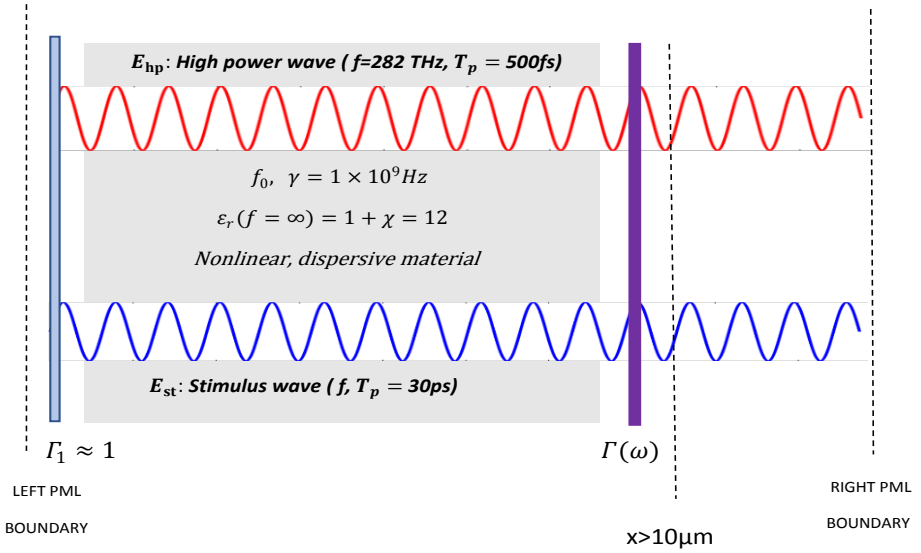

Figure 4.26 The setting for gain spectrum computation (Simulation1) at $f_0 = 590\ THz$.

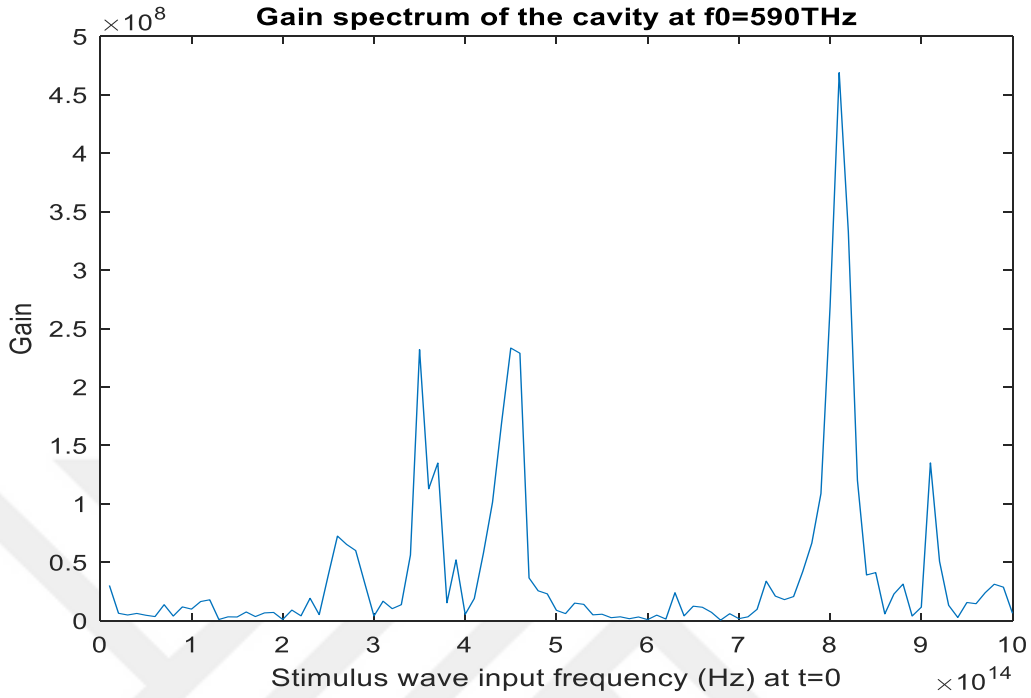

Figure 4.27 Stimulus wave gain spectrum for $f_0 = 590\ THz$.

Table 4.9: Tabulated stimulus wave gain spectrum (in THz)

fs	Gain	fs	Gain	fs	Gain	fs	Gain	fs	Gain
10	30146501	210	9073455	410	18995936	610	4745551	810	4.69E+08
20	6315998	220	4143911	420	57818957	620	1387913	820	3.33E+08
30	4856142	230	19179642	430	1.01E+08	630	23927640	830	1.2E+08
40	6196092	240	5165912	440	1.7E+08	640	4104084	840	39081126
50	4644096	250	39191087	450	2.33E+08	650	12407045	850	41146885
60	3520963	260	72396979	460	2.29E+08	660	11480627	860	5811195
70	13694626	270	65253901	470	36571306	670	7139056	870	22822690
80	3963803	280	59980997	480	25562630	680	460438.1	880	31321327
90	11806260	290	31820617	490	22958180	690	5972771	890	3974897
100	9887131	300	3971916	500	8880452	700	1744340	900	11546997
110	16369671	310	16678550	510	6049155	710	3298178	910	1.35E+08
120	17883189	320	10275157	520	15035671	720	9744849	920	50681316
130	1011830	330	13669901	530	13971732	730	33825692	930	13150568
140	3281272	340	56145982	540	4989822	740	21018890	940	2744665
150	3160314	350	2.32E+08	550	5520565	750	18017909	950	15563149
160	7462489	360	1.13E+08	560	2561821	760	20640943	960	14521315
170	3517446	370	1.35E+08	570	3321717	770	41988101	970	23910817
180	6653450	380	15293782	580	1688068	780	66391643	980	31200048
190	7045155	390	52030388	590	3174574	790	1.09E+08	990	28690920
200	1027926	400	5360851	600	905915.7	800	2.69E+08	1000	6297730

CHAPTER 5

NUMERICAL EXPERIMENTS ON THE OPTIMIZATION OF NONLINEAR WAVE AMPLIFICATION EFFICIENCY USING THE BFGS ALGORITHM

5.1 Formulation of the problem

The source term of the stimulus wave, which is the polarization density of the stimulus wave, is dependent on the source term (polarization density) of the high-intensity pump wave. This means that in order to solve for the stimulus wave E_1, we need to solve for the pump wave E_2 as the equations for the stimulus wave and the pump wave are coupled to each other. Therefore, the stimulus wave can be solved by simultaneously solving for the pump wave.

Our goal is to maximize the stimulus wave magnitude at a given stimulus wave frequency $f_{st} = f'$; **max** $|E_1(f_{st} = f')|$. In order to achieve this, we will make a dispersion analysis that is based on the high-intensity pump wave frequency. By sweeping the excitation frequency of the pump wave (f_p) in a large spectral interval that extends from the far-infrared region to the near ultraviolet region, we can investigate the pump wave frequency dependent variation of the maximum stimulus wave magnitude for $f_{st} = f'$, and we can select the optimum pump wave frequency value that maximizes the magnitude of the stimulus wave for $f_{st} = f'$. Mathematically our optimization problem can be stated as:

$$f_{min} < f_p < f_{max} \rightarrow \quad \textbf{max}\,|E_1(f_{st} = f')| \;\; based\ on\ the\ following\ equations$$

$$\nabla^2\big(E_2(f_p)\big) - \mu_0\varepsilon_\infty \frac{\partial^2\left(E_2(f_p)\right)}{\partial t^2} = \mu_0\sigma\frac{\partial\left(E_2(f_p)\right)}{\partial t} + \mu_0\frac{\partial^2 P_2}{\partial t^2} \qquad (109-112)$$

$$\frac{\partial^2 P_2}{\partial t^2} + \gamma\frac{\partial P_2}{\partial t} + {\omega_0}^2(P_2) - \frac{{\omega_0}^2}{Ned}(P_2)^2 + \frac{{\omega_0}^2}{N^2e^2d^2}(P_2)^3 = \frac{Ne^2}{m}\big(E_2(f_p)\big)$$

$$\nabla^2\big(E_1(f_p)\big) - \mu_0\varepsilon_\infty \frac{\partial^2\big(E_1(f_p)\big)}{\partial t^2} = \mu_0\sigma\frac{\partial\big(E_1(f_p)\big)}{\partial t} + \mu_0\frac{\partial^2(P_1)}{\partial t^2}$$

$$\frac{\partial^2(P_1)}{\partial t^2} + \gamma\frac{\partial(P_1)}{\partial t} + {\omega_0}^2(P_1) - \frac{{\omega_0}^2}{Ned}\{{P_1}^2 + 2P_1P_2\} + \frac{{\omega_0}^2}{N^2e^2d^2}\{{P_1}^3 + 3{P_1}^2P_2 + 3P_1{P_2}^2\} = \frac{Ne^2}{m}(E_1(f_p))$$

Where

$$E_2\big(x = x_{input}, t\big) = A_p\cos\big(2\pi f_p t + \psi_p\big)\big(u(t) - u\big(t - \Delta T_p\big)\big)\frac{V}{m}$$

$$E_1\big(x = x_{input}, t\big) = A_{st}\cos(2\pi f_{st} t + \psi_{st})\,\big(u(t) - u(t - \Delta T_{st})\big)\frac{V}{m}$$

$$A_p \gg A_{st}, \qquad \Delta T_p \ll \Delta T_{st}$$

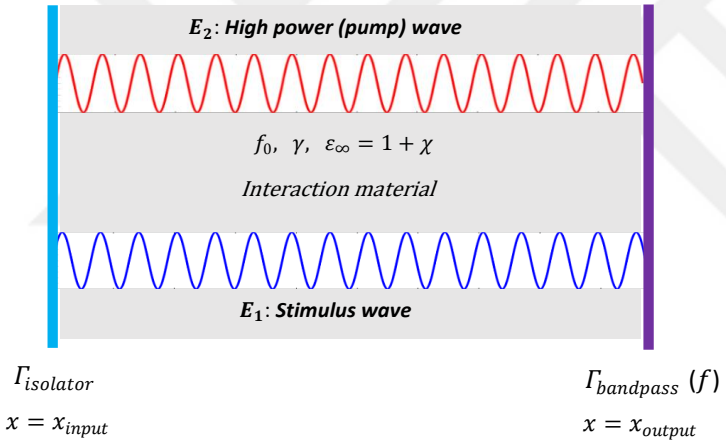

Figure 5.1 Configuration of the cavity.

If we are using N ultrashort high-intensity pulse excitations to amplify the low-intensity stimulus wave:

$$E_1\big(x = x_{input}, t\big) = \sum_{i=1}^{N} A_i\cos(2\pi f_i t + \psi_i)\,\big(u(t) - u(t - \Delta T_i)\big)\ V/m$$

$$E_2(x = x_{input}, t) = A_{st}\cos(2\pi(f_{st})t + \psi_{st})\big(u(t) - u(t - \Delta T_{st})\big)\ V/m$$

Where $A_i \gg A_{st},\ \Delta T_i \ll \Delta T_{st},\ i = 1,2,\dots,N$

Then the dispersion analysis-based optimization problem is stated as follows:

$$\boldsymbol{f_p} = \{ f_1 , f_2 , \dots , f_N \}$$

$$\boldsymbol{f_{min}} = \{ f_{min,1} , f_{min,2} , \dots , f_{min,N} \}, \qquad \boldsymbol{f_{max}} = \{ f_{max,1} , f_{max,2} , \dots , f_{max,N} \}$$

$$\boldsymbol{f_{min}} < \boldsymbol{f_p} < \boldsymbol{f_{max}} ; \quad \textbf{max} \, |E_1(f_{st} = f')| \;\; based\ on\ the\ following\ equations$$

$$\nabla^2\big(E_2(\boldsymbol{f_p})\big) - \mu_0 \varepsilon_\infty \frac{\partial^2 \left(E_2(\boldsymbol{f_p})\right)}{\partial t^2} = \mu_0 \sigma \frac{\partial \left(E_2(\boldsymbol{f_p})\right)}{\partial t} + \mu_0 \frac{\partial^2 P_2}{\partial t^2} \qquad (113-116)$$

$$\frac{\partial^2 P_2}{\partial t^2} + \gamma \frac{\partial P_2}{\partial t} + {\omega_0}^2 (P_2) - \frac{{\omega_0}^2}{Ned} (P_2)^2 + \frac{{\omega_0}^2}{N^2 e^2 d^2} (P_2)^3 = \frac{Ne^2}{m} \big(E_2(\boldsymbol{f_p})\big)$$

$$\nabla^2\big(E_1(\boldsymbol{f_p})\big) - \mu_0 \varepsilon_\infty \frac{\partial^2 \big(E_1(\boldsymbol{f_p})\big)}{\partial t^2} = \mu_0 \sigma \frac{\partial \big(E_1(\boldsymbol{f_p})\big)}{\partial t} + \mu_0 \frac{\partial^2 (P_1)}{\partial t^2}$$

$$\frac{\partial^2 (P_1)}{\partial t^2} + \gamma \frac{\partial (P_1)}{\partial t} + {\omega_0}^2 (P_1) - \frac{{\omega_0}^2}{Ned} \{ {P_1}^2 + 2 P_1 P_2 \} + \frac{{\omega_0}^2}{N^2 e^2 d^2} \{ {P_1}^3 + 3 {P_1}^2 P_2 + 3 P_1 {P_2}^2 \} = \frac{Ne^2}{m} (E_1(\boldsymbol{f_p}))$$

Note that in this case the pump wave is comprised of N ultrashort pulses instead of a single ultrashort pulse. Therefore, we have a multiparameter optimization problem.

The physics behind the efficient amplification of the stimulus wave involves the simultaneous maximization of the stored electric energy density and the polarization density originated by the pump wave in the resonator. This can be explained in two steps, first we need to maximize the stored energy in the cavity in order to transfer a high amount of energy to the stimulus wave. Second, we need to maximize the polarization density of the pump wave, which acts as the energy coupling coefficient based on Eq.116.

Even if we maximize the stored electric energy density in a resonator, if the nonlinear coupling coefficient P_2 is not high, then we cannot efficiently transfer the accumulated energy into the stimulus wave and high-gain amplification of the stimulus wave does not occur. In order to perform the optimization of the stimulus wave magnitude at a given stimulus wave frequency ($\textbf{max} \, |E_1(f_{st} = f')|$), we need an efficient optimization algorithm. In the next section, we will use the computationally efficient Quasi-Newton

BFGS algorithm to perform the maximization of the stimulus wave magnitude at a desired frequency.

5.2. Optimization of optical parametric amplification gain factor in a micro-resonator

Assume that we are using N ultrashort high-power pulses to amplify the stimulus wave. These ultrashort pulses have similar pulse energies so that each of them affects the amplification performance in the same degree. The ultrashort high-power pulses are summed up to form the pump wave. At a given spatial input point, the pump wave and the stimulus wave are given as

$$E_p\big(x = x_{input}, t\big) = \sum_{i=1}^{N} A_i \cos(2\pi\nu_i t + \psi_i)\,\big(u(t) - u(t - \Delta T_i)\big)\ V/m$$

$$E_{st}(x = x_{input}, t) = A_{st}\cos(2\pi(\nu_{st})t + \psi_{st})\big(u(t) - u(t - \Delta T_{st})\big)\ V/m$$

Where $A_i \gg A_{st},\ \Delta T_i \ll \Delta T_{st},\ i = 1,2,\dots,N$

We want to tune the frequencies $(\nu_1, \nu_2, \dots, \nu_N)$ of these ultrashort pulses so that the gain factor is maximized. In order to do that, we use the Broyden-Fletcher-Goldfarb-Shanno (BFGS) algorithm, so that the Hessian matrix of each iteration is recursively updated. The BFGS algorithm is one of the Quasi-Newton Methods that are used to compute the Hessian matrix. Recursive computation reduces the computational cost of the optimization by eliminating the need to compute the second derivative at each iteration. We will use the BFGS algorithm because of its accuracy and simplicity. The most general form of the Quasi-Newton method is given as [20]

$$\boldsymbol{x^{(k)}} = \boldsymbol{x^{(k-1)}} - \alpha_k\big(\boldsymbol{H}^{(k-1)}\big)^{-1}(\boldsymbol{\nabla} f\big(\boldsymbol{x}^{(k-1)}\big),\quad k = 1,2,3,\dots \qquad (117)$$

$f\big(\boldsymbol{x}^{(k-1)}\big)$: $Cost\ function$, $\boldsymbol{x}^{(k)}$: $Optimization\ parameters$, $\boldsymbol{H}^{(k-1)}$: $Hessian\ matrix$, α_k: $Step\ size$

Quasi-Newton methods, like steepest descent, require only the gradient of the objective function to be supplied at each iteration. The Hessian is updated by analyzing successive gradient vectors. The whole BFGS algorithm is as described below [20]:

Given a starting point x_0, convergence tolerance ε>0, inverse Hessian approximation H_0;

$$k \leftarrow 0;$$

while $\|\nabla f_k\| > \varepsilon;$

Compute search direction

$p_k = -H_k \nabla f_k;$

Set $x_{k+1} = x_k + \alpha_k p_k$ *where* α_k *is computed from a line search procedure to satisfy the Wolfe conditions.*

Define $s_k = x_{k+1} - x_k$ *and* $y_k = \nabla f_{k+1} - \nabla f_k;$

Compute H_{k+1} *using;*

$H_{k+1} = (I - \rho_k s_k y_k{}^T) H_k (I - \rho_k y_k s_k{}^T) + \rho_k s_k s_k{}^T$ *(BFGS)*

Where $\rho_k = \frac{1}{y_k{}^T s_k}$

$$k \leftarrow k + 1;$$

end (while)

The step size α_k can be computed from a line search procedure to satisfy the *Wolfe conditions*:

$$f(x_k + \alpha_k p_k) \leq f(x_k) + c_1 \alpha_k \nabla f_k{}^T p_k \qquad (118\text{-}119)$$

$$|\nabla f(x_k + \alpha_k p_k)^T p_k| \leq c_2 |\nabla f_k{}^T p_k| \qquad 0 < c_1 < c_2 < 1$$

Alternatively, the step size α_k can be computed from the so-called *Backtracking Approach:*

Choose $\alpha > 0$, $\rho \in (0,1)$, $c \in (0,1)$

repeat until $f(x_k + \alpha p_k) \leq f(x_k) + c\alpha \nabla f_k{}^T p_k$

$$\alpha \leftarrow \rho\alpha$$

end

Since our problem is the amplification of a stimulus (input) wave via nonlinear wave mixing with a high-power pump wave, for this problem, the optimization parameters are the frequencies of the N ultrashort pulses $\nu_1, \nu_2, \dots, \nu_N$ that constitute the total pump wave. Assume that E_1 is the low power stimulus wave to be amplified, and E_2 is the high-power pump wave, which is the combination of N ultrashort pulses. The general formulation for the maximization of the stimulus wave magnitude (gain factor) is summarized as follows:

Optimization parameters: $\boldsymbol{\nu} = [\nu_1, \nu_2, \dots, \nu_N]$, **Cost function to be maximized**: $f = |E_1(\boldsymbol{\nu})|$

Constraints: $g_1(\boldsymbol{\nu}) \le c_1,\ g_2(\boldsymbol{\nu}) \le c_2, \dots,\ g_N(\boldsymbol{\nu}) \le c_N$

Equations:

$$\nabla^2(E_2(\boldsymbol{\nu})) - \mu_0\varepsilon_\infty \frac{\partial^2\big(E_2(\boldsymbol{\nu})\big)}{\partial t^2} = \mu_0\sigma \frac{\partial\big(E_2(\boldsymbol{\nu})\big)}{\partial t} + \mu_0 \frac{d^2P_2}{\partial t^2} \qquad (120-123)$$

$$\frac{d^2P_2}{dt^2} + \gamma\frac{dP_2}{dt} + {\omega_0}^2P_2 - \frac{{\omega_0}^2{P_2}^2}{Ned} + \frac{{\omega_0}^2{P_2}^3}{N^2e^2d^2} = \frac{Ne^2(E_2(\boldsymbol{\nu}))}{m}$$

$$\nabla^2(E_1(\boldsymbol{\nu})) - \mu_0\varepsilon_\infty \frac{\partial^2\big(E_1(\boldsymbol{\nu})\big)}{\partial t^2} = \mu_0\sigma \frac{\partial\big(E_1(\boldsymbol{\nu})\big)}{\partial t} + \mu_0 \frac{d^2(P_1)}{\partial t^2}$$

$$\frac{d^2(P_1)}{dt^2} + \gamma\frac{d(P_1)}{dt} + {\omega_0}^2(P_1) - \frac{{\omega_0}^2({P_1}^2 + 2P_1P_2)}{Ned} + \frac{{\omega_0}^2({P_1}^3 + 3{P_1}^2P_2 + 3P_1{P_2}^2)}{N^2e^2d^2} = \frac{Ne^2\big(E_1(\boldsymbol{\nu})\big)}{m}$$

This problem is a constrained optimization problem, we can convert this problem into an unconstrained optimization problem by modifying the cost function via the addition of *penalty functions*. In the case of a maximization problem, these penalty functions yield a decrease in the cost function when the constraints are violated. In our case, the penalty for violating the constraints is adjusted to yield a quadratic decrease.

Augmented cost function: (Penalty function method)

$$f = |E_1(\boldsymbol{\nu})| - L\left\{\sum_{i=1}^{N} \delta_i\,(g_i(\boldsymbol{\nu}) - c_i)\right\}^q, \qquad \delta_i = \begin{cases} 0 & if\ \ g_i(\boldsymbol{\nu}) \le c_i \\ > 0 & if\ \ g_i(\boldsymbol{\nu}) > c_i \end{cases} \qquad (124)$$

q: Positive valued penalty exponent, L: Positive valued penalty constant, δ_i: Penalty coefficients

Optimization process:

$$\boldsymbol{v}_{k+1} = \boldsymbol{v}_k + \alpha_k \, \boldsymbol{p}_k$$

$$\boldsymbol{p}_k = -\boldsymbol{H}_k \, \boldsymbol{\nabla f}_k \quad , \quad \boldsymbol{s_k} = \boldsymbol{v_{k+1}} - \boldsymbol{v_k} \quad , \quad \boldsymbol{y_k} = \boldsymbol{\nabla f_{k+1}} - \boldsymbol{\nabla f_k}$$

$$\boldsymbol{H_{k+1}} = \left(\boldsymbol{I} - \rho_k \boldsymbol{s_k} \boldsymbol{y_k}^{\boldsymbol{T}}\right) \boldsymbol{H_k} \left(\boldsymbol{I} - \rho_k \boldsymbol{y_k} \boldsymbol{s_k}^{\boldsymbol{T}}\right) + \rho_k \boldsymbol{s_k} \boldsymbol{s_k}^{\boldsymbol{T}} \quad \textit{(BFGS)}$$

$$\boldsymbol{\nabla f} = \begin{bmatrix} \dfrac{f(v_1 + \epsilon, v_2, \dots, v_N) - f(v_1, v_2, \dots, v_N)}{\epsilon} \\ \dfrac{f(v_1, v_2 + \epsilon, \dots, v_N) - f(v_1, v_2, \dots, v_N)}{\epsilon} \\ \vdots \\ \dfrac{f(v_1, v_2, \dots, v_N + \epsilon) - f(v_1, v_2, \dots, v_N)}{\epsilon} \end{bmatrix} \quad , \quad \rho_k = \frac{1}{\boldsymbol{y_k}^{\boldsymbol{T}} \boldsymbol{s_k}}$$

The convergence rate of the BFGS algorithm is super-linear, but our formulated problem is a nonlinear optimization problem (nonlinear programming). Therefore, the convergence is not reached immediately. Furthermore, the recursive computation of the Hessian matrix slows down the convergence rate. For these reasons, the computation of the optimum frequency values takes a great amount of time.

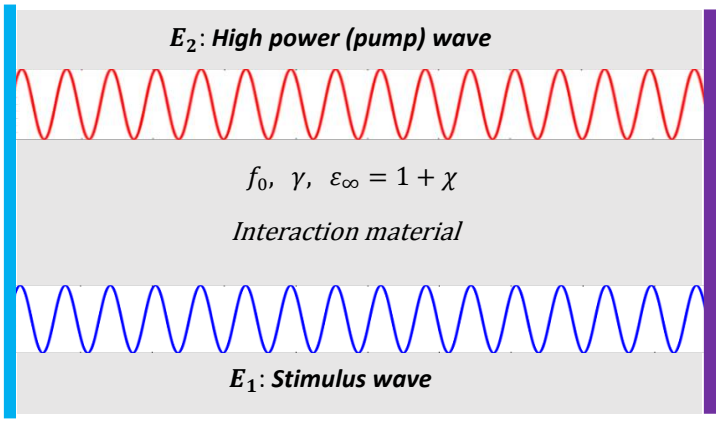

Figure 5.2 Configuration of the cavity

5.3. Finite difference time domain formulation-based solution of the gain factor optimization problem in optical parametric amplification

We can discretize equations (120-123) using the finite difference time domain (FDTD) method as shown in equations (125-128) at each iteration k of the optimization problem. Our first aim is to discretize equations (120,123) and solve for $E_{2,k}(i,j+1)$ i.e. the value of $E_{2,k}$ at a given point at the next time step. Since $E_{2,k}$ is coupled to $P_{2,k}$, we first solve for $P_{2,k}(i,j+1)$ and then substitute it into the equation for $E_{2,k}(i,j+1)$. We keep on solving these two equations iteratively for all time steps and for all points in the spatial domain of a given one dimensional problem. For a higher accuracy of the resulting solution, we choose Δt and Δx as small as possible [11,12]. Then we discretize equations (7a,7b) and substitute the value of $P_{2,k}(i,j)$ obtained from equations (120,121) to solve for $E_{1,k}(i,j+1)$ in equations (122,123). Finally, we modify the values of the optimization parameters based on the BFGS algorithm, and we repeat this procedure for each iteration of the optimization process until the desired gain factor is attained.

***FDTD Equations*:** (125-128)

$$\frac{E_{2,k}(i+1,j)-2E_{2,k}(i,j)+E_{2,k}(i-1,j)}{\Delta x^2}-\mu_0\varepsilon_\infty(i,j)\frac{E_{2,k}(i,j+1)-2E_{2,k}(i,j)+E_{2,k}(i,j-1)}{\Delta t^2}$$
$$=\mu_0\sigma(i,j)\frac{E_{2,k}(i,j)-E_{2,k}(i,j-1)}{\Delta t}+\mu_0\frac{P_{2,k}(i,j+1)-2P_{2,k}(i,j)+P_{2,k}(i,j-1)}{\Delta t^2}$$

$$\frac{P_{2,k}(i,j+1)-2P_{2,k}(i,j)+P_{2,k}(i,j-1)}{\Delta t^2}+\gamma\frac{P_{2,k}(i,j)-P_{2,k}(i,j-1)}{\Delta t}+4\pi^2{f_0}^2\left(P_{2,k}(i,j)\right)$$
$$-\frac{4\pi^2{f_0}^2}{Ned}\left(P_{2,k}(i,j)\right)^2+\frac{4\pi^2{f_0}^2}{N^2e^2d^2}\left(P_{2,k}(i,j)\right)^3=\frac{Ne^2}{m}\left(E_{2,k}(i,j)\right).$$

$$\frac{E_{1,k}(i+1,j)-2E_{1,k}(i,j)+E_{1,k}(i-1,j)}{\Delta x^2}-\mu_0\varepsilon_\infty(i,j)\frac{E_{1,k}(i,j+1)-2E_{1,k}(i,j)+E_{1,k}(i,j-1)}{\Delta t^2}$$
$$=\mu_0\sigma(i,j)\frac{E_{1,k}(i,j)-E_{1,k}(i,j-1)}{\Delta t}+\mu_0\frac{P_{1,k}(i,j+1)-2P_{1,k}(i,j)+P_{1,k}(i,j-1)}{\Delta t^2}$$

$$\frac{P_{1,k}(i,j+1)-2P_{1,k}(i,j)+P_{1,k}(i,j-1)}{\Delta t^2}+\gamma\frac{P_{1,k}(i,j)-P_{1,k}(i,j-1)}{\Delta t}+4\pi^2{f_0}^2\left(P_{1,k}(i,j)\right)$$
$$-\frac{4\pi^2{f_0}^2}{Ned}\left\{\left(P_{1,k}(i,j)\right)^2+2P_{1,k}(i,j)P_{2,k}(i,j)\right\}+\frac{4\pi^2{f_0}^2}{N^2e^2d^2}\{\left(P_{1,k}(i,j)\right)^3$$
$$+3\left(P_{1,k}(i,j)\right)^2P_{2,k}(i,j)\ \ +3P_{1,k}(i,j)\left(P_{2,k}(i,j)\right)^2\}=\frac{Ne^2}{m}(E_{1,k}(i,j)).$$

x: Spatial coordinate, t: Time, k: Iteration number, $E_k(\mathrm{x},\mathrm{t}) = E_k(\mathrm{i}\Delta\mathrm{x}, \mathrm{j}\Delta\mathrm{t}) \rightarrow E_k(\mathrm{i},\mathrm{j})$

$E_{2,k}$: *High intensity pump wave at iteration k*

$E_{1,k}$: *Stimulus wave at iteration k*

Cost function: $|E_1(\boldsymbol{v})|$

Augmented cost function: (Penalty function method)

$$f = |E_1(\boldsymbol{v})| + L_1\left\{\sum_{i=1}^{N} \delta_i \left(g_i(\boldsymbol{v}) - c_i\right)^2\right\} + L_2\left\{\sum_{j=1}^{M} \zeta_j \left(b_j(\boldsymbol{v}) - a_j\right)^2\right\}$$

$$\delta_i = \begin{cases} 0 & if \quad g_i(\boldsymbol{v}) \le c_i \\ > 0 & if \quad g_i(\boldsymbol{v}) > c_i \end{cases}, \quad \zeta_j \neq 0 \quad if \quad b_j(\boldsymbol{v}) \neq a_j$$

Iterations:

$$\boldsymbol{v}_{k+1} = \boldsymbol{v}_k + \alpha_k \, \boldsymbol{p}_k$$

$$\boldsymbol{p}_k = -\boldsymbol{H}_k \, \boldsymbol{\nabla f}_k$$

$$\boldsymbol{s_k} = \boldsymbol{x_{k+1}} - \boldsymbol{x_k}$$

$$\boldsymbol{y_k} = \boldsymbol{\nabla f_{k+1}} - \boldsymbol{\nabla f_k}$$

$$\boldsymbol{H_{k+1}} = \left(\boldsymbol{I} - \rho_k \boldsymbol{s_k y_k}^{\boldsymbol{T}}\right)\boldsymbol{H_k}\left(\boldsymbol{I} - \rho_k \boldsymbol{y_k s_k}^{\boldsymbol{T}}\right) + \rho_k \boldsymbol{s_k s_k}^{\boldsymbol{T}} \quad (BFGS)$$

$$\rho_k = \frac{1}{\boldsymbol{y_k}^{\boldsymbol{T}} \boldsymbol{s_k}}$$

Wolfe conditions for α_k :

$$f(x_k + \alpha_k \, p_k) \le f(x_k) + c_1 \, \alpha_k \nabla {f_k}^T p_k$$

$$\left|\nabla f(x_k + \alpha_k \, p_k)^T p_k\right| \le c_2 \left|\nabla {f_k}^T p_k\right| \qquad 0 < c_1 < c_2 < 1$$

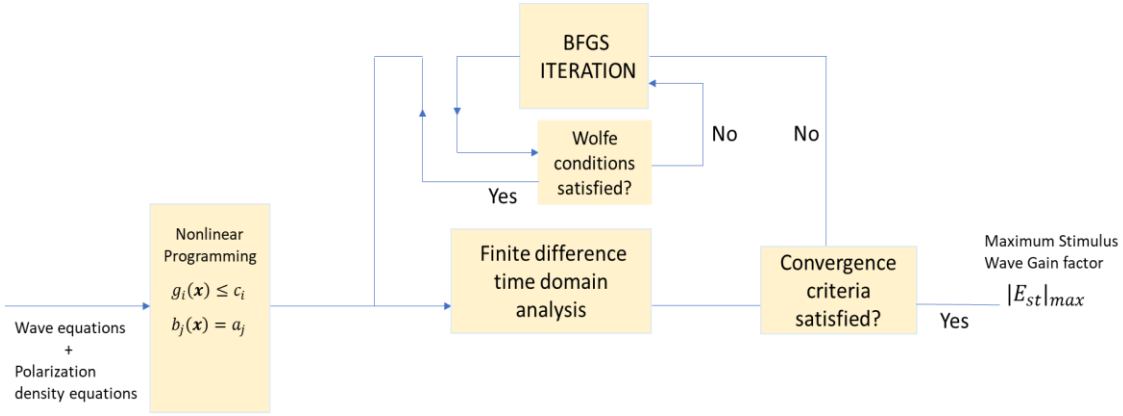

Figure 5.3 Flowchart diagram of BFGS based nonlinear programming in FDTD analysis.

5.4 Numerical experiment

5.4.1. Double frequency tuning for gain factor optimization

Assume that a 250 THz infrared stimulus wave E_{st} and a high power pump wave E_{hp} that is composed of two high-intensity ultrashort pulses (frequencies are to be determined) are propagating inside a low-loss (high Q) cavity that has two reflecting walls. The reflecting wall on the left side can be thought as an optical isolator and has a reflection coefficient of $\Gamma_1 \approx 1$, the one on the right side represents an optical band-pass filter with a frequency dependent reflection coefficient $\Gamma(f)$. Both waves are generated at x=0 μm, at the time instant t=0 s. The waves and the parameters of the gain medium are as given below:

$$E_{hp}(x = 0\ \mu m, t) = \sum_{i=1}^{2} A_i \cos(2\pi f_i t + \psi_i)\left(u(t) - u(t - \Delta T_i)\right) \quad V/m$$

Where $A_1 = 2 \times 10^8,\ A_2 = 1.5 \times 10^8,\ \psi_1 = 0,\ \psi_2 = 0,\ \Delta T_1 = 0.5\ ps,\ \Delta T_2 = 1\ ps$

$E_{st}(x = 0\mu m, t) = 1 \times \sin(2\pi(2.5 \times 10^{14})t)\ \ V/m,\ \ for\ \ 0 \le t \le 10\ ps$

$Dielectric\ constant\ of\ the\ gain\ medium = \ \varepsilon_\infty = 1 + \chi = 12 \quad (\mu_r = 1)$

$Resonance\ frequency\ of\ the\ gain\ medium:\ f_0 = 500\ THz$

$Damping\ coefficient\ of\ the\ gain\ medium:\ \gamma = 1 \times 10^9\ Hz$

$Time\ interval\ and\ duration\ of\ simulation:\ 0 \le t \le 10\ ps$

$Spatial\ range\ of\ the\ gain\ medium: 0\ \mu m < x < 10\ \mu m$

$Right\ cavity\ wall\ location:\ x = 10\ \mu m\ \ ;\ \ Left\ cavity\ wall\ location:\ x = 0\ \mu m$

$Electron\ density\ of\ the\ gain\ medium:\ N = 3.5 \times 10^{28}/m^3\ \ ;\ \ Atomic\ diameter:$
$d = 0.3\ nm$

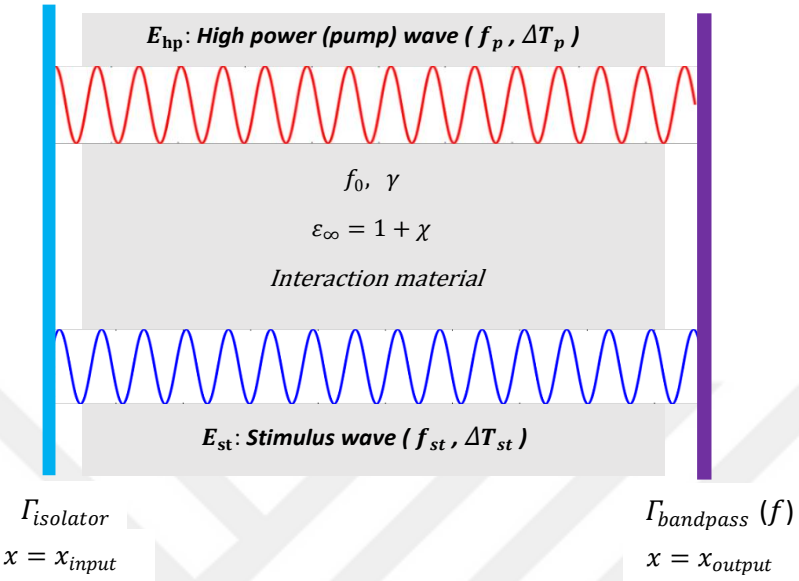

Figure 5.4 Configuration of the cavity and the parameters for subsection 5.4.1.

Our problem: Find the optimum pump wave pulse frequencies f_{p1}, f_{p2} that maximize the magnitude of the monochromatic stimulus wave in the cavity ($|E_{st}(f_{st} = 250\,THz)|$), in the cavity, for 10 THz $< \{f_{p1}, f_{p2}\} < 1000\,THz$ (THz to UV), and for $0\,\mu m < x < 10\,\mu m,\ 0 \le t \le 10\,ps$, such that

$$\nabla^2 E_{hp}(f_{p1}, f_{p2}) - \mu_0 \varepsilon_\infty \frac{\partial^2 E_{hp}(f_{p1}, f_{p2})}{\partial t^2} = \mu_0 \sigma \frac{\partial E_{hp}(f_{p1}, f_{p2})}{\partial t} + \mu_0 \frac{\partial^2 P_{hp}}{\partial t^2}.$$

$$\frac{\partial^2 P_{hp}}{\partial t^2} + \gamma \frac{\partial P_{hp}}{\partial t} + {\omega_0}^2 (P_{hp}) - \frac{{\omega_0}^2}{Ned} (P_{hp})^2 + \frac{{\omega_0}^2}{N^2 e^2 d^2} (P_{hp})^3 = \frac{Ne^2}{m} E_{hp}(f_{p1}, f_{p2}).$$

$$\nabla^2 E_{st}(f_{p1}, f_{p2}) - \mu_0 \varepsilon_\infty \frac{\partial^2 E_{st}(f_{p1}, f_{p2})}{\partial t^2} = \mu_0 \sigma \frac{\partial E_{st}(f_{p1}, f_{p2})}{\partial t} + \mu_0 \frac{\partial^2 P_{st}}{\partial t^2}.$$

$$\frac{\partial^2 (P_{st})}{\partial t^2} + \gamma \frac{\partial (P_{st})}{\partial t} + {\omega_0}^2 (P_{st}) - \frac{{\omega_0}^2}{Ned} \{{P_{st}}^2 + 2 P_{st} P_{hp}\} + \frac{{\omega_0}^2}{N^2 e^2 d^2} \{{P_{st}}^3 + 3 {P_{st}}^2 P_{hp} + 3 P_{st} {P_{hp}}^2\}$$
$$= \frac{Ne^2}{m} E_{st}(f_{p1}, f_{p2})$$

Our aim is to maximize the magnitude of the stimulus wave at its original frequency $f_{st} = 250\,THz$ (monochromatic form). This is a precaution against any degree of spectral broadening that the stimulus wave may go through while being amplified. Therefore, our cost function is chosen as (at any spatial point $x = x'$ inside the cavity)

$$Q = |E_{st}(f_{st} = 250\ THz)| = \left| \int_{2.5\times10^{14}-\Delta f}^{2.5\times10^{14}+\Delta f} \left\{ \int_{0}^{\Delta T} \{E_{st}(x = x', t)\, e^{-i(2\pi\Omega)t}\} dt \right\} e^{i(2\pi\Omega)t} d\Omega \right|$$

$$where\ \Delta T = 10\ ps, \quad 0 \le t \le 10\ ps, \quad (2.5\times10^{14} - \Delta f) < \Omega < (2.5\times10^{14} + \Delta f), \quad \Delta f = 1\ THz$$

Initial conditions:

$$P_{hp}(x,0) = P_{hp}{}'(x,0) = E_{hp}(x,0) = E_{hp}{}'(x,0) = P_{st}(x,0) = P_{st}{}'(x,0) = E_{st}(x,0) = E_{st}{}'(x,0) = 0$$

Boundary and excitation conditions:

$$E_{hp}(x = 0\mu m, t) = \sum_{i=1}^{2} A_i \cos(2\pi f_i t + \psi_i)\left(u(t) - u(t - \Delta T_i)\right) \quad V/m$$

Where $A_1 = 2\times10^{14},\ A_2 = 1.5\times10^{14},\ \psi_1 = 0,\ \psi_2 = 0,\ \Delta T_1 = 0.5\ ps,\ \Delta T_2 = 1\ ps$

$$E_{st}(x = 0\ \mu m, t) = 1 \times \sin(2\pi(2.5\times10^{14})t)\ \ V/m,\ \ for\ \ 0 \le t \le 10\ ps$$

$$E_{hp}(x = 15\ \mu m, t) = E_{st}(x = 15\ \mu m, t) = 0, \quad for\ 0 < t < 10ps$$

Absorbing boundary condition (perfectly matched layer):

$$\sigma(x) = \{\ (x - (L - \Delta))\sigma_0\ ,\ \ (L - \Delta) \le\ x < L\ \ \},\ for\ L = 15\ \mu m,\ \ \Delta = 2.5\ \mu m,\ \sigma_0 = 4.5\times10^8\ S/m$$

Optical isolator condition: Full reflection at x = 0 μm

$$\Gamma(x = 0\mu m, t) = 1 \quad (Reflection\ coefficient\ is\ equal\ to\ 1)$$

Optical bandpass filter condition: Frequency dependent reflection at x = 10 μm

$$|\Gamma(f')| = 1 - e^{-\left(\frac{(f' - 250THz)}{\sqrt{2}THz}\right)^2}$$

Cost function to be maximized: $Q(f_{p1}, f_{p2}) = |E_{st}(f_{st} = 250\ THz)| - \delta_1\left(f_{p1} - f_{max}\right)^2 - \delta_2\left(f_{min} - f_{p1}\right)^2 - \delta_3\left(f_{p2} - f_{max}\right)^2 - \delta_4\left(f_{min} - f_{p2}\right)^2$

Where:

$$\delta_1 = \begin{Bmatrix} 0 & if\ \ f_{p1} \le f_{max} \\ \frac{|E_{st}(f_{st}=250THz)|}{10^{27}} & if\ \ f_{p1} > f_{max} \end{Bmatrix}, \quad \delta_2 = \begin{Bmatrix} 0 & if\ \ f_{p1} \ge f_{min} \\ \frac{|E_{st}(f_{st}=250THz)|}{10^{27}} & if\ \ f_{p1} < f_{min} \end{Bmatrix}$$

$$\delta_3 = \begin{Bmatrix} 0 & if\ \ f_{p2} \le f_{max} \\ \frac{|E_{st}(f_{st}=250THz)|}{10^{27}} & if\ \ f_{p2} > f_{max} \end{Bmatrix}, \quad \delta_4 = \begin{Bmatrix} 0 & if\ \ f_{p2} \ge f_{min} \\ \frac{|E_{st}(f_{st}=250THz)|}{10^{27}} & if\ \ f_{p2} < f_{min} \end{Bmatrix}$$

Optimization algorithm (BFGS):

$$Set\ \ \boldsymbol{H_1} = \begin{bmatrix} 1 & 0 \\ 0 & 1 \end{bmatrix}, f_{p1,0} = 100\ THz,\ f_{p1,1} = 102\ THz,$$

$$f_{p2,0} = 100\ THz, \qquad f_{p2,1} = 103\ THz, \qquad \alpha_1 = 0.5$$

$$\boldsymbol{\nabla Q}_k = \begin{bmatrix} \dfrac{Q(f_{p1,k}, f_{p2,k}) - Q(f_{p1,k-1}, f_{p2,k})}{f_{p1,k} - f_{p1,k-1}} \\ \dfrac{Q(f_{p1,k}, f_{p2,k}) - Q(f_{p1,k}, f_{p2,k-1})}{f_{p2,k} - f_{p2,k-1}} \end{bmatrix}$$

$$\boldsymbol{p}_k = -\boldsymbol{H}_k \boldsymbol{\nabla Q}_k$$

$$\boldsymbol{f}_{p,k+1} = \boldsymbol{f}_{p,k} + \alpha_k \boldsymbol{p}_k\ , \quad \boldsymbol{f}_{p,k} = \begin{bmatrix} f_{p1,k} \\ f_{p2,k} \end{bmatrix}$$

$$\boldsymbol{s}_k = \boldsymbol{f}_{p,k+1} - \boldsymbol{f}_{p,k}$$

$$\boldsymbol{\nabla Q}_{k+1} = \begin{bmatrix} \dfrac{Q(f_{p1,k+1}, f_{p2,k}) - Q(f_{p1,k}, f_{p2,k})}{f_{p1,k+1} - f_{p1,k}} \\ \dfrac{Q(f_{p1,k}, f_{p2,k+1}) - Q(f_{p1,k}, f_{p2,k})}{f_{p2,k+1} - f_{p2,k}} \end{bmatrix}$$

$$\boldsymbol{y}_k = \boldsymbol{\nabla Q}_{k+1} - \boldsymbol{\nabla Q}_k$$

$$\rho_k = \frac{1}{\boldsymbol{y}_k{}^T \boldsymbol{s}_k}$$

$$\boldsymbol{H}_{k+1} = (\boldsymbol{I} - \rho_k \boldsymbol{s}_k \boldsymbol{y}_k{}^T)\boldsymbol{H}_k(\boldsymbol{I} - \rho_k \boldsymbol{y}_k \boldsymbol{s}_k{}^T) + \rho_k \boldsymbol{s}_k \boldsymbol{s}_k{}^T \quad \textit{(BFGS)}$$

$$\boldsymbol{I}: Identity\ matrix$$

In order to satisfy the Wolfe conditions, the step size at each iteration is chosen as

$$\alpha_k = C^{\left(\log\left|\frac{Q(\boldsymbol{f_{p,k}})}{Q(\boldsymbol{f_{p,k}}) - Q(\boldsymbol{f_{p,k-1}})}\right|\right) / \left(\left|\frac{Q(\boldsymbol{f_{p,k}})}{Q(\boldsymbol{f_{p,k}}) - Q(\boldsymbol{f_{p,k-1}})}\right|\right)} \qquad (129)$$

Where C is just a constant ($1 < C < 1.5$) and α_k is the step size at iteration k. This formula (Eq.129) was determined by trial and error and was found to satisfy the Wolfe's conditions automatically at each iteration. This saves us from the huge computational cost of running another iteration loop to determine the step size at each iteration of the optimization process. In this simulation C=1.445. Based on the above formulations, the maximum

stimulus wave amplitude that has been reached in the cavity (for 0<t<10ps) is determined as $Gain_{max} = |E_{st}(\, f_{st} = 250\, THz)|_{max} = 4.67 \times 10^8\, V/m$, which corresponds to $f_{p1} = 387.2\, THz,\ f_{p2} = 319.4\, THz$ (see Table 5.1).

$$W_{e,p} = Stored\ electric\ energy\ density\ via\ pump\ wave$$
$$= \frac{1}{2}\varepsilon_\infty {E_{pump}}^2 + \frac{1}{2} E_{pump} P_{pump}.\ (\frac{Joules}{m^3})$$

P_{pump}: $Polarization\ density\ created\ by\ the\ pump\ wave\ (\frac{Coulomb}{m^2})$

E_{pump}: $Pump\ wave\ electric\ field\ intensity,\ \ \varepsilon_\infty$: $Background\ permittivity$

Table 5.1: BFGS algorithm-based optimization process

f_{p1}	f_{p2}	$Gain_{max}$	$W_{e,p}\ (\frac{J}{m^3})$	$P_{pump}(\frac{C}{m^2})$	k (iteration #)
100THz	100THz	0.84	1.29×10^7	0.08	1
107.2THz	115.7THz	6.23	1.80×10^7	0.09	4
154.9THz	156.6THz	4.44	3.36×10^7	0.08	7
218.6THz	199.5THz	313.52	4.48×10^7	0.10	10
198.3THz	214.5THz	37.16	1.67×10^7	0.10	13
229.5THz	243.0THz	240.58	5.97×10^7	0.09	16
263.1THz	227.2THz	646.72	5.54×10^7	0.10	19
322.7THz	278.9THz	1.57×10^3	6.12×10^7	0.12	22
396.0THz	299.8THz	4.28×10^4	9.39×10^8	0.15	25
391.6THz	293.4THz	9.16×10^4	1.76×10^8	0.16	28
380.7THz	311.7THz	3.85×10^5	1.26×10^8	0.20	30
383.4THz	317.2THz	8.11×10^4	6.40×10^7	0.20	32
386.0THz	318.4THz	6.32×10^6	2.89×10^8	0.23	34
386.8THz	318.8THz	9.79×10^7	2.63×10^8	0.27	36
387.2THz	319.3THz	3.96×10^8	2.51×10^8	0.29	38
387.2THz	319.4THz	4.67×10^8	2.95×10^8	0.29	39

As we can see from Table 5.1, the optimum ultrashort pulse frequencies correspond to a very high stored electric energy density and a high polarization density. The stored electric energy density and the polarization density must be simultaneously high for a significant stimulus wave amplification. The stored electric energy density indicates the achievable order of stimulus wave amplification [13,14], and the polarization density acts as a

coupling coefficient, which is a measure of how much stored electric energy can be coupled to the stimulus wave.

The time variation of the spectrally broadened (polychromatic) stimulus wave between t=6.6 picoseconds and t=10 picoseconds is shown in Figure 5.5. From the figure, we can see that the polychromatic stimulus wave reaches an amplitude of approximately $8 \times 10^8\ V/m$.

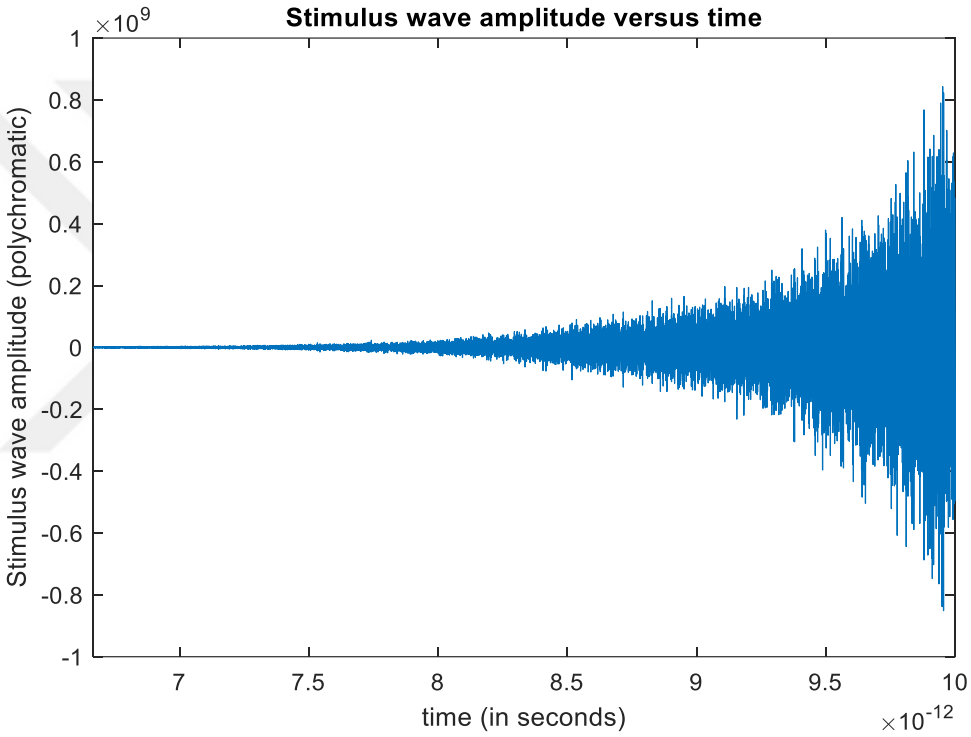

Figure 5.5 Stimulus wave amplification (in polychromatic form) inside the cavity at x= 5.73µm

CHAPTER 6

SUPER-GAIN PARAMETRIC AMPLIFICATION IN MULTIRESONANT OPTICAL MICROCAVITIES VIA NON-LINEAR PROGRAMMING

Up until this point it was assumed that an interaction medium has a single dominant resonance, although this is a valid assumption for many materials (especially for excitonic materials), most materials have more than one dominant resonance, in this case the total polarization density is the sum of all polarization densities that arise from each dominant resonance. Based on quantum mechanics, if there are k different dominant resonances, each resonance has an oscillator strength ξ_i, and the sum of all oscillator strengths is equal to 1. The mathematical description of this paragraph can be formulated as follows:

$$\sum_{i=1}^{k} \xi_i = 1 \qquad (135)$$

$$P = \sum_{i=1}^{k} P_i = \sum_{i=1}^{k} N_i p_i = N \sum_{i=1}^{k} \xi_i p_i \qquad (136)$$

$$P: Polarization\ density, \quad N: Electron\ density$$

In this case, the wave equation and the corresponding dispersion equations can be formulated as follows:

$$\nabla^2(E) - \mu_0 \varepsilon_\infty \frac{\partial^2(E)}{\partial t^2} = \mu_0 \sigma \frac{\partial(E)}{\partial t} + \mu_0 \frac{d^2 P}{\partial t^2} \qquad (137)$$

$$\frac{d^2 P_1}{dt^2} + \gamma_1 \frac{dP_1}{dt} + {\omega_1}^2 P_1 - \frac{{\omega_1}^2 {P_1}^2}{N_1 e d} + \frac{{\omega_1}^2 {P_1}^3}{{N_1}^2 e^2 d^2} = \frac{N_1 e^2 E}{m} \qquad (138)$$

$$\frac{d^2 P_2}{dt^2} + \gamma_2 \frac{dP_2}{dt} + {\omega_2}^2 P_2 - \frac{{\omega_2}^2 {P_2}^2}{N_2 e d} + \frac{{\omega_2}^2 {P_2}^3}{{N_2}^2 e^2 d^2} = \frac{N_2 e^2 E}{m} \qquad (139)$$

$$\vdots$$

$$\frac{d^2P_k}{dt^2} + \gamma_k \frac{dP_k}{dt} + {\omega_k}^2 P_k - \frac{{\omega_k}^2 {P_k}^2}{N_k e d} + \frac{{\omega_k}^2 {P_k}^3}{{N_k}^2 e^2 d^2} = \frac{N_k e^2 E}{m} \quad (140)$$

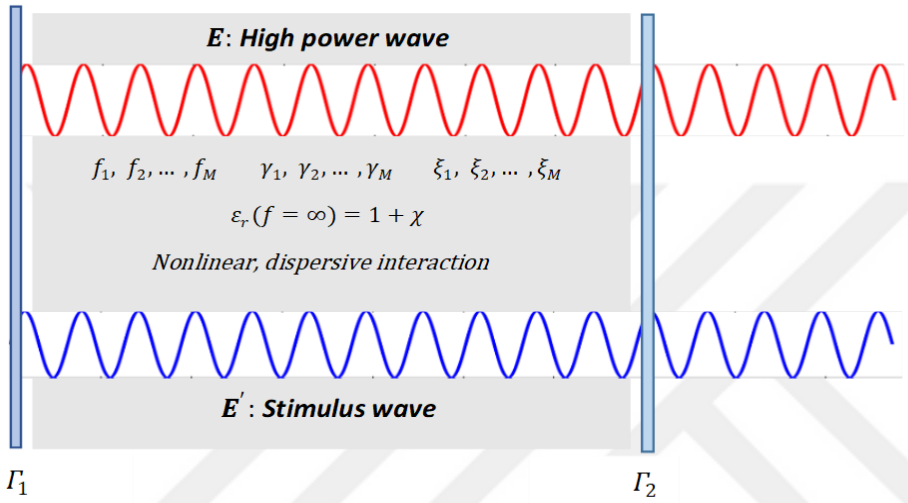

Figure 6.1 Parametric amplification in a multi-resonant cavity.

Where $N_1, N_2, \dots, N_k$ are the number of electrons oscillating at each resonance frequency. Assume that we have a medium with three dominant resonance frequencies f_1, f_2, f_3 with oscillator strengths ξ_1, ξ_2, ξ_3, in order to formulate the optical parametric amplification problem, we denote the pump wave as E and the stimulus wave as E'.

The equations that solely model the propagation of the pump wave (excluding the stimulus wave) are given as

$$\nabla^2(E) - \mu_0 \varepsilon_\infty \frac{\partial^2(E)}{\partial t^2} = \mu_0 \sigma \frac{\partial(E)}{\partial t} + \mu_0 \frac{d^2P}{\partial t^2} \quad (141)$$

$$\frac{d^2P_1}{dt^2} + \gamma_1 \frac{dP_1}{dt} + {\omega_1}^2 P_1 - \frac{{\omega_1}^2 {P_1}^2}{N_1 e d} + \frac{{\omega_1}^2 {P_1}^3}{{N_1}^2 e^2 d^2} = \frac{N_1 e^2 E}{m} \quad (142)$$

$$\frac{d^2P_2}{dt^2} + \gamma_2 \frac{dP_2}{dt} + {\omega_2}^2 P_2 - \frac{{\omega_2}^2 {P_2}^2}{N_2 e d} + \frac{{\omega_2}^2 {P_2}^3}{{N_2}^2 e^2 d^2} = \frac{N_2 e^2 E}{m} \quad (143)$$

$$\frac{d^2P_3}{dt^2} + \gamma_3 \frac{dP_3}{dt} + {\omega_3}^2 P_3 - \frac{{\omega_3}^2 {P_3}^2}{N_3 e d} + \frac{{\omega_3}^2 {P_3}^3}{{N_3}^2 e^2 d^2} = \frac{N_3 e^2 E}{m} \quad (144)$$

$$N = N_1 + N_2 + N_3, \; P = P_1 + P_2 + P_3 \quad (145)$$

Similarly, when both waves are present in the micro-resonator, the equations that describe the propagation of the total wave in the interaction medium are given as

$$\nabla^2(E + E') - \mu_0 \varepsilon_\infty \frac{\partial^2(E + E')}{\partial t^2} = \mu_0 \sigma \frac{\partial(E + E')}{\partial t} + \mu_0 \frac{d^2(P + P')}{\partial t^2} \quad (146 - 149)$$

$$\frac{d^2(P_1 + {P_1}')}{dt^2} + \gamma_1 \frac{d(P_1 + {P_1}')}{dt} + {\omega_1}^2 (P_1 + {P_1}') - \frac{{\omega_1}^2 (P_1 + {P_1}')^2}{N_1 e d} + \frac{{\omega_1}^2 (P_1 + {P_1}')^3}{{N_1}^2 e^2 d^2} = \frac{N_1 e^2 (E + E')}{m}$$

$$\frac{d^2(P_2 + {P_2}')}{dt^2} + \gamma_2 \frac{d(P_2 + {P_2}')}{dt} + {\omega_2}^2 (P_2 + {P_2}') - \frac{{\omega_2}^2 (P_2 + {P_2}')^2}{N_2 e d} + \frac{{\omega_2}^2 (P_2 + {P_2}')^3}{{N_2}^2 e^2 d^2} = \frac{N_2 e^2 (E + E')}{m}$$

$$\frac{d^2(P_3 + {P_3}')}{dt^2} + \gamma_3 \frac{d(P_3 + {P_3}')}{dt} + {\omega_3}^2 (P_3 + {P_3}') - \frac{{\omega_3}^2 (P_3 + {P_3}')^2}{N_3 e d} + \frac{{\omega_3}^2 (P_3 + {P_3}')^3}{{N_3}^2 e^2 d^2} = \frac{N_3 e^2 (E + E')}{m}$$

By subtracting equations 141-144 from equations 146-149 respectively, we can get the equations that model the propagation of the stimulus wave under the influence of the pump wave:

$$\nabla^2(E') - \mu_0 \varepsilon_\infty \frac{\partial^2(E')}{\partial t^2} = \mu_0 \sigma \frac{\partial(E')}{\partial t} + \mu_0 \frac{d^2(P')}{\partial t^2} \quad (150 - 153)$$

$$P' = {P_1}' + {P_2}' + {P_3}'$$

$$\frac{d^2({P_1}')}{dt^2} + \gamma_1 \frac{d({P_1}')}{dt} + {\omega_1}^2({P_1}') - \frac{{\omega_1}^2({{P_1}'}^2 + 2P_1{P_1}')}{N_1 e d} + \frac{{\omega_1}^2({{P_1}'}^3 + 3P_1{{P_1}'}^2 + 3{P_1}^2{P_1}')}{{N_1}^2 e^2 d^2} = \frac{N_1 e^2(E')}{m}$$

$$\frac{d^2({P_2}')}{dt^2} + \gamma_2 \frac{d({P_2}')}{dt} + {\omega_2}^2({P_2}') - \frac{{\omega_2}^2({{P_2}'}^2 + 2P_2{P_2}')}{N_2 e d} + \frac{{\omega_2}^2({{P_2}'}^3 + 3P_2{{P_2}'}^2 + 3{P_2}^2{P_2}')}{{N_2}^2 e^2 d^2} = \frac{N_2 e^2(E')}{m}$$

$$\frac{d^2({P_3}')}{dt^2} + \gamma_3 \frac{d({P_3}')}{dt} + {\omega_3}^2({P_3}') - \frac{{\omega_3}^2({{P_3}'}^2 + 2P_3{P_3}')}{N_3 e d} + \frac{{\omega_3}^2({{P_3}'}^3 + 3P_3{{P_3}'}^2 + 3{P_3}^2{P_3}')}{{N_3}^2 e^2 d^2} = \frac{N_3 e^2(E')}{m}$$

From equations 150-153, we can get the time variation of the stimulus wave at a given point in a micro-resonator and by using the non-linear programming approach, we can maximize the amplitude of the stimulus wave in a micro-resonator. In this chapter, instead of the previously applied BFGS algorithm, we will use Newton's algorithm in its plain form. The reason of this preference is that we will now use a single ultra-short pump wave pulse as the number of equations is now increased due to the presence of multiple resonance frequencies and we want to save on the computational cost. Since there is only a single frequency to be tuned, the BFGS approach is not necessary. As we can remember from the previous chapter, the Newton algorithm is given as

$$\boldsymbol{\nu^{(k)}} = \boldsymbol{\nu^{(k-1)}} - \mu_k (\boldsymbol{\nabla}^2 f(\boldsymbol{\nu^{(k-1)}}))^{-1} (\boldsymbol{\nabla} f(\boldsymbol{\nu^{(k-1)}})), \quad k = 1,2,3,\ldots \qquad (154)$$

For a single optimization parameter, Equation 154 can be rewritten as

$$\nu^{(k)} = \nu^{(k-1)} - \mu_k \frac{f(\nu^{(k-1)}) - f(\nu^{(k-2)})}{f'(\nu^{(k-1)}) - f'(\nu^{(k-2)})} (\nu^{(k-1)} - \nu^{(k-2)}), \quad k = 1,2,3,\ldots \qquad (155)$$

The step size μ_k can be determined by the Wolfe conditions and the corresponding formula described in Chapter 5. Hence, there are 8 equations to be solved at each iteration of the optimization algorithm. These equations (156-163) are given below

$$\nu_p: Pump\ wave\ frequency$$

$$\nabla^2\big(E(\nu_p)\big) - \mu_0\varepsilon_\infty \frac{\partial^2\big(E(\nu_p)\big)}{\partial t^2} = \mu_0\sigma\frac{\partial\big(E(\nu_p)\big)}{\partial t} + \mu_0\frac{d^2P}{\partial t^2}$$

$$\frac{d^2P_1}{dt^2} + \gamma_1\frac{dP_1}{dt} + {\omega_1}^2P_1 - \frac{{\omega_1}^2{P_1}^2}{N_1ed} + \frac{{\omega_1}^2{P_1}^3}{{N_1}^2e^2d^2} = \frac{N_1e^2\big(E(\nu_p)\big)}{m}$$

$$\frac{d^2P_2}{dt^2} + \gamma_2\frac{dP_2}{dt} + {\omega_2}^2P_2 - \frac{{\omega_2}^2{P_2}^2}{N_2ed} + \frac{{\omega_2}^2{P_2}^3}{{N_2}^2e^2d^2} = \frac{N_2e^2\big(E(\nu_p)\big)}{m}$$

$$\frac{d^2P_3}{dt^2} + \gamma_3\frac{dP_3}{dt} + {\omega_3}^2P_3 - \frac{{\omega_3}^2{P_3}^2}{N_3ed} + \frac{{\omega_3}^2{P_3}^3}{{N_3}^2e^2d^2} = \frac{N_3e^2\big(E(\nu_p)\big)}{m}$$

$$\nabla^2\big(E'(\nu_p)\big) - \mu_0\varepsilon_\infty \frac{\partial^2\big(E'(\nu_p)\big)}{\partial t^2} = \mu_0\sigma\frac{\partial\big(E'(\nu_p)\big)}{\partial t} + \mu_0\frac{d^2(P')}{\partial t^2}$$

$$\frac{d^2({P_1}')}{dt^2} + \gamma_1\frac{d({P_1}')}{dt} + {\omega_1}^2({P_1}') - \frac{{\omega_1}^2({{P_1}'}^2 + 2P_1{P_1}')}{N_1ed} + \frac{{\omega_1}^2({{P_1}'}^3 + 3P_1{{P_1}'}^2 + 3{P_1}^2{P_1}')}{{N_1}^2e^2d^2} = \frac{N_1e^2(E'(\nu_p))}{m}$$

$$\frac{d^2({P_2}')}{dt^2} + \gamma_2\frac{d({P_2}')}{dt} + {\omega_2}^2({P_2}') - \frac{{\omega_2}^2({{P_2}'}^2 + 2P_2{P_2}')}{N_2ed} + \frac{{\omega_2}^2({{P_2}'}^3 + 3P_2{{P_2}'}^2 + 3{P_2}^2{P_2}')}{{N_2}^2e^2d^2} = \frac{N_2e^2(E'(\nu_p))}{m}$$

$$\frac{d^2({P_3}')}{dt^2} + \gamma_3\frac{d({P_3}')}{dt} + {\omega_3}^2({P_3}') - \frac{{\omega_3}^2({{P_3}'}^2 + 2P_3{P_3}')}{N_3ed} + \frac{{\omega_3}^2({{P_3}'}^3 + 3P_3{{P_3}'}^2 + 3{P_3}^2{P_3}')}{{N_3}^2e^2d^2} = \frac{N_3e^2(E'(\nu_p))}{m}$$

$$P = P_1 + P_2 + P_3,\ P' = {P_1}' + {P_2}' + {P_3}'$$

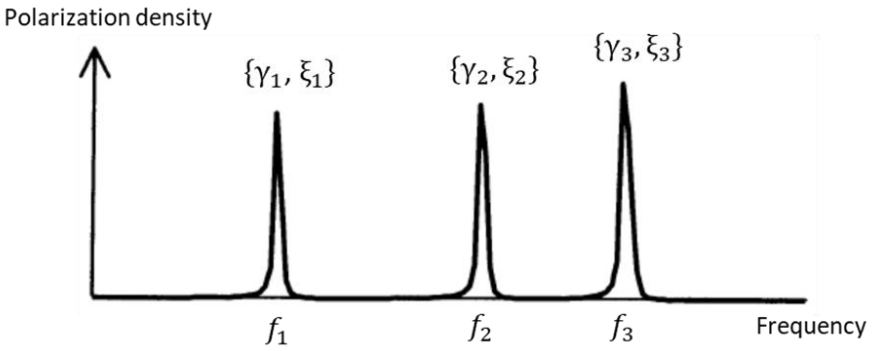

Figure 6.2 Dispersion plot of the polarization density in a multiresonant medium.

***FDTD Equations*:** (163-170)

Equations (156-163) are discretized using the finite difference time domain as follows:

$$\frac{E_k(i+1,j)-2E_k(i,j)+E_k(i-1,j)}{\Delta x^2}-\mu_0\varepsilon_\infty(i,j)\frac{E_k(i,j+1)-2E_k(i,j)+E_k(i,j-1)}{\Delta t^2}$$
$$=\mu_0\sigma(i,j)\frac{E_k(i,j)-E_k(i,j-1)}{\Delta t}+\mu_0\frac{P_k(i,j+1)-2P_k(i,j)+P_k(i,j-1)}{\Delta t^2}$$

$$\frac{P_{1,k}(i,j+1)-2P_{1,k}(i,j)+P_{1,k}(i,j-1)}{\Delta t^2}+\gamma_1\frac{P_{1,k}(i,j)-P_{1,k}(i,j-1)}{\Delta t}+4\pi^2{f_1}^2\left(P_{1,k}(i,j)\right)$$
$$-\frac{4\pi^2{f_1}^2}{N_1 ed}\left(P_{1,k}(i,j)\right)^2+\frac{4\pi^2{f_1}^2}{{N_1}^2e^2d^2}\left(P_{1,k}(i,j)\right)^3=\frac{N_1e^2}{m}\left(E_k(i,j)\right).$$

$$\frac{P_{2,k}(i,j+1)-2P_{2,k}(i,j)+P_{2,k}(i,j-1)}{\Delta t^2}+\gamma_2\frac{P_{2,k}(i,j)-P_{2,k}(i,j-1)}{\Delta t}+4\pi^2{f_2}^2\left(P_{2,k}(i,j)\right)$$
$$-\frac{4\pi^2{f_2}^2}{N_2 ed}\left(P_{2,k}(i,j)\right)^2+\frac{4\pi^2{f_2}^2}{{N_2}^2e^2d^2}\left(P_{2,k}(i,j)\right)^3=\frac{N_2e^2}{m}\left(E_k(i,j)\right).$$

$$\frac{P_{3,k}(i,j+1)-2P_{3,k}(i,j)+P_{3,k}(i,j-1)}{\Delta t^2}+\gamma_3\frac{P_{3,k}(i,j)-P_{3,k}(i,j-1)}{\Delta t}+4\pi^2{f_3}^2\left(P_{3,k}(i,j)\right)$$
$$-\frac{4\pi^2{f_3}^2}{N_3 ed}\left(P_{3,k}(i,j)\right)^2+\frac{4\pi^2{f_3}^2}{{N_3}^2e^2d^2}\left(P_{3,k}(i,j)\right)^3=\frac{N_3e^2}{m}\left(E_k(i,j)\right).$$

$$\frac{{E_k}'(i+1,j)-2{E_k}'(i,j)+{E_k}'(i-1,j)}{\Delta x^2}-\mu_0\varepsilon_\infty(i,j)\frac{{E_k}'(i,j+1)-2{E_k}'(i,j)+{E_k}'(i,j-1)}{\Delta t^2}$$
$$=\mu_0\sigma(i,j)\frac{{E_k}'(i,j)-{E_k}'(i,j-1)}{\Delta t}+\mu_0\frac{{P_k}'(i,j+1)-2{P_k}'(i,j)+{P_k}'(i,j-1)}{\Delta t^2}$$

$$\frac{{P_{1,k}}'(i,j+1)-2{P_{1,k}}'(i,j)+{P_{1,k}}'(i,j-1)}{\Delta t^2}+\gamma_1\frac{{P_{1,k}}'(i,j)-{P_{1,k}}'(i,j-1)}{\Delta t}+4\pi^2{f_1}^2\left({P_{1,k}}'(i,j)\right)$$
$$-\frac{4\pi^2{f_1}^2}{N_1 ed}\left\{\left({P_{1,k}}'(i,j)\right)^2+2{P_{1,k}}'(i,j)P_{1,k}(i,j)\right\}+\frac{4\pi^2{f_1}^2}{{N_1}^2e^2d^2}\{\left({P_{1,k}}'(i,j)\right)^3$$
$$+3\left({P_{1,k}}'(i,j)\right)^2P_{1,k}(i,j)\ \ +3{P_{1,k}}'(i,j)\left(P_{1,k}(i,j)\right)^2\}=\frac{N_1e^2}{m}({E_k}'(i,j)).$$

$$\frac{{P_{2,k}}'(i,j+1)-2{P_{2,k}}'(i,j)+{P_{2,k}}'(i,j-1)}{\Delta t^2}+\gamma_2\frac{{P_{2,k}}'(i,j)-{P_{2,k}}'(i,j-1)}{\Delta t}+4\pi^2{f_2}^2\left({P_{2,k}}'(i,j)\right)$$
$$-\frac{4\pi^2{f_2}^2}{N_2 ed}\left\{\left({P_{2,k}}'(i,j)\right)^2+2{P_{2,k}}'(i,j)P_{2,k}(i,j)\right\}+\frac{4\pi^2{f_2}^2}{{N_2}^2e^2d^2}\{\left({P_{2,k}}'(i,j)\right)^3$$
$$+3\left({P_{2,k}}'(i,j)\right)^2P_{2,k}(i,j)\ \ +3{P_{2,k}}'(i,j)\left(P_{2,k}(i,j)\right)^2\}=\frac{N_2e^2}{m}({E_k}'(i,j)).$$

$$\frac{{P_{3,k}}'(i,j+1)-2{P_{3,k}}'(i,j)+{P_{3,k}}'(i,j-1)}{\Delta t^2}+\gamma_3\frac{{P_{3,k}}'(i,j)-{P_{3,k}}'(i,j-1)}{\Delta t}+4\pi^2{f_3}^2\left({P_{3,k}}'(i,j)\right)$$
$$-\frac{4\pi^2{f_3}^2}{N_3 ed}\left\{\left({P_{3,k}}'(i,j)\right)^2+2{P_{3,k}}'(i,j)P_{3,k}(i,j)\right\}+\frac{4\pi^2{f_3}^2}{{N_3}^2e^2d^2}\{\left({P_{3,k}}'(i,j)\right)^3$$
$$+3\left({P_{3,k}}'(i,j)\right)^2P_{3,k}(i,j)\ \ +3{P_{3,k}}'(i,j)\left(P_{3,k}(i,j)\right)^2\}=\frac{N_3e^2}{m}({E_k}'(i,j)).$$

$$P=P_1+P_2+P_3,\ P'={P_1}'+{P_2}'+{P_3}' \qquad (171)$$

x: Space coordinate, t: Time, k: Iteration, $E_k(\mathrm{x},\mathrm{t})=E_k(\mathrm{i}\Delta\mathrm{x},\mathrm{j}\Delta\mathrm{t})\ \rightarrow E_k(\mathrm{i},\mathrm{j})$

E_k: *pump wave at each iteration*

${E_k}'$: *Input (stimulus) wave at each iteration*

Cost function: $f=\left|E'(\nu_p{}^{(k)})\right|$

Newton's Algorithm:

$$\nu_p{}^{(k)}=\nu_p{}^{(k-1)}-\mu_k\frac{f\left(\nu_p{}^{(k-1)}\right)-f\left(\nu_p{}^{(k-2)}\right)}{f'\left(\nu_p{}^{(k-1)}\right)-f'\left(\nu_p{}^{(k-2)}\right)}\left(\nu_p{}^{(k-1)}-\nu_p{}^{(k-2)}\right),\quad k=1,2,3,\ldots$$

6.1. Simulations of wave amplification in multi-resonant nonlinear optical cavities

Simulation 6.1.1:

The low-intensity input wave $\boldsymbol{E_1}$ to be amplified and the high-intensity pump wave $\boldsymbol{E_2}$ are propagating in a simple Fabry-Perot type optical microcavity with an optical isolator acting as the left cavity wall and a bandpass-filter acting as the right cavity wall. The waves are simultaneously originated at x=2.5 μm at time t=0 s. The input wave $\boldsymbol{E_1}$ has a normalized electric field amplitude of 1 V/m and a frequency of 350 THz. The intense pump wave $\boldsymbol{E_2}$ has an amplitude of 1.75×10^8 V/m (frequency to be determined). The waves and the values of the cavity parameters are as stated below:

$$\boldsymbol{E_1}(x = 2.5\ \mu m, t) = 1 \times \sin(2\pi(3.5 \times 10^{14})t)\ \ V/m$$

$$\boldsymbol{E_2}(x = 2.5\ \mu m, t) = 1.75 \times 10^8 \times \sin\left(2\pi\left(\nu_p\right)t\right)\ \ V/m$$

$$Spatial\ and\ temporal\ parameters\colon\ 0 \le x \le 10\ \mu m, 0 \le t \le 30\ ps$$

$$Cavity\ resonances\colon\ \boldsymbol{f_r} = \{4 \times 10^{14}\ Hz, 6.3 \times 10^{14}\ Hz, 8.8 \times 10^{14}\ Hz\}$$

$$Damping\ rates\ of\ the\ cavity\colon\ \boldsymbol{\gamma} = \{1 \times 10^{9}\ Hz, 2 \times 10^{9}\ Hz, 4 \times 10^{9}\ Hz\}$$

$$Relative\ permittivity\colon (\varepsilon_r) = 12 \quad (\mu_r = 1)$$

$$Optical\ isolator\ location\ (left\ wall)\colon\ x = 0\ \mu m$$

$$Bandpass\ filter\ (right\ wall)\ location\colon\ x = 10\ \mu m$$

$$Interaction\ medium\ range\ \colon 0\mu m < x < 10\ \mu m$$

$$Number\ of\ electrons\ per\ volume\colon\ N = 3.5 \times 10^{28}/m^3$$

$$Atomic\ diameter\colon d = 0.3\ nanometers$$

$$Cost\ function\colon C$$

Problem definition: Determine the optimal excitation frequency of the pump wave ν_p in order to maximize the absolute value of the peak amplitude of the input wave at 350 THz ($|E_{in}(\ f = 350\ THz)|$) inside the cavity, for 10 THz < $\{\nu_p\} < 500\ THz$, and for $0\ \mu m < x < 10\ \mu m,\ 0 \le t \le 10\ ps$.

$$C = |E_{in}(f = 350\,THz)| = \left| \int_{3.5\times10^{14}-\Delta f}^{3.5\times10^{14}+\Delta f} \left\{ \int_{0}^{\Delta T} \{E_{in}(x = x', t)\, e^{-i(2\pi\Omega)t}\} dt \right\} e^{i(2\pi\Omega)t} d\Omega \right|$$

$$\Delta T = 30\,ps, (3.5 \times 10^{14} - \Delta f)\,Hz < \Omega < (3.5 \times 10^{14} + \Delta f)\,Hz, \qquad \Delta f = 1.2\,THz$$

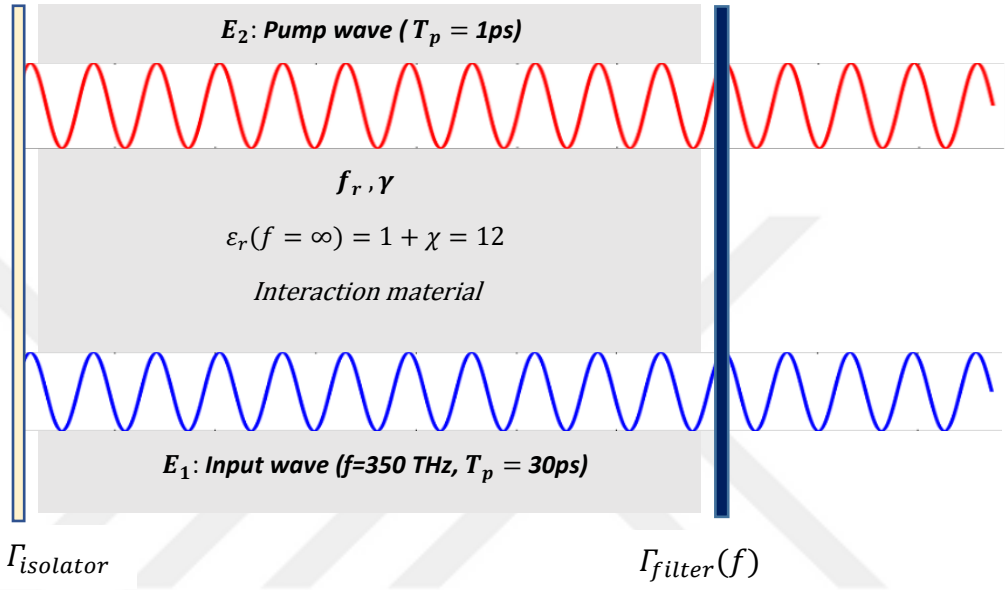

Figure 6.3 Configuration of the cavity for simulation 6.1.1

Initial conditions: (Prime indicates derivative)

$$P_2(x,0) = P_2'(x,0) = E_2(x,0) = E_2'(x,0) = P_1(x,0) = P_1'(x,0) = E_1(x,0) = E_1'(x,0) = 0$$

Band-pass filter: Frequency dependent reflection at x = 10 μm

$$|\Gamma(f')| = 1 - e^{-(\frac{(f'-350\,THz)}{\sqrt{3}\,THz})^2}$$

Objective (cost) function via penalties: $C(\nu_p) = |E_{st}(f_{st} = 350\,THz)| - \delta_1(\nu_p - \nu_{max})^2 - \delta_2(\nu_{min} - \nu_p)^2$

$$\delta_1 = \begin{Bmatrix} 0 & \nu_p \le \nu_{max} \\ \frac{|E_1(f=350\,THz)|}{(0.5\times10^{26})} & if\ \nu_p > \nu_{max} \end{Bmatrix}, \quad \delta_2 = \begin{Bmatrix} 0 & \nu_p \ge \nu_{min} \\ \frac{|E_1(f=350\,THz)|}{(0.5\times10^{26})} & \nu_p < \nu_{min} \end{Bmatrix}$$

***FDTD Equations*:**

Equations for the pump wave: (172-175)

$$\frac{E_{2,k}(i+1,j)-2E_{2,k}(i,j)+E_{2,k}(i-1,j)}{\Delta x^2}-\mu_0\varepsilon_\infty(i,j)\frac{E_{2,k}(i,j+1)-2E_{2,k}(i,j)+E_{2,k}(i,j-1)}{\Delta t^2}$$
$$=\mu_0\sigma(i,j)\frac{E_{2,k}(i,j)-E_{2,k}(i,j-1)}{\Delta t}+\mu_0\frac{P_{2,k}(i,j+1)-2P_{2,k}(i,j)+P_{2,k}(i,j-1)}{\Delta t^2}$$

$$\frac{P_{21,k}(i,j+1)-2P_{21,k}(i,j)+P_{21,k}(i,j-1)}{\Delta t^2}+\gamma_1\frac{P_{21,k}(i,j)-P_{21,k}(i,j-1)}{\Delta t}+4\pi^2{f_1}^2\left(P_{21,k}(i,j)\right)$$
$$-\frac{4\pi^2{f_1}^2}{N_1ed}\left(P_{21,k}(i,j)\right)^2+\frac{4\pi^2{f_1}^2}{{N_1}^2e^2d^2}\left(P_{21,k}(i,j)\right)^3=\frac{N_1e^2}{m}\left(E_{2,k}(i,j)\right).$$

$$\frac{P_{22,k}(i,j+1)-2P_{22,k}(i,j)+P_{22,k}(i,j-1)}{\Delta t^2}+\gamma_2\frac{P_{22,k}(i,j)-P_{22,k}(i,j-1)}{\Delta t}+4\pi^2{f_2}^2\left(P_{22,k}(i,j)\right)$$
$$-\frac{4\pi^2{f_2}^2}{N_2ed}\left(P_{22,k}(i,j)\right)^2+\frac{4\pi^2{f_2}^2}{{N_2}^2e^2d^2}\left(P_{22,k}(i,j)\right)^3=\frac{N_2e^2}{m}\left(E_{2,k}(i,j)\right).$$

$$\frac{P_{23,k}(i,j+1)-2P_{23,k}(i,j)+P_{23,k}(i,j-1)}{\Delta t^2}+\gamma_3\frac{P_{23,k}(i,j)-P_{23,k}(i,j-1)}{\Delta t}+4\pi^2{f_3}^2\left(P_{23,k}(i,j)\right)$$
$$-\frac{4\pi^2{f_3}^2}{N_3ed}\left(P_{23,k}(i,j)\right)^2+\frac{4\pi^2{f_3}^2}{{N_3}^2e^2d^2}\left(P_{23,k}(i,j)\right)^3=\frac{N_3e^2}{m}\left(E_{2,k}(i,j)\right).$$

$$P_2=P_{21}+P_{22}+P_{23},\ \ N=N_1+N_2+N_3$$

Equations for the input wave: (176-179)

$$\frac{E_{1,k}(i+1,j)-2E_{1,k}(i,j)+E_{1,k}(i-1,j)}{\Delta x^2}-\mu_0\varepsilon_\infty(i,j)\frac{E_{1,k}(i,j+1)-2E_{1,k}(i,j)+E_{1,k}(i,j-1)}{\Delta t^2}$$
$$=\mu_0\sigma(i,j)\frac{E_{1,k}(i,j)-E_{1,k}(i,j-1)}{\Delta t}+\mu_0\frac{P_{1,k}(i,j+1)-2P_{1,k}(i,j)+P_{1,k}(i,j-1)}{\Delta t^2}$$

$$\frac{P_{11,k}(i,j+1)-2P_{11,k}(i,j)+P_{11,k}(i,j-1)}{\Delta t^2}+\gamma_1\frac{P_{11,k}(i,j)-P_{11,k}(i,j-1)}{\Delta t}+4\pi^2{f_1}^2\left(P_{11,k}(i,j)\right)$$
$$-\frac{4\pi^2{f_1}^2}{N_1 ed}\left\{\left(P_{11,k}(i,j)\right)^2+2P_{11,k}(i,j)P_{21,k}(i,j)\right\}+\frac{4\pi^2{f_1}^2}{{N_1}^2e^2d^2}\{\left(P_{11,k}(i,j)\right)^3$$
$$+3\left(P_{11,k}(i,j)\right)^2P_{21,k}(i,j)\ \ +3P_{11,k}(i,j)\left(P_{21,k}(i,j)\right)^2\}=\frac{N_1e^2}{m}(E_{1,k}(i,j)).$$

$$\frac{P_{12,k}(i,j+1)-2P_{12,k}(i,j)+P_{12,k}(i,j-1)}{\Delta t^2}+\gamma_2\frac{P_{12,k}(i,j)-P_{12,k}(i,j-1)}{\Delta t}+4\pi^2{f_2}^2\left(P_{12,k}(i,j)\right)$$
$$-\frac{4\pi^2{f_2}^2}{N_2 ed}\left\{\left(P_{12,k}(i,j)\right)^2+2P_{12,k}(i,j)P_{22,k}(i,j)\right\}+\frac{4\pi^2{f_2}^2}{{N_2}^2e^2d^2}\{\left(P_{12,k}(i,j)\right)^3$$
$$+3\left(P_{12,k}(i,j)\right)^2P_{22,k}(i,j)\ \ +3P_{12,k}(i,j)\left(P_{22,k}(i,j)\right)^2\}=\frac{N_2e^2}{m}(E_{1,k}(i,j)).$$

$$\frac{P_{13,k}(i,j+1)-2P_{13,k}(i,j)+P_{13,k}(i,j-1)}{\Delta t^2}+\gamma_3\frac{P_{13,k}(i,j)-P_{13,k}(i,j-1)}{\Delta t}+4\pi^2{f_3}^2\left(P_{13,k}(i,j)\right)$$
$$-\frac{4\pi^2{f_3}^2}{N_3 ed}\left\{\left(P_{13,k}(i,j)\right)^2+2P_{13,k}(i,j)P_{23,k}(i,j)\right\}+\frac{4\pi^2{f_3}^2}{{N_3}^2e^2d^2}\{\left(P_{13,k}(i,j)\right)^3$$
$$+3\left(P_{13,k}(i,j)\right)^2P_{23,k}(i,j)\ \ +3P_{13,k}(i,j)\left(P_{23,k}(i,j)\right)^2\}=\frac{N_3e^2}{m}(E_{1,k}(i,j)).$$

$$P_1=P_{11}+P_{12}+P_{13},\ \ N=N_1+N_2+N_3$$

x: Space coordinate, t: Time, k: Iteration, $E_k(\mathrm{x},\mathrm{t})=E_k(\mathrm{i}\Delta\mathrm{x},\mathrm{j}\Delta\mathrm{t})\ \rightarrow E_k(\mathrm{i},\mathrm{j})$

$E_{2,k}$: *Pump wave at iteration k*

$E_{1,k}$: *Input (stimulus) wave at iteration k*

These equations for the pump wave and the input wave are solved at every iteration of the optimization process until the desired gain factor at a specific input wave frequency is obtained. If N is the number of resonances for a given multi-resonant interaction medium, then there are (2N+2) equations to solve at each iteration. Therefore, as the number of resonances in the cavity increase, the computational cost increases. For this reason, we will only use a single pump wave pulse in order to perform an optimization based on a single parameter, which is the center (excitation) frequency of the pump wave pulse.

Newton's method:

Cost function: $C = |E_1(f = 350\,THz)|$

Newton's Algorithm: (C' *indicates derivative*)

$$\nu_p{}^{(k)} = \nu_p{}^{(k-1)} - \mu_k \frac{C\left(\nu_p{}^{(k-1)}\right) - C\left(\nu_p{}^{(k-2)}\right)}{C'\left(\nu_p{}^{(k-1)}\right) - C'\left(\nu_p{}^{(k-2)}\right)}\left(\nu_p{}^{(k-1)} - \nu_p{}^{(k-2)}\right), \quad k = 1,2,3,\ldots$$

For each iteration, the optimal step size is determined as

$$\mu_k = c^{\left(\log\left|\frac{C(\boldsymbol{\nu_p}^{(k)})}{C(\boldsymbol{\nu_p}^{(k)}) - C(\boldsymbol{\nu_p}^{(k-1)})}\right|\right) / \left(\left|\frac{C(\boldsymbol{\nu_p}^{(k)})}{C(\boldsymbol{\nu_p}^{(k)}) - C(\boldsymbol{\nu_p}^{(k-1)})}\right|\right)} \quad (180)$$

Where c is a constant ($1.001 < c < 1.499$). Equation eliminates the necessity of running an additional iteration to identify the optimal step size. For this simulation, the constant c is selected as c=1.37. According to the stated formulations, the highest intracavity input wave amplitude (for 0<t<30ps) is determined as

$Gain_{max} = \left|E_1(\,\nu_p = 350\,THz)\right|_{max} = 3.32 \times 10^8\ V/m$, which occurs at a pump wave excitation frequency of $\nu_p = 234.1\,THz$ (see Table 6.1).

$W_e = Intracavity\ electric\ energy\ density,\ \ P_{pump}$: $Induced\ polarization\ density$

Table 6.1: Newton's algorithm-based optimization

ν_p	$Gain_{max}$	$W_{e,p}\ (\frac{J}{m^3})$	$P_{pump}(\frac{C}{m^2})$	k (iteration #)
225.0THz	1.84	1.88×10^7	0.05	1
275.8THz	21.32	2.15×10^7	0.05	3
332.4THz	59196.44	8.62×10^7	0.16	5
389.4THz	1.72	2.3×10^5	0.06	7
381.4THz	2.23	3.5×10^5	0.07	9
392.3THz	1.47	1.6×10^5	0.05	10
345.5THz	146.13	1.0×10^5	0.11	11
272.3THz	3.53×10^3	5.85×10^7	0.12	12
199.1THz	4.28×10^4	6.90×10^7	0.14	13
234.1THz	3.32×10^8	2.56×10^8	0.16	14

In table 6.1, it is clearly shown that the optimal excitation frequency concurrently yields to a high intracavity energy and a high polarization density.

Therefore, we can deduce that the intracavity electric energy density and the intracavity polarization density should be simultaneously high for intense input wave amplification.

The polychromatic input wave is plotted in Figure6.4 between t=15 picoseconds and t=30 picoseconds. This figure shows that the polychromatic input wave gradually increases to an amplitude of nearly $8 \times 10^8\ V/m$.

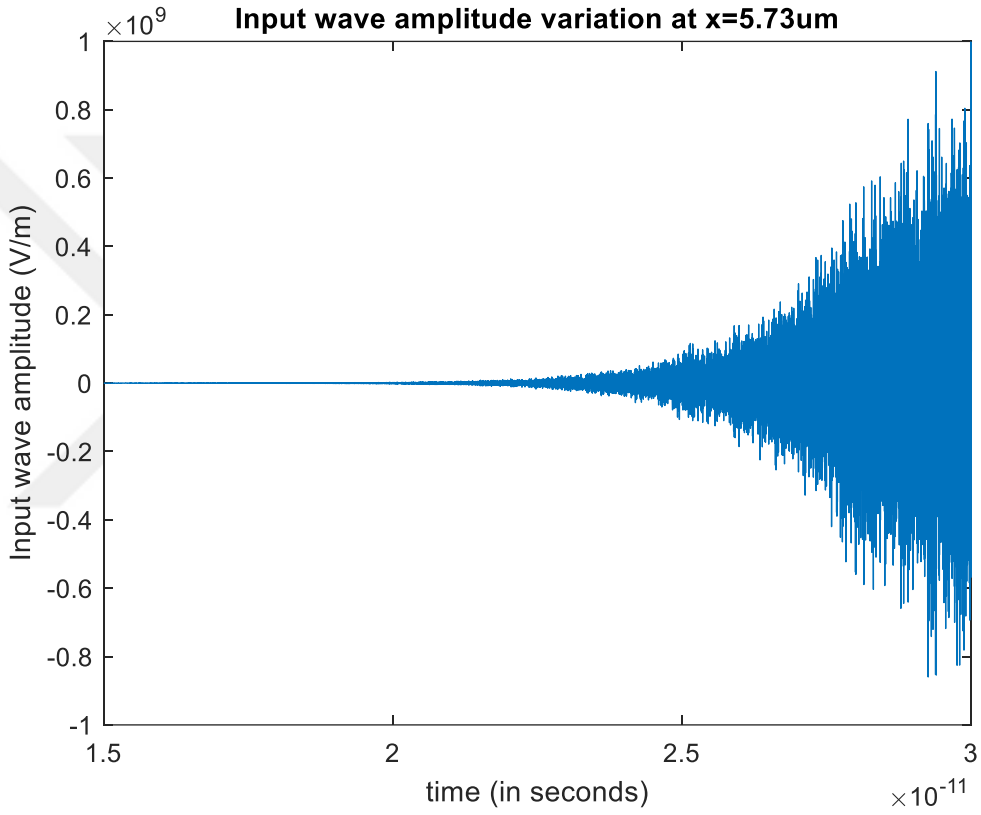

Figure 6.4 Input wave amplification (polychromatic) in the cavity versus time.

Note that although the input wave is spectrally broadened while being amplified, we are actually maximizing the magnitude of the peak amplitude of the input wave at its excitation frequency $\nu_p = 350\ THz$ (quasi-monochromatic). Therefore, we exclude the other spectral components. A direct frequency independent approach to optimize the magnitude of the input wave results in an amplified input wave with many additional spectral components. These additional spectral components would most likely be more prominent than the initial excitation frequency of the input wave.

Simulation 6.1.2:

The low-intensity input wave $\boldsymbol{E_1}$ to be amplified and the high-intensity pump wave $\boldsymbol{E_2}$ are propagating in a simple Fabry-Perot type optical microcavity with an optical isolator acting as the left cavity wall and a bandpass-filter acting as the right cavity wall. The waves are simultaneously originated at x=0 μm at time t=0 s. The input wave $\boldsymbol{E_1}$ has a normalized electric field amplitude of 1 V/m and a frequency of 440 THz. The intense pump wave $\boldsymbol{E_2}$ has an amplitude of 3×10^8 V/m (frequency to be determined). The waves and the values of the cavity parameters are as stated below:

$$\boldsymbol{E_1}(x = 0\ \mu m, t) = 1 \times \sin(2\pi(4.4 \times 10^{14})t)\ \ V/m$$

$$\boldsymbol{E_2}(x = 0\ \mu m, t) = 3 \times 10^8 \times \sin\left(2\pi\left(\nu_p\right)t\right)\ \ V/m$$

$$Spatial\ and\ temporal\ parameters\colon\ 0 \le x \le 10\ \mu m, 0 \le t \le 10\ ps$$

$$Cavity\ resonances\colon\ \boldsymbol{f_r} = \{5.2 \times 10^{14}\ Hz, 7.6 \times 10^{14}\ Hz\}$$

$$Damping\ rates\ of\ the\ cavity\colon\ \boldsymbol{\gamma} = \{2 \times 10^9\ Hz, 4 \times 10^9\ Hz\}$$

$$Relative\ permittivity\colon (\varepsilon_r) = 10 \quad (\mu_r = 1)$$

$$Optical\ isolator\ location\ (left\ wall)\colon\ x = 0\ \mu m$$

$$Bandpass\ filter\ location\ (right\ wall)\ location\colon\ x = 10\ \mu m$$

$$Interaction\ medium\ range\ \colon 0\ \mu m < x < 10\ \mu m$$

$$Number\ of\ electrons\ per\ volume\colon\ N = 3.5 \times 10^{28}/m^3$$

$$Atomic\ diameter\colon d = 0.3\ nanometers$$

$$Cost\ function\colon C$$

Problem definition: Determine the optimal excitation frequency of the pump wave ν_p in order to maximize the absolute value of the peak amplitude of the input wave at 440 THz ($|E_{in}(f = 440\ THz)|$) inside the cavity, for 120 THz < $\{\nu_p\} < 400\ THz$, and for $0\ \mu m < x < 10\ \mu m,\ 0 \le t \le 10\ ps$.

$$C = |E_{in}(f = 440\ THz)| = \left| \int_{4.4\times10^{14}-\Delta f}^{4.4\times10^{14}+\Delta f} \left\{ \int_{0}^{\Delta T} \{E_{in}(x = x', t)\, e^{-i(2\pi\Omega)t}\} dt \right\} e^{i(2\pi\Omega)t} d\Omega \right|$$

$$\Delta T = 10\ ps, (4.4 \times 10^{14} - \Delta f)\ Hz < \Omega < (4.4 \times 10^{14} + \Delta f)\ Hz, \qquad \Delta f = 1.2\ THz$$

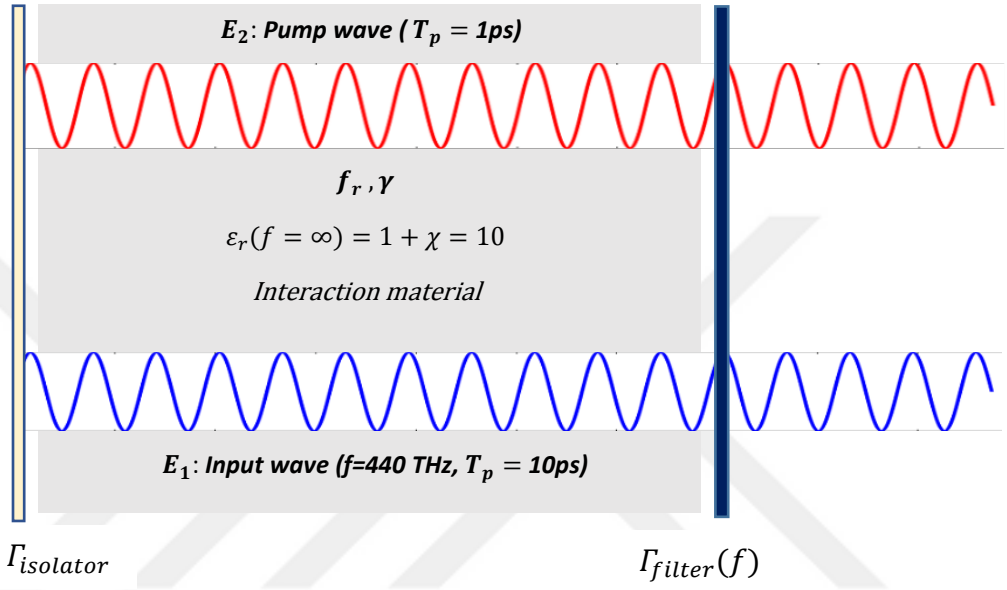

Figure 6.5 Configuration of the cavity for simulation 6.1.2

Initial conditions: (Prime indicates derivative)

$$P_2(x,0) = P_2'(x,0) = E_2(x,0) = E_2'(x,0) = P_1(x,0) = P_1'(x,0) = E_1(x,0) = E_1'(x,0) = 0$$

Band-pass filter: Frequency dependent reflection at x = 10 μm

$$|\Gamma(f')| = 1 - e^{-(\frac{(f'-440\ THz)}{\sqrt{3}\ THz})^2}$$

Objective (cost) function via penalties: $C(\nu_p) = |E_{st}(f_{st} = 440\ THz)| - \delta_1(\nu_p - \nu_{max})^2 - \delta_2(\nu_{min} - \nu_p)^2$

$$\delta_1 = \begin{Bmatrix} 0 & \nu_p \le \nu_{max} \\ \frac{|E_1(f=440THz)|}{(0.5\times10^{26})} & if\ \nu_p > \nu_{max} \end{Bmatrix}, \quad \delta_2 = \begin{Bmatrix} 0 & \nu_p \ge \nu_{min} \\ \frac{|E_1(f=440THz)|}{(0.5\times10^{26})} & \nu_p < \nu_{min} \end{Bmatrix}$$

***FDTD Equations*:**

Equations for the pump wave: (181-183)

$$\frac{E_{2,k}(i+1,j)-2E_{2,k}(i,j)+E_{2,k}(i-1,j)}{\Delta x^2}-\mu_0\varepsilon_\infty(i,j)\frac{E_{2,k}(i,j+1)-2E_{2,k}(i,j)+E_{2,k}(i,j-1)}{\Delta t^2}$$
$$=\mu_0\sigma(i,j)\frac{E_{2,k}(i,j)-E_{2,k}(i,j-1)}{\Delta t}+\mu_0\frac{P_{2,k}(i,j+1)-2P_{2,k}(i,j)+P_{2,k}(i,j-1)}{\Delta t^2}$$

$$\frac{P_{21,k}(i,j+1)-2P_{21,k}(i,j)+P_{21,k}(i,j-1)}{\Delta t^2}+\gamma_1\frac{P_{21,k}(i,j)-P_{21,k}(i,j-1)}{\Delta t}+4\pi^2{f_1}^2\left(P_{21,k}(i,j)\right)$$
$$-\frac{4\pi^2{f_1}^2}{N_1ed}\left(P_{21,k}(i,j)\right)^2+\frac{4\pi^2{f_1}^2}{{N_1}^2e^2d^2}\left(P_{21,k}(i,j)\right)^3=\frac{N_1e^2}{m}\left(E_{2,k}(i,j)\right).$$

$$\frac{P_{22,k}(i,j+1)-2P_{22,k}(i,j)+P_{22,k}(i,j-1)}{\Delta t^2}+\gamma_2\frac{P_{22,k}(i,j)-P_{22,k}(i,j-1)}{\Delta t}+4\pi^2{f_2}^2\left(P_{22,k}(i,j)\right)$$
$$-\frac{4\pi^2{f_2}^2}{N_2ed}\left(P_{22,k}(i,j)\right)^2+\frac{4\pi^2{f_2}^2}{{N_2}^2e^2d^2}\left(P_{22,k}(i,j)\right)^3=\frac{N_2e^2}{m}\left(E_{2,k}(i,j)\right).$$

$$P_2=P_{21}+P_{22},\ \ N=N_1+N_2$$

Equations for the input wave: (184-186)

$$\frac{E_{1,k}(i+1,j)-2E_{1,k}(i,j)+E_{1,k}(i-1,j)}{\Delta x^2}-\mu_0\varepsilon_\infty(i,j)\frac{E_{1,k}(i,j+1)-2E_{1,k}(i,j)+E_{1,k}(i,j-1)}{\Delta t^2}$$
$$=\mu_0\sigma(i,j)\frac{E_{1,k}(i,j)-E_{1,k}(i,j-1)}{\Delta t}+\mu_0\frac{P_{1,k}(i,j+1)-2P_{1,k}(i,j)+P_{1,k}(i,j-1)}{\Delta t^2}$$

$$\frac{P_{11,k}(i,j+1)-2P_{11,k}(i,j)+P_{11,k}(i,j-1)}{\Delta t^2}+\gamma_1\frac{P_{11,k}(i,j)-P_{11,k}(i,j-1)}{\Delta t}+4\pi^2{f_1}^2\left(P_{11,k}(i,j)\right)$$
$$-\frac{4\pi^2{f_1}^2}{N_1 ed}\left\{\left(P_{11,k}(i,j)\right)^2+2P_{11,k}(i,j)P_{21,k}(i,j)\right\}+\frac{4\pi^2{f_1}^2}{{N_1}^2e^2d^2}\{\left(P_{11,k}(i,j)\right)^3$$
$$+3\left(P_{11,k}(i,j)\right)^2P_{21,k}(i,j)\ +3P_{11,k}(i,j)\left(P_{21,k}(i,j)\right)^2\}=\frac{N_1e^2}{m}(E_{1,k}(i,j)).$$

$$\frac{P_{12,k}(i,j+1)-2P_{12,k}(i,j)+P_{12,k}(i,j-1)}{\Delta t^2}+\gamma_2\frac{P_{12,k}(i,j)-P_{12,k}(i,j-1)}{\Delta t}+4\pi^2{f_2}^2\left(P_{12,k}(i,j)\right)$$
$$-\frac{4\pi^2{f_2}^2}{N_2 ed}\left\{\left(P_{12,k}(i,j)\right)^2+2P_{12,k}(i,j)P_{22,k}(i,j)\right\}+\frac{4\pi^2{f_2}^2}{{N_2}^2e^2d^2}\{\left(P_{12,k}(i,j)\right)^3$$
$$+3\left(P_{12,k}(i,j)\right)^2P_{22,k}(i,j)\ +3P_{12,k}(i,j)\left(P_{22,k}(i,j)\right)^2\}=\frac{N_2e^2}{m}(E_{1,k}(i,j)).$$

$$P_1=P_{11}+P_{12},\ \ N=N_1+N_2 \quad (187)$$

x: Space coordinate, t: Time, k: Iteration, $E_k(\mathrm{x,t})=E_k(\mathrm{i\Delta x,j\Delta t})\ \rightarrow E_k(\mathrm{i,j})$

$E_{2,k}$: *pump wave at each iteration k*

$E_{1,k}$: *Input (stimulus)wave at iteration k*

Newton's method:

Cost function: $C=|E_1(f=440\,THz)|$

Newton's Algorithm: (C' *indicates derivative*)

$$\nu_p{}^{(k)}=\nu_p{}^{(k-1)}-\mu_k\frac{C\left(\nu_p{}^{(k-1)}\right)-C\left(\nu_p{}^{(k-2)}\right)}{C'\left(\nu_p{}^{(k-1)}\right)-C'\left(\nu_p{}^{(k-2)}\right)}\left(\nu_p{}^{(k-1)}-\nu_p{}^{(k-2)}\right),\quad k=1,2,3,\ldots$$

For each iteration, the optimal step size is determined as

$$\mu_k=c^{\left(\log\left|\frac{C(\boldsymbol{\nu_p}^{(k)})}{C(\boldsymbol{\nu_p}^{(k)})-C(\boldsymbol{\nu_p}^{(k-1)})}\right|\right)/\left(\left|\frac{C(\boldsymbol{\nu_p}^{(k)})}{C(\boldsymbol{\nu_p}^{(k)})-C(\boldsymbol{\nu_p}^{(k-1)})}\right|\right)} \quad (188)$$

Where c is a constant ($1.001<c<1.499$). For this simulation, the constant c is selected as c=1.35. According to the stated formulations, the highest intracavity input wave amplitude (for 0<t<10ps) is determined as

$Gain_{max} = \left|E_1(\nu_p = 440\ THz)\right|_{max} = 2.26 \times 10^8\ V/m$, which occurs at a pump wave excitation frequency of $\nu_p = 302.9\ THz$ (see Table6.2).

$W_e = Intracavity\ electric\ energy\ density,\ \ P_{pump}$: $Induced\ polarization\ density$

Table 6.2: Newton's algorithm-based optimization

ν_p	$Gain_{max}$	$W_{e,p}\ (\frac{J}{m^3})$	$P_{pump}(\frac{C}{m^2})$	k (iteration #)
175.0THz	17.09	3.37×10^8	0.202	1
250.0THz	13.21	4.02×10^8	0.166	2
158.0THz	4.08	0.42×10^8	0.051	3
238.5THz	43.85	2.26×10^8	0.246	4
320.2THz	340.84	1.79×10^8	0.160	5
403.9THz	58.84	0.95×10^8	0.127	6
339.4THz	5.13×10^4	3.06×10^8	0.224	7
275.0THz	3.86	0.97×10^8	0.090	8
288.3THz	8.87	0.89×10^8	0.095	9
302.9THz	2.26×10^8	3.67×10^8	0.253	10

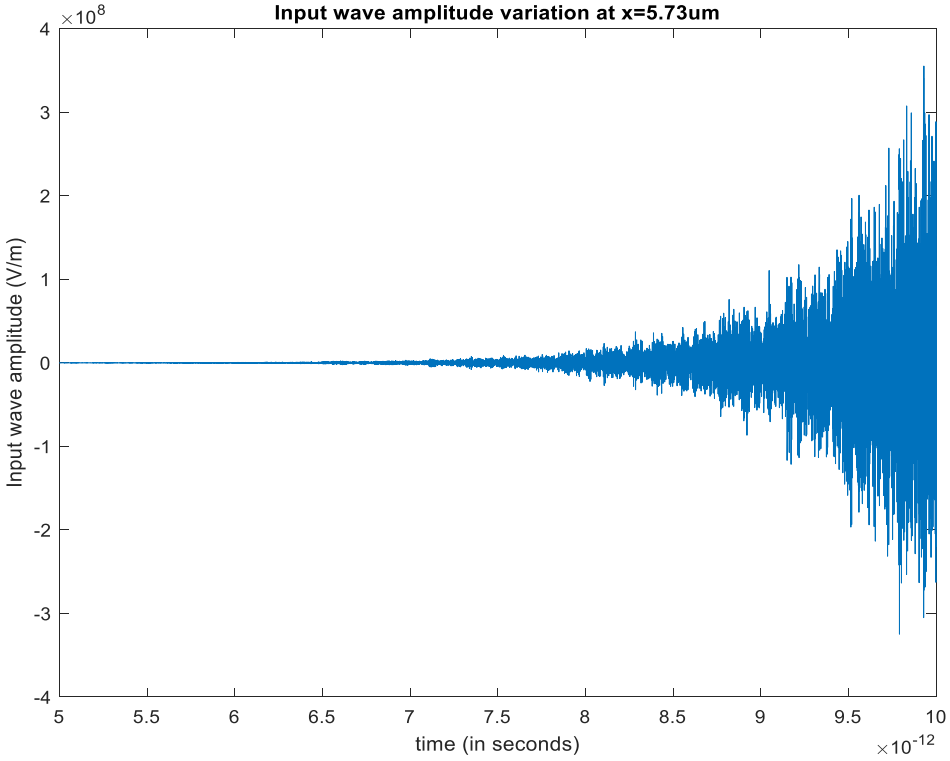

Figure 6.6 Input wave amplification (polychromatic) in the cavity versus time.

6.2. Validation of the numerical model

The results of our numerical model that is based on the FDTD equations given in equations and the embedded Newton's algorithm that is given in equation, are compared with the results available from the experimentally validated theoretical formulas of nonlinear wave mixing in the following examples. In the first example we will compare our numerical model with the experimental formula in the context of optical frequency conversion. In the second example, the numerical model will be compared with the experimental formula in the context of second harmonic generation.

Example 6.2.1: Optical frequency conversion by nonlinear wave mixing

In this example, a higher frequency component (ω_3) is generated via interaction of two quasi monochromatic waves with frequencies ω_1 and ω_2. The high-intensity wave has an angular frequency of ω_2 and the relatively low-intensity signal wave has an angular frequency of ω_1. The resulting high frequency wave has an angular frequency of $\omega_3 = \omega_1 + \omega_2$. The numerical conversion efficiency will be tested based on theory.

The 180 THz high-intensity source wave $\boldsymbol{E_2}$ is originated at x=2.6 μm. The 120 THz input wave $\boldsymbol{E_1}$ is also generated at x=2.6 μm. The amplitudes of the waves are A_2 and A_1 respectively.

$$\boldsymbol{E_2}(x = 2.6\,\mu m, t) = A_2 \times \sin(2\pi(1.8 \times 10^{14})t + \varphi_2)\ \ V/m$$

$$\boldsymbol{E_1}(x = 2.6\,\mu m, t) = A_1 \times \sin(2\pi(1.2 \times 10^{14})t + \varphi_1)\ \ V/m\ \ \ (\varphi_1 = 0, \varphi_2 = 0)$$

Spatial and temporal simulation parameters: $0 \le x \le 10\ \mu m,\ 0 \le t \le 30\ ps$

$Emission\ (resonance)\ frequencies\ of\ the\ cavity\ material$: $\boldsymbol{f_r} = \{1 \times 10^{15}\ Hz, 1.2 \times 10^{15}\ Hz,\ 1.5 \times 10^{15}\ Hz\}$

$Damping\ (decay)\ rates\ of\ the\ cavity\ material$: $\boldsymbol{\gamma} = \{3 \times 10^{12}\ Hz, 1 \times 10^{12}\ Hz, 2 \times 10^{12}\ Hz\}$

$$Permittivity\ of\ the\ cavity\ material\ (\varepsilon_\infty) = 1 + \chi = 12 \quad (\mu_r = 1)$$

$$Left\ termination\ layer\ (absorber)\ is\ from\ x = 0\ to\ x = 2.3\ \mu m$$

$$Right\ termination\ layer\ (absorber) is\ from\ x = 7.7\ \mu m\ to\ x = 10\ \mu m$$

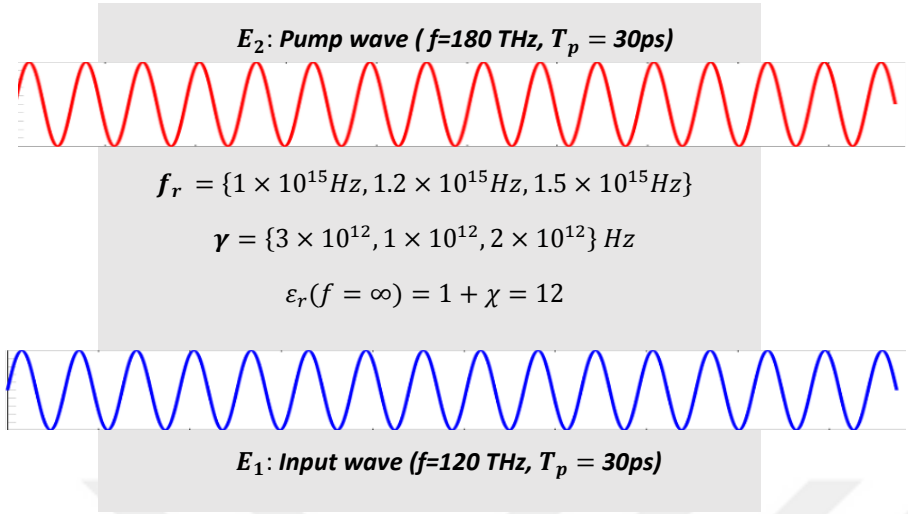

Figure 6.7 Configuration for example 6.2.1

$$\eta_{theoretical} = \frac{\omega_3}{\omega_2}\left(\sin\sqrt{2d^2\eta^3{\omega_3}^2(cn\varepsilon_0{A_2}^2)L^2}\ \right)^2 \qquad (189)$$

d= Strength of Nonlinearity, η = Intrinsic impedance, n= Refractive index

A_2= High-intensity source wave amplitude

A_1= Input wave amplitude, L= Interaction (medium) length

$$\omega_3 = \omega_1 + \omega_2 = Frequency\ of\ the\ generated\ harmonic$$

The numerical model is implemented based on Equations (163-170).

For a simulation duration of $0 \le t \le t_{max}$, the numerical expression for *harmonic (frequency) conversion efficiency* is given as

$$\eta_{numerical} = \frac{\text{Power of the new } \omega_3 \text{ harmonic of the total wave at t} = t_{max}}{\text{Power of the } \omega_2 \text{ harmonic of the total wave at t} = 0} \qquad (190)$$

The values of each parameter are as stated below:

$$\omega_2 = Source\ (pump)\ wave\ angular\ frequency = (2\pi \times 180)\ THz,$$

$$\omega_1 = Input\ wave\ angular\ frequency = (2\pi \times 120)\ THz$$

L=Cavity medium length=3.33 micrometers (from x=3.33 μm to 6.66 μm)

$\omega_3 = Converted\ harmonic\ angular\ frequency = 2\pi \times 300\ THz,$ n $= \sqrt{12}$

d= *Strength of nonlinearity*= 3.31×10^{-23} (The experimental and the numerical results match for this value at a source wave amplitude of $A_2 = 10^9\ V/m$. Hence this value is our initial estimate)

A_2= *Amplitude of the source wave (Swept from* $1 \times 10^8\ V/m$ *to* $2.5 \times 10^9\ V/m$ *)*

A_1= *Amplitude of the input wave* = $A_2/10$

Resonator (oscillator) strengths = $\xi = \{\frac{1}{3}, \frac{1}{3}, \frac{1}{3}\}$

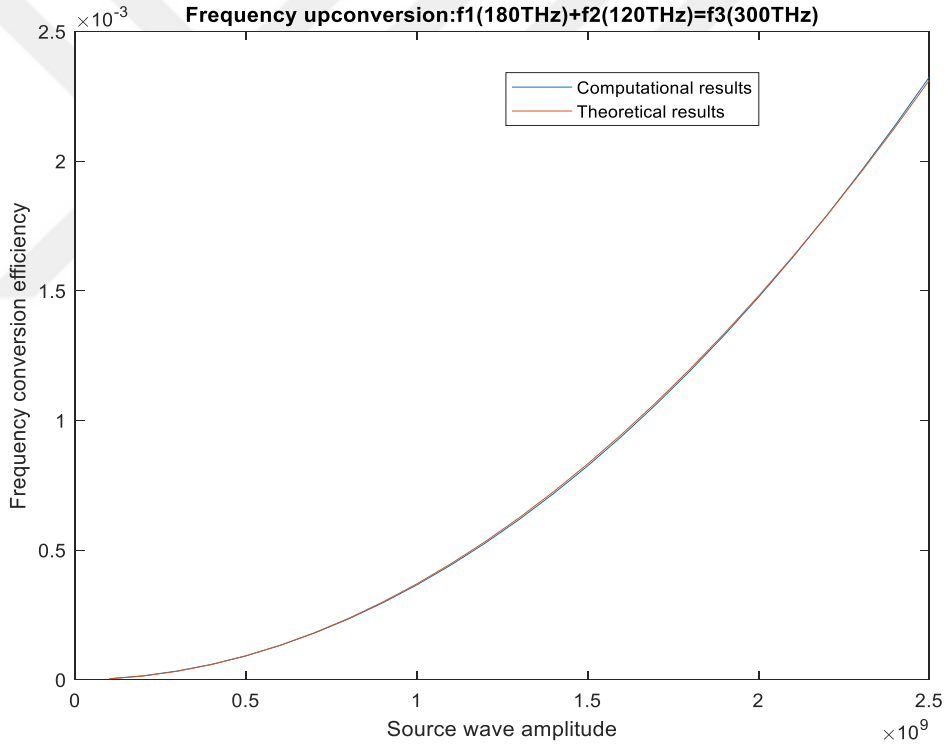

Figure6.8: Comparison of the frequency up-conversion efficiencies for f_3=300 THz and d= 3.31×10^{-22}, versus the pump wave amplitude.

The numerical and the theoretical results perfectly agree as shown in Figure6.8. This figure shows that once we obtain an initial estimate of the nonlinearity coefficient at a sample pump wave amplitude (preferably for a high pump wave amplitude), that initial estimate often turns out to be a very accurate one. This example proves that our numerical model is quite accurate based on the experimentally verified theoretical results.

Example 6.2.2: Second harmonic generation by nonlinear wave mixing

In this example, the second harmonic generation efficiency of a source wave is investigated in a nonlinear medium. The initially monochromatic source wave has an angular frequency of ω_1. The second harmonic of the source wave has an angular frequency of $\omega_2 = 2\omega_1$. Theoretical and numerical results are compared.

The 100 THz high-intensity source wave $\boldsymbol{E_1}$ is originated at x=2.4 μm. The amplitude of the wave is A_1 (V/m).

$$\boldsymbol{E_1}(x = 2.4\ \mu m, t) = A_1 \times \sin(2\pi(1 \times 10^{14})t + \varphi_1)\ \ V/m \quad (\varphi_1 = 0)$$

Spatial and temporal simulation parameters: $0 \le x \le 10\ \mu m,\ 0 \le t \le 30\ ps$

$Emission\ (resonance)\ frequencies\ of\ the\ cavity\ material$: $\boldsymbol{f_r} = \{7.8 \times 10^{14}\ Hz, 9.5 \times 10^{14}\ Hz,\ 1.4 \times 10^{15}\ Hz\}$

$Damping\ (decay)\ rates\ of\ the\ cavity\ material$: $\boldsymbol{\gamma} = \{4 \times 10^{12}\ Hz, 3 \times 10^{12}\ Hz, 1 \times 10^{12}\ Hz\}$

$$Permittivity\ of\ the\ cavity\ material\ (\varepsilon_\infty) = 1 + \chi = 12 \quad (\mu_r = 1)$$

$$Left\ termination\ layer\ (absorber)\ is\ from\ x = 0\ to\ x = 2.35\ \mu m$$

$$Right\ termination\ layer\ (absorber) is\ from\ x = 7.65\ \mu m\ to\ x = 10\ \mu m$$

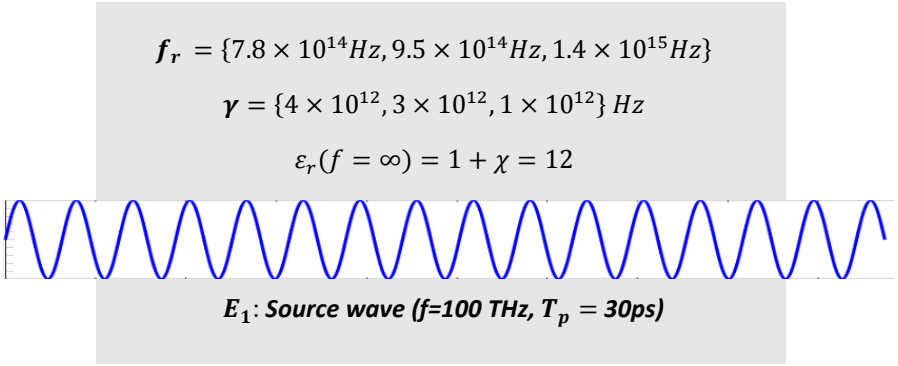

Figure6.9: Configuration for Example 6.2.2

The experimentally validated theoretical efficiency of the second harmonic generation process is given as

$$\eta = (\tanh\sqrt{d^2\eta^3\omega^2cn\varepsilon_0{A_1}^2L^2})^2 \qquad (191)$$

d= Strength of Nonlinearity, η = Intrinsic impedance, n= Refractive index

A_1= High-intensity source wave amplitude

L= Interaction (medium) length

$\omega_2 = Angular\ frequency\ of\ the\ second\ harmonic$

The numerical model is implemented based on Equations (163-170).

For a simulation duration of $0 \leq t \leq t_{max}$, the numerical expression for second *harmonic generation efficiency* is given as

$$\eta_{numerical} = \frac{\text{Power of the second harmonic of the source wave at t} = t_{max}}{\text{Power of the first harmonic of the source wave at t} = 0} \qquad (192)$$

The value of each parameter is as stated below:

$\omega_1 = Source\ wave\ first\ harmonic\ angular\ frequency = (2\pi \times 100)\ THz$

L=Cavity medium length=3.33 micrometers (from x=3.33 μm to 6.66 μm)

$\omega_2 = Second\ harmonic\ angular\ frequency = 2\pi \times 300\ THz,\ \text{n} = \sqrt{12}$

d= *Strength of nonlinearity*= 1.21×10^{-22} (The experimental and the numerical results match for this value at a source wave amplitude of $A_1 = 10^9\ V/m$. Hence this value is chosen as our initial estimate)

A_1= Amplitude of the source wave (Swept from $1 \times 10^8\ V/m$ to $2.5 \times 10^9\ V/m$)

Resonator (oscillator) strengths = $\xi = \{\ 0.3, 0.4, 0.3\ \}$

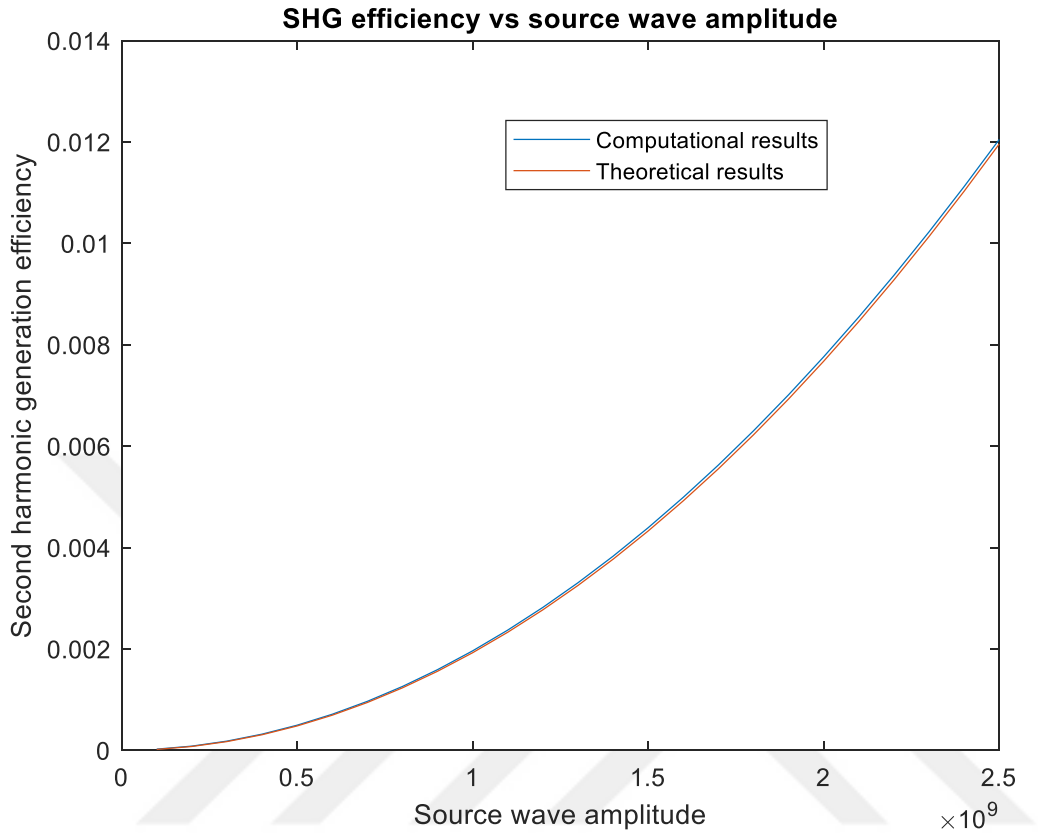

Figure6.10: Comparison of the numerical and theoretical second harmonic generation efficiencies for f_1=100 THz and d= 1.21×10^{-21}, versus the source wave amplitude.

CHAPTER 7

CONCLUSION

Micrometer scale amplification of electromagnetic waves is well known to be possible via stimulated emission. However, optical amplification using nonlinear wave mixing has poor performance in the micrometer range as the gain medium length is too small for considerable amplification. Without the use of a resonator, optical amplification using nonlinear wave mixing is negligible. Even with the use of a resonator, achieving significant amplification is not feasible as the resonator loss factor for a nonlinear interaction is very high. Detectable amplification inside a micro-resonator via nonlinear wave interaction may only be possible if the pump wave is too strong, the cavity loss factor is very small, the frequencies of the interacting waves are relatively high, and the interaction time is very long. Achieving a long interaction time is especially very difficult as the high-intensity pump wave usually has an ultrashort pulse duration. Considering all these difficulties, optical amplification is much more feasible using the stimulated emission technique unless the interaction medium displays an unusually strong nonlinearity. A strongly nonlinear gain (or interaction) medium might be able to yield a comparable amplification efficiency with that of amplification by stimulated emission. Such highly nonlinear materials are of significant interest for the nonlinear optics community not only for amplification purposes but also for purposes other than wave amplification such as harmonic generation or frequency conversion, in fact artificially materials such as materials that are doped with highly nonlinear nanoparticles (e.g. gold nanoparticles doped in glass) already display unusually high nonlinear response. However, for optical amplification purposes such materials are not feasible as they also display a strong absorption around their resonant nonlinear response frequency. Furthermore, these artificial materials can be both very costly and very hard to fabricate. Production of nanoparticles and their embedding in a host material is of high challenge.

Most importantly, such materials are produced in thin film form, which is of no use for wave amplification purposes. Apart from the trivial technique of using very intense pump wave pulses in extremely low-loss (High-Q) resonators, optical amplification in a micro-resonator cannot be achieved by nonlinear wave mixing. This trivial technique also carries the risk of damaging the gain medium due to very high-intensity levels as a result of dielectric breakdown. Hence, an alternative technique for nonlinear wave amplification in the micrometer scale is of high importance and that is why we have chosen a computational approach, in which we can tune every parameter to investigate the wave amplification performance.

We have determined that in order to have a strong amplification in a micro-resonator using nonlinear wave mixing, the electric energy density and the polarization density in the micro-resonator must be concurrently high. Having a high intracavity energy alone is not enough, since a coupling mechanism to transfer some of that stored energy to the wave to be amplified is necessary. The polarization density in the micro-resonator acts as a coupling coefficient between the high-intensity pump wave and the input wave and therefore must also be maximized. Simultaneous maximization of the electric energy and the polarization density is computationally plausible by embedding a nonlinear programming (nonlinear optimization) algorithm in a wave equation discretization method such as the finite difference time domain method. Since the combined numerical algorithm is of high computational cost, we have chosen a method of optimization (BFGS) that computes the second derivative (Hessian) of each iteration in a recursive manner, thereby reducing the computational cost. The results of our numerical experiments show that the frequencies of high-intensity ultrashort pulses (pump waves) can be adjusted via nonlinear programming to optimize the gain factor of the nonlinear optical amplification, and the gain factor can be further enhanced by choosing an interaction medium with a low polarization damping coefficient and by choosing the micro-resonator walls to be highly reflective. We believe these results indicate that nonlinear electromagnetic wave amplification or optical amplification by nonlinear wave mixing may be an alternative of the stimulated emission technique for amplification in the micrometer scale, provided that the resonator parameters and the pump wave frequencies are adjusted accordingly.

The suggested experimental setup is shown in Figure 7.1. The frequencies of the intense ultrashort pulses that form the excitation can be tuned via a controller device that takes the micro-resonator parameters as inputs and adjusts the frequencies of the ultrashort pulses accordingly through interfacing with a wavelength tuner, such as a simple movable slit. The controller device may perform the maximization of the output intensity of the input beam by executing the algorithm presented in this study. The input parameters for the controller involve the resonance frequencies and the polarization damping rates of the micro-resonator medium, the length of the resonator, background permittivity and conductivity of the medium, and the electric field amplitudes of the excitation pulses. Based on these parameters, the controller device can adjust the position of the movable slit (wavelength tuner) that is depicted in Figure 7.2 to select the wavelength of the maximum transmission for each excitation pulse. Figure 7.1 illustrates the simple experimental configuration for implementation and Figure 7.2 illustrates the configuration of the source device (such as a tunable solid-state bulk laser [24]) and its' integration with the movable slit that acts as a wavelength tuner. Note that although the numerical simulations that are performed in this study assumes a micrometer scale micro-resonator, the suggested BFGS nonlinear optimization can be used to enhance the cavity gain of a nonlinear wave mixing process at any scale.

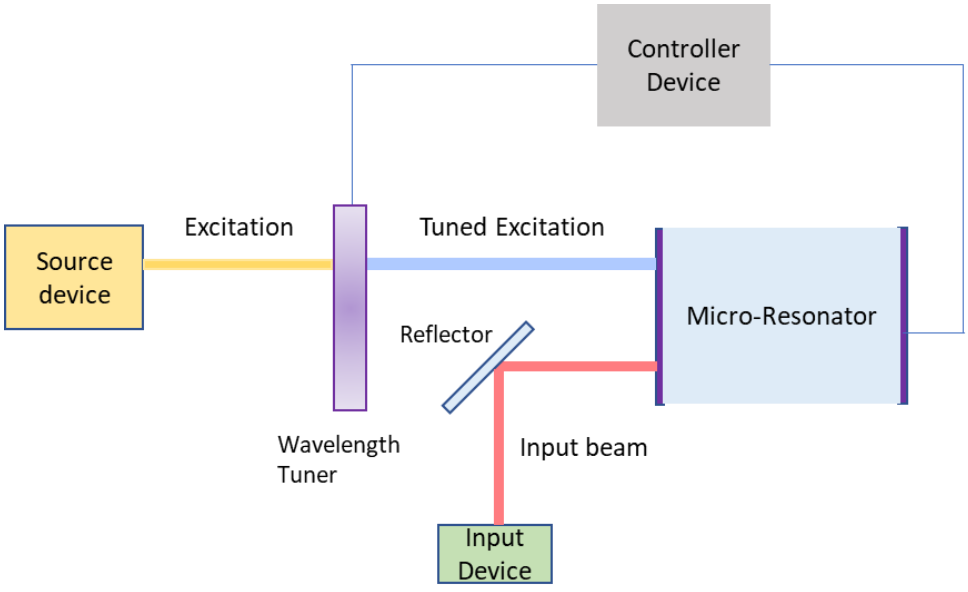

Figure 7.1 Proposed experimental setup for the implementation of the process.

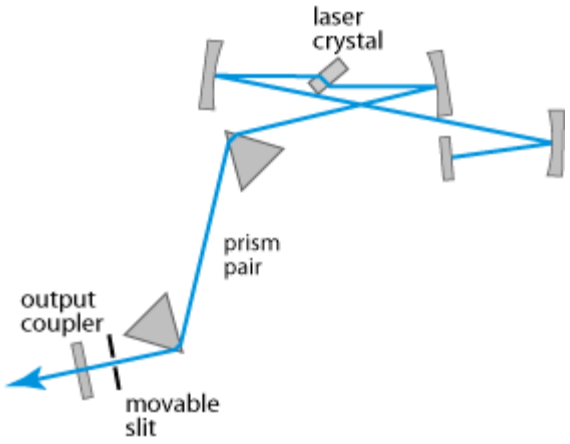

Figure 7.2 Configuration of a tunable solid-state bulk laser [24].

For a high parametric cavity-gain, the cavity walls should be highly reflective. However, the most important criteria for high-gain amplification are the resonance frequencies of a material, which should reside in the near infra-red frequency range. Germanium and Gallium-Arsenide are two nice examples of the semiconductor class that can be used as an interaction medium due to their strong resonance features in the infra-red region and low polarization decay rate. Fused silica, crystalline quartz and borosilicate crown glass are also suitable for use as an interaction medium for their strong near-infrared emission features. As a good dielectric, Lithium-Niobate is one of the best materials to be used as an interaction medium due its' high permittivity, low polarization decay rate, and strong near-infrared emission attributes. Other possible candidates for use as an interaction medium for parametric amplification are zinc selenide and sapphire for their low polarization decay rate and fair infra-red emission features. In short, any material that has a strong emission in the near infra-red frequency range is a good choice for parametric wave amplification regardless of their polarization decay rate as low polarization decay rate can be easily compensated by increasing the reflection coefficients of the cavity walls.

The algorithm presented in this study features a simple optical set-up, and an enhanced gain factor for the parametric wave amplification process in the microscale. Further studies can be done to examine the optical beam cross section, optical power, and other features via a two-dimensional analysis using a suitable discretization algorithm.

REFERENCES

[1] Boyd Robert.W., Nonlinear Optics, pp. 105-107, Academic Press, New York, 2008.

[2] Fox Mark, Optical properties of solids, pp. 237-239, Oxford University Press, New York, 2002.

[3] Balanis Constantine.A., Advanced Engineering Electromagnetics, pp. 66-67, John Wiley & Sons, New York, 1989.

[4] Bahaa E. A. Saleh, Malvin Carl Teich, Fundamentals of Photonics, pp. 885-917, Wiley-Interscience, New York, 2007

[5] Silfvast William.T., Laser Fundamentals, pp. 24-35, Cambridge University Press, New York, 2004

[6] Junkichi Satsuma, Nobuo Yajima, "Initial Value Problems of One-Dimensional Self-Modulation of Nonlinear Waves in Dispersive Media", Progress of Theoretical Physics Supplement, Volume 55, January 1974

[7] Taflove Allen, Hagness Susan.C., Computational Electrodynamics: The Finite-Difference Time-Domain Method, pp. 353-361, Artech House, Boston, 2005

[8] Amit S. Nagra, Robert A. York, "FDTD Analysis of Wave Propagation in Nonlinear Absorbing and Gain Media", IEEE Transactions on Antennas and Propagation, Vol. 46, No. 3, March 1998

[9] Murray K. Reed, Michael K. Steiner-Shepard, Michael S. Armas, Daniel K. Negus, "Microjoule-energy ultrafast optical parametric amplifiers", Journal of the Optical Society of America B, Volume 12, Issue 11, 1995

[10] Anna G. Ciriolo, Matteo Negro, Michele Devetta, Eugenio Cinquanta, Davide Faccialà, Aditya Pusala, Sandro De Silvestri, Salvatore Stagira, and Caterina Vozzi, "Optical Parametric Amplification Techniques for the Generation of High-Energy Few-Optical-Cycles IR Pulses for Strong Field Applications", MDPI Applied Sciences, March 2017

[11] E. A. Migal, F. V. Potemkin, and V. M. Gordienko, "Highly efficient optical parametric amplifier tunable from near-to mid-IR for driving extreme nonlinear optics in solids", Optics Letters, Vol. 42, Issue 24, pp. 5218-5221, June 2017

[12] Chaohua Wu, Jingtao Fan, Gang Chen, and Suotang Jia, "Symmetry-breaking-induced dynamics in a nonlinear microresonator", Optics Express (20), pp. 28133-28142, July 2019.

[13] György Tóth, József A. Fülöp, and János Hebling, "Periodically intensity-modulated pulses by optical parametric amplification for multicycle tunable terahertz pulse generation", Optics Express Vol. 25, Issue 23, pp. 28258-28272, May 2017

[14] Fabian Kaufmann, Anton Sergeyev, Marc Reig Escalé, and Rachel Grange, "On-Chip Optical Parametric Amplification in Subwavelength Lithium Niobate Nanowaveguides", Advanced Photonics 2018

[15] V. Gruson, G. Ernotte, P. Lassonde, A. Laramée, M. R. Bionta, M. Chaker, L. Di Mauro, P. B. Corkum, H. Ibrahim, B. E. Schmidt, and F. Legaré, "2.5 TW, two-cycle IR laser pulses via frequency domain optical parametric amplification", Optics Express Vol. 25, Issue 22, pp. 27706-27714, (2017)

[16] Guilmot Ernotte, Philippe Lassonde, Mathieu Giguère, Bruno E. Schmidt, and François Légaré, "Towards TW Few-Cycle Infrared Laser Pulses via Fourier Optical Parametric Amplification", International Conference on Ultrafast Phenomena, 2016

[17] Keisuke Kaneshima, Nobuhisa Ishii, Kengo Takeuchi, and Jiro Itatani, "Generation of carrier-envelope phase-stable mid-infrared pulses via dual-wavelength optical parametric amplification", Optics Express Vol. 24, Issue 8, pp. 8660-8665, (2016)

[18] Yanchun Yin, Andrew Chew, Xiaoming Ren, Jie Li, Yang Wang, Yi Wu & Zenghu Chang, "Towards Terawatt Sub-Cycle Long-Wave Infrared Pulses via Chirped Optical Parametric Amplification and Indirect Pulse Shaping", Scientific Reports volume 7, Article number: 45794, (2017)

[19] Adam S Wyatt, Paloma Matía-Hernando, Allan S Johnson, Danylo T Matselyukh, Alfred J H Jones, Richard T Chapman, Cephise Cacho, Dane R Austin, John W G Tisch, Jon P Marangos, Emma Springate, "Optical Parametric Amplification of Mid-Infrared Few-Cycle Pulses", arXiv:1909.05954 [physics.optics]

[20] Yuxi Fu, Eiji J. Takahashi, Katsumi Midorikawa, "Energy Scaling of Infrared Femtosecond Pulses by Dual-Chirped Optical Parametric Amplification", IEEE Photonics Journal (Volume: 9, Issue: 3, June 2017)

[21] E. Smetanina, E. Migal, I. Thiele, F. Potemkin, "Light Bullets from Chirped High-Power Femtosecond Pulses under Normal GVD for Mid-IR Optical Parametric Amplification", 2019 Conference on Lasers and Electro-Optics Europe & European Quantum Electronics Conference (CLEO/Europe-EQEC)

[22] Bingjie Zhou, Jingui Ma, Jing Wang, Peng Yuan, Guoqiang Xie, and Liejia Qian, "Ultrafast group-velocity control via cascaded quadratic nonlinearities in optical parametric amplification", Optics Letters Vol. 43, Issue 15, pp. 3790-3793 (2018)

[23] C. R. Phillips, N. Bigler, J. Pupeikis, S. Hrisafov, L. Gallmann, H. Ishizuki, T. Taira, and U. Keller, "Broadband and high power mid-infrared optical parametric amplification via quasi-phase-matching devices", High-Brightness Sources and Light-driven Interactions, Optical Society of America, 2018

[24] Özüm Emre Aşırım, Mustafa Kuzuoğlu, "Numerical Study of Resonant Optical Parametric Amplification via Gain Factor Optimization in Dispersive Microresonators", Photonics 2020

[25] Zhong Zuo, Chenglin Gu, Daowang Peng, Xing Zou, Daping Luo, Lian Zhou, Zhiwei Zhu, Zejiang Deng, Yang Liu, and Wenxue Li, "Few-cycle mid-infrared ultrafast pulses generation based on continuous-wave seeded optical parametric amplification", Laser Congress 2019

[26] Sung Bo Lee, Hyeon Sang Bark, and Tae-In Jeon, "Enhancement of THz resonance using a multilayer slab waveguide for a guided-mode resonance filter", Opt. Express (20), pp. 29357-29366, (2019)

[27] Houssein El Dirani, Laurene Youssef, Camille Petit-Etienne, Sebastien Kerdiles, Philippe Grosse, Christelle Monat, Erwine Pargon, and Corrado Sciancalepore, "Ultralow-loss tightly confining Si_3N_4 waveguides and high-Q microresonators", Opt. Express, Vol. 27, Issue 21, pp. 30726-30740 (2019)

[28] Ivan S. Maksymov; Andrey A. Sukhorukov; Andrei V. Lavrinenko ; Yuri S. Kivshar, "Comparative Study of FDTD-Adopted Numerical Algorithms for Kerr Nonlinearities", IEEE Antennas and Wireless Propagation Letters, Volume 10, 2011

[29] E. Valentinuzzi, "Dispersive properties of Kerr-like nonlinear optical structures", Journal of Lightwave Technology, Volume 16, Issue 1, 1998

[30] Mohammad Amin Izadi, Rahman Nouroozi, "Adjustable Propagation Length Enhancement of the Surface Plasmon Polariton Wave via Phase Sensitive Optical Parametric Amplification", Scientific Reports Volume 8, Article number: 15495 (2018)

[31] Özüm Emre Aşırım, Mustafa Kuzuoğlu, "Enhancement of Optical Parametric Amplification in Micro-resonators via Gain Medium Parameter Selection and Mean Cavity Wall Reflectivity Adjustment", Journal of Physics-B: Atomic Molecular and Optical Physics, 2020

[32] Özüm Emre Aşırım, Mustafa Kuzuoğlu, "Super-Gain Optical Parametric Amplification in Dielectric Micro-Resonators via BFGS Algorithm-Based Non-Linear Programming", Appl. Sci. 2020, 10(5), 1770

ÖZÜM EMRE AŞIRIM

E-mail: ozumasirim88@gmail.com
https://orcid.org/0000-0003-0531-401X

Education

Undergraduate Study

B.S 2005-2009

FMV IŞIK University/ Electronics Engineering Department/Turkey.

Ranked 1st in the engineering faculty (among 227 graduates). Ranked 8th in overall with a GPA of 3.74 /4.00

Areas of Focus: Signal Processing (Image & Biomedical), Communication Engineering, Electromagnetics, Computational Physics

B.S Thesis: *Simulation of Resource Allocation in WIMAX Networks.*

Graduate Study

MSc 2010-2013

Middle East Technical University (METU), Electrical and Electronics Eng. (GPA: 3.64/4.00)
Areas of focus: Signal processing, Electromagnetics, Optics, Computational Electromagnetics

Thesis Subject: Investigation of Rough Surface Scattering of Electromagnetic Waves Using Finite Element Method (FEM).
Thesis advisors: Prof. Dr. Mustafa Kuzuoğlu, Prof. Dr. Özlem Özgün

PhD 2014 –2020
Middle East Technical University (METU), Electrical and Electronics Engineering **(**GPA: 3.78/4.00)

Areas of focus: Photonics, Nonlinear Optics, Electromagnetic Wave Theory, Computational Electromagnetics, Numerical Optimization

Thesis Subject: Super-Gain Parametric Wave Amplification in Optical Micro-resonators Using Ultrashort Pump Waves

Thesis advisor: Prof.Dr. Mustafa Kuzuoğlu

Research Interests

- **Computational Physics (Electromagnetics, Optics & Photonics, Plasma Physics)**
- **Nonlinear Optics**
- **Wave matter interactions**
- **Wave propagation in nonlinear & dispersive media**
- **Wave propagation in artificial media**
- **Laser-plasma interactions**
- **Antenna Theory**
- **Physical & Quantum Optics**
- **Numerical Optimization**
- **Statistical & Adaptive Signal Processing**

Journal Papers

Aşırım, Ö.E.; Kuzuoğlu, M. Numerical Study of Resonant Optical Parametric Amplification via Gain Factor Optimization in Dispersive Microresonators. *Photonics* 2020, *7*, 5.

Aşırım, Ö.E.; Kuzuoğlu, M. Super-Gain Optical Parametric Amplification in Dielectric Micro-Resonators via BFGS Algorithm-Based Non-Linear Programming. *Appl. Sci.* 2020, *10*, 1770.

Özüm Emre Aşırım, Mustafa Kuzuoğlu, "Enhancement of Optical Parametric Amplification in Micro-resonators via Gain Medium Parameter Selection and Mean Cavity Wall Reflectivity Adjustment", Journal of Physics-B: Atomic Molecular and Optical Physics, 2020

Özüm Emre Aşırım, Mustafa Kuzuoğlu, Wideband Electromagnetic Wave Generation via Supercontinuum Formation in Infrared-Resonant Optical Microcavities, *International Journal of Optics and Applications*, Vol. 8 No. 2, 2019, pp. 21-31. doi: 10.5923/j.optics.20190802.01.

Programming Skills: MATLAB, C, C++

Languages:

Turkish (Native)
English (Fluent)
German (Fluent)

Professional Experience

2009-2010 Turk Telekom - Network operation Center
2014-2016 Lime Finance – Forecasting Specialist in FOREX Trading

Awards

2014
TUBITAK – Ph.D Scholarship for education in Turkey
Given by assessing the average of the ALES exam score and GPA.

2013
King Abdullah University of Science & Technology (KAUST) – Full PhD Scholarship

2010
Işık University – Electronics Engineering, Engineering Faculty Valedictorian Award

Courses Taken During PhD:

- **Quantum Optics**
- **Quantum Mechanics**
- **Photonics**
- **Laser Physics**
- **Applications of Laser Physics**
- **Optical Properties of Semiconductors**
- **Optoelectronics**
- **Optical Materials & Spectroscopy**
- **Electromagnetic Waves & Electro-Optics**
- **Nano-Optics**
- **Introduction to Nanoscience & Nanotechnology**
- **Fourier Optics**
- **Simulations & Modeling of Many Particle Systems**
- **Molecular Spectroscopy**
- **Plasma Physics & Controlled Fusion**
- **Plasma Physics**
- **Applications of Plasma physics**
- **Statistical Signal Processing**
- **Adaptive Signal Processing**
- **Spectral Estimation**

Major Field in PhD Qualification Exam: Electromagnetic Waves, Optics, Photonics
Minor Field in PhD Qualification Exam: Signal Processing (Random & Deterministic)